University of Alberta

# NEW FLUORESCENT PROTEINS AND GENETICALLY ENCODED BIOSENSORS

by

Huiwang Ai

A thesis submitted to the Faculty of Graduate Studies and Research
in partial fulfillment of the requirements for the degree of

Doctor of Philosophy

Department of Chemistry

Edmonton, Alberta
Fall 2008

Library and Archives Canada

Published Heritage Branch

395 Wellington Street
Ottawa ON K1A 0N4
Canada

Bibliothèque et Archives Canada

Direction du Patrimoine de l'édition

395, rue Wellington
Ottawa ON K1A 0N4
Canada

*Your file Votre référence*
*ISBN: 978-0-494-46269-0*
*Our file Notre référence*
*ISBN: 978-0-494-46269-0*

NOTICE:
The author has granted a non-exclusive license allowing Library and Archives Canada to reproduce, publish, archive, preserve, conserve, communicate to the public by telecommunication or on the Internet, loan, distribute and sell theses worldwide, for commercial or non-commercial purposes, in microform, paper, electronic and/or any other formats.

The author retains copyright ownership and moral rights in this thesis. Neither the thesis nor substantial extracts from it may be printed or otherwise reproduced without the author's permission.

AVIS:
L'auteur a accordé une licence non exclusive permettant à la Bibliothèque et Archives Canada de reproduire, publier, archiver, sauvegarder, conserver, transmettre au public par télécommunication ou par l'Internet, prêter, distribuer et vendre des thèses partout dans le monde, à des fins commerciales ou autres, sur support microforme, papier, électronique et/ou autres formats.

L'auteur conserve la propriété du droit d'auteur et des droits moraux qui protège cette thèse. Ni la thèse ni des extraits substantiels de celle-ci ne doivent être imprimés ou autrement reproduits sans son autorisation.

---

In compliance with the Canadian Privacy Act some supporting forms may have been removed from this thesis.

While these forms may be included in the document page count, their removal does not represent any loss of content from the thesis.

Conformément à la loi canadienne sur la protection de la vie privée, quelques formulaires secondaires ont été enlevés de cette thèse.

Bien que ces formulaires aient inclus dans la pagination, il n'y aura aucun contenu manquant.

Canada

# University of Alberta

## Library Release Form

**Name of Author:** Huiwang Ai

**Title of Thesis:** New fluorescent proteins and genetically encoded biosensors

**Degree:** Doctor of Philosophy

**Year this Degree Granted:** 2008

Permission is hereby granted to the University of Alberta Library to reproduce single copies of this thesis and to lend or sell such copies for private, scholarly or scientific research purposes only.

The author reserves all other publication and other rights in association with the copyright in the thesis, and except as herein before provided, neither the thesis nor any substantial portion thereof may be printed or otherwise reproduced in any material form whatsoever without the author's prior written permission.

*Signature*

*To my home country China*

*To my parents*

*Also to the 26th year of myself*

# ABSTRACT

Fluorescent proteins (FPs) emerged in the mid 1990s as a powerful tool for life science research. FPs with a variety of fluorescent colors, ranging from blue to the far-red, are now used in thousands of labs around the world as non-intrusive genetically encoded markers. Although much work has already gone into the development of these various colors of FP, a few members in the 'toolbox' are considerably less optimal than others. The initial goal of this thesis was to engineer new and superior alternatives to these FPs.

To address the limitations of cyan FP (CFP), an alternative known as monomeric teal FP1 (mTFP1) was engineered from the naturally tetrameric *Clavularia* FP484, by screening rationally designed and randomly created libraries. The mechanism of the color of mTFP1 was further investigated and it led to a new green FP known as mWasabi. Both mTFP1 and mWasabi were thoroughly characterized and proven to be useful additions to the FP 'toolbox'.

In the directed evolution process, it was noticed that some variants underwent fast and reversible photoswitching. One mutant, designated as mTFP0.7, was subjected to further characterization and the x-ray crystal structure of both isomers was solved in collaboration with Prof. S.J. Remington. The research on the reversible photoswitching phenomenon elucidated its mechanism, which might be universal to photoswitchable FPs.

The *Aequorea* GFP-derived blue FP (BFP) is of low brightness, and bleaches exceptionally fast. By undertaking the parallel creation, evolution, and comparison of a series of new BFPs with different chromophore structures, several superior variants (e.g. EBFP2 and mKalama1) were produced and characterized.

In the process of creating mKalama1, I fortunately discovered a violet-excitable yellow-fluorescing mutant that was further evolved to be mAmetrine. It has been demonstrated that the combination of mAmetrine, mTFP1, and two other FPs from the 'toolbox' provides two compatible FRET pairs that can be ratiometrically imaged in the same cell. These new FRET pairs have been used to monitor caspase activation in apoptotic cells. To further expand the technique, compatible calcium sensors based on the dual FRET pairs were designed, created and optimized. The development of compatible FRET pairs is an important expansion of FPs into a new exciting research area.

# ACKNOWLEDGEMENTS

The very first thanks should be given to my research supervisor, Dr Robert E Campbell. When I came to Canada in 2003, I knew very little about biochemistry. Fortunately I initiated my project without too much difficulty because of the crucial help and education from him. It was so wonderful that I started my research with the '24/7' technical support. In the course of approaching the PhD degree, sometimes I was depressed and was thinking about giving up because of other personal affairs. The encouragement from him has strongly supported me to get out of the negatives. Besides that I also sincerely thank him to help me to write this thesis. The education, inspiration, friendship from him, everything together made up my most unforgettable memory in Canada.

I sincerely thank the professors ever involved in my supervisory committee: Dr. John Vederas, Dr Chris Le, Dr Rik Tykwinski, Dr David Bundle, and Dr Ing Swie Goping from the Department of Biochemistry, as well as Dr Patrick Daugherty from Chemical Engineering at the University of California Santa Barbara, to attend my candidacy exam and/or my final oral exam, and/or to provide me thorough reviews and comments on this thesis.

I would also like to thank the other professors in the Department of Chemistry. They interacted with me by teaching me courses and/or attending my 502 seminar, and/or supporting me through other ways. Also thanks to other staffs in the Department. Special thanks to Dr Sandra Marcus for teaching me to culture cells, and to the machine shop for building up the LED arrays for my experiments.

Important supports from the collaborators J. Nathan Henderson and S. James Remington at the University of Oregon, Nathan C. Shaner and Roger Y. Tsien at the University of California San Diego, Michael W. Davidson and Kristin L. Hazelwood as well as Scott G. Olenych at the National High Magnetic Field Laboratory and the Florida State University, are highly appreciated. Without their support, portions of the work described here would not have been possible.

I highly value the friendship from the members in the Campbell group, and other friends in the Department who make my life more wonderful in Edmonton.

# TABLE OF CONTENTS

**ABSTRACT** ..... 1

**ACKNOWLEDGEMENTS** ..... 2

**TABLE OF CONTENTS** ..... 3

**LIST OF TABLES** ..... 8

**LIST OF FIGURES** ..... 9

**ABBREVIATIONS AND SYMBOLS** ..... 12

**CHAPTER 1: PROTEIN ENGINEERING AND ITS APPLICATION TO FLUORESCENT PROTEINS** ..... 1

1.1 INTRODUCTION ..... 2

1.2 PROTEIN ENGINEERING ..... 2

1.2.1 Structure-based rational design ..... 4

1.2.2 Directed protein evolution ..... 4

1.2.3 Semi-rational engineering ..... 7

1.3 FLUORESCENCE AND FLUORESCENCE MICROSCOPY ..... 7

1.3.1 Fluorescence ..... 8

1.3.2 Photobleaching ..... 10

1.3.3 Fluorescence resonance energy transfer ..... 10

1.3.4 Fluorescence lifetime ..... 12

1.3.5 Spectrofluorometer ..... 13

1.3.6 Fluorescence microscopy ..... 14

1.4 FLUOROPHORES ..... 16

1.5 FLUORESCENT PROTEINS AND EVOLUTION ..... 18

1.5.1 *Aequorea victoria* green fluorescent protein ..... 18

1.5.2 Unnatural colors and enhanced mutants of avGFP ..... 21

1.5.3 *Anthozoa* FPs ..... 23

1.5.4 Circularly permutated FPs ..... 26

1.5.5 Standard applications of FPs ..... 28

1.5.6 FRET applications of FPs ..... 28

1.6 THE SCOPE OF THE THESIS ..... 30

**CHAPTER 2: DIRECTED EVOLUTION OF A MONOMERIC, BRIGHT, AND PHOTOSTABLE VERSION OF CLAVULARIA CYAN FLUORESCENT PROTEIN ..... 32**

2.1 INTRODUCTION ..... 33
2.2 EXPERIMENTAL ..... 36
2.2.1 General methods and materials ..... 36
2.2.2 Library construction, mutagenesis, and genes encoding fusion proteins ..... 36
2.2.3 Library Screening ..... 38
2.2.4 Protein purification and characterization ..... 39
2.2.5 Spectroscopy ..... 39
2.2.6 Protein expression and imaging in HeLa cells ..... 40
2.3 RESULTS AND DISCUSSION ..... 41
2.3.1 Design of a synthetic gene library encoding dimeric variants of cFP484 ..... 41
2.3.2 Directed evolution of a monomeric teal fluorescent protein ..... 45
2.3.3 Structural analysis of mTFP1 ..... 48
2.3.4 mTFP1 as a FRET donor to mCitrine and mOrange ..... 52
2.3.5 Live cell imaging of mTFP1 fusions and FRET reporters ..... 54
2.4 CONCLUSIONS ..... 56

**CHAPTER 3: CHROMOPHORE CIS-TRANS PHOTOISOMERIZATION: CHARACTERIZATION OF THE REVERSIBLY PHOTOSWITCHABLE VARIANT mTFP0.7 ..... 58**

3.1 INTRODUCTION ..... 59
3.2 EXPERIMENTAL ..... 60
3.2.1 General methods ..... 60
3.2.2 Protein purification ..... 61
3.2.3 Absorption measurements ..... 61
3.2.4 Kinetics ..... 61
3.3 RESULTS AND DISCUSSION ..... 62
3.3.1 Photophysical characterization of mTFP0.7 ..... 62

3.3.2 Prospects for use of mTFP0.7 in live cell imaging ..... 65
3.4 CONCLUSIONS ..... 65

**CHAPTER 4: HUE-SHIFTED VARIANTS OF mTFP1: IDENTIFICATION OF THE MOLECULAR DETERMINANTS OF COLOR AND APPLICATIONS IN FLUORESCENCE IMAGING ..... 67**

4.1 INTRODUCTION ..... 68
4.2 EXPERIMENTAL ..... 70
4.2.1 General methods ..... 70
4.2.2 Mutagenesis and library construction ..... 70
4.2.3 Library screening ..... 71
4.2.4 Protein purification and characterization ..... 71
4.2.5 Photostability measurements ..... 72
4.2.6 Mammalian expression vectors ..... 72
4.2.7 Live cell imaging ..... 73
4.3 RESULTS AND DISCUSSION ..... 74
4.3.1 Blue shifted variants of mTFP1 ..... 74
4.3.2 Red shifted variants of mTFP1 ..... 77
4.3.3 Directed evolution of the red shifted variant of mTFP1 ..... 80
4.3.4 Two color imaging with mWasabi and Sapphire ..... 81
4.3.5 Imaging of mTFP1 and mWasabi fusion proteins ..... 82
4.4 CONCLUSIONS ..... 87

**CHAPTER 5: EXPLORATION OF NEW CHROMOPHORE STRUCTURES LEADS TO THE IDENTIFICATION OF IMPROVED BLUE FLUORESCENT PROTEINS ..... 89**

5.1 INTRODUCTION ..... 90
5.2 EXPERIMENTAL ..... 93
5.2.1 General Methods ..... 93
5.2.2 Library construction and mutagenesis ..... 93
5.2.3 Screening ..... 93
5.2.4 Protein purification ..... 94

5.2.5 Protein characterization ..... 94
5.2.6 Live Cell Imaging ..... 95
5.3 RESULTS ..... 95
5.3.1 *Aequorea* GFP variants with a tyrosine-derived chromophore ..... 95
5.3.2 Improved versions of *Aequorea*-derived EBFP ..... 97
5.3.3 *Discosoma* RFP variants ..... 99
5.4 DISCUSSION ..... 101

**CHAPTER 6: FLUORESCENT PROTEIN FRET PAIRS FOR RATIOMETRIC IMAGING OF DUAL CASPASE BIOSENSORS ..... 105**

6.1 INTRODUCTION ..... 106
6.2 EXPERIMENTAL ..... 107
6.2.1 General methods and materials ..... 107
6.2.2 Mutagenesis and screening ..... 108
6.2.3 Protein characterization ..... 108
6.2.4 Construction of 10-AA linker FRET constructs for spectral imaging ..... 109
6.2.5 Construction of fusion proteins for imaging and photostability measurements ..... 110
6.2.6 Construction of fusion proteins for 4-color widefield imaging ..... 110
6.2.7 Construction of caspase-3 sensors ..... 111
6.2.8 Spectral imaging of FRET constructs ..... 112
6.2.9 4-color widefield imaging ..... 112
6.2.10 Imaging of mAmetrine fusion proteins ..... 112
6.2.11 Photostability measurements in live cells ..... 113
6.2.12 Widefield imaging of staurospaurine-induced apoptosis ..... 114
6.2.13 Image processing ..... 115
6.3 RESULTS AND DISCUSSION ..... 115
6.3.1 Directed evolution of mAmetrine ..... 115
6.3.2 Further characterization of mAmetrine ..... 117
6.3.3 Identification of FRET acceptor for mAmetrine ..... 120
6.3.4 4-color live cell imaging ..... 121
6.3.5 Compatible dual FRET imaging of single cells ..... 122

6.3.6 Spectral bleed-through and correction ..... 127
6.3.7 Comparison of mAmetrine to mT-sapphire ..... 129
6.4 CONCLUSIONS ..... 130

**CHAPTER 7: SPECTRALLY COMPATIBLE FP-BASED FRET SENSORS FOR SIMULTANEOUS CALCIUM IMAGING ..... 131**

7.1 INTRODUCTION ..... 132
7.2 EXPERIMENTAL ..... 135
7.2.1. General methods ..... 135
7.2.2. Evolution of circularly permutated mAmetrine 173 (cpmAmetrine-173) ..... 136
7.2.3. Construction of Cameleons (CaYang and CaYin) for in vitro study ..... 137
7.2.4. Protein purification and characterization ..... 138
7.2.5. Construction of Cameleon mammalian expression vectors ..... 139
7.2.6. Live cell imaging ..... 140
7.3 RESULTS AND DISCUSSION ..... 140
7.3.1. Circularly permutated mAmetrine 173 ..... 140
7.3.2. Endoplasmic reticulum calcium sensors (CaYangs) ..... 143
7.3.3. Cytoplasm calcium sensors (CaYins) ..... 145
7.3.4. Compatible dual-compartmental calcium imaging ..... 147
7.4 CONCLUSIONS ..... 148

**CHAPTER 8: CONCLUSIONS AND FUTURE WORK ..... 150**

**REFERENCES ..... 154**

# LIST OF TABLES


**Table 2.1** Rationale for design of the synthetic dimeric gene library of cFP484..... 43

**Table 2.2** Mutations in dimeric and monomeric TFP variants..... 46

**Table 2.3** Fluorescent properties of CFPs and TFPs..... 47

**Table 2.4** Experimentally determined relative fluorescence intensities for identical concentrations of mTFP1, mCerulean, and mCitrine imaged on an epi-fluorescence microscope with xenon arc lamp illumination..... 56

**Table 3.1** The kinetics of the fluorescence recovery of mTFP0.7 at different temperatures..... 65

**Table 4.1** Properties of hue-shifted mTFP1 variants..... 77

**Table 5.1** Overview of mutations in blue-fluorescing FPs..... 98

**Table 5.2** Properties of new blue-fluorescing FPs..... 99

**Table 6.1** Properties of FPs of the spectrally compatible FRET pairs..... 116

**Table 6.2** Photobleaching rates for FPs of the spectrally compatible FRET pairs... 119

**Table 6.3** Filters used for widefield dual FRET or four-color imaging..... 121

**Table 6.4** Relative emission intensities for each protein of the spectrally compatible FRET pairs when imaged with each of the filter sets listed in **Table 6.3**.. ..... 128

**Table 7.1** Fluorescence properties of mAmetrine and cpmAmetrine-173..... 142

**Table 7.2** Cameleon constructs and their $Ca^{2+}$ response..... 145

# LIST OF FIGURES


**Figure 1.1** An example of directed evolution. ..... 6

**Figure 1.2** Jablonski diagram. ..... 9

**Figure 1.3** FRET efficiency (*E*) is highly dependent on the distance (*r*) between donor and acceptor. ..... 12

**Figure 1.4** A general schematic of a spectrofluorometer with 90° geometry. ..... 13

**Figure 1.5** (A) A simplified light pathway for an inverted wide-field microscope. (B) Schematic transmission profiles for an ideal pair of excitation filter, dichroic filter and emission filter. ..... 15

**Figure 1.6** Structures of some intrinsic and extrinsic fluorophores. ..... 16

**Figure 1.7** Labeling proteins with extrinsic fluorophores. (A). FITC reacts with the primary amine of the protein. (B). Nonfluorescent ReAsH-EDT reacts with the tetracysteine tag and turns to a highly fluorescent form. ..... 17

**Figure 1.8** avGFP structure and a proposed mechanism of chromophore formation. . 19

**Figure 1.9** The fluorescent protein color palette. ..... 21

**Figure 1.10** The chromophore structure of (A) wild-type avGFP in the ground state (major); (B) wild-type avGFP in the ground state (minor), or wild-type GFP in the excited state, or EGFP in the both states; (C) BFP; (D) CFP; and (E) YFP. ..... 22

**Figure 1.11** The chromophore structures of (A) cFP484; (B) ZsYellow; (C) DsRed; and (D) eqFP611. ..... 24

**Figure 1.12** An illustration of creating a circularly permutated variant of a FP. ..... 27

**Figure 1.13** The representative structure of Cameleon. ..... 29

**Figure 2.1** Absorbance and fluorescence emission spectra of a selection of FPs. (A) Fluorescence emission spectra of mCerulean, mTFP1, EGFP, Citrine, and mOrange. (B) Absorbance and fluorescence emission spectra of dTFP0.2 and mTFP1. ..... 34

**Figure 2.2** Protein sequence alignments of mTFP1, coral CFPs, and homologues. ..... 42

**Figure 2.3** Characterization of oligomeric structure and pH sensitivity of mTFP1. ..... 44

**Figure 2.4** Fluorescence photobleaching of mTFP1, mCerulean and mTFP0.7 under epi-fluorescence microscope. ..... 48

**Figure 2.5** Crystal packing of mTFP1 and amFP486. ..... 49
**Figure 2.6** Location of beneficial mutations in mTFP1. ..... 51
**Figure 2.7** mTFP1 as a FRET donor to a YFP or mOrange acceptor. ..... 53
**Figure 2.8** Localization of mTFP1 fusion proteins in live HeLa cells. ..... 54
**Figure 2.9** FRET imaging of mTFP1 with a YFP acceptor. ..... 55
**Figure 3.1** The chromophore structures of mTFP0.7 in (A) fluorescent state and (B) dark state. ..... 63
**Figure 3.2** (A) The absorbance of mTFP0.7 in the fluorescent state and dark state. (B) The fluorescence loss of mTFP0.7 under different light intensities and the respective recovery. (C) The dependence of the rates of fluorescence loss of mTFP0.7 on light intensities. (D) The Arrhenius plot of the fluorescence recovery of mTFP0.7. ..... 64
**Figure 4.1** Chromophore structures of mTFP1 and its hue-shifted variants. ..... 69
**Figure 4.2** The chromophore environment of mTFP1, amFP486, and avGFP-S65T.. 69
**Figure 4.3** Spectra of hue-shifted variants of mTFP1. ..... 75
**Figure 4.4** Two color imaging with Sapphire/EGFP ..... 82
**Figure 4.5** Fluorescence imaging of mTFP1 fusion constructs. ..... 84
**Figure 4.6** (A – D) Laser scanning confocal images of a single HeLa cell expressing mTFP1-H2B progressing through prophase, metaphase, anaphase, and interphase, respectively. (E - H) Spinning disk confocal images selected from a time-lapse series of HeLa cells expressing mTFP1-annexin during ionomycin-induced translocation to the plasma and nuclear membranes.. 85
**Figure 4.7** Live cell imaging of mWasabi fusion vectors. ..... 86
**Figure 5.1** Representative covalent structures of chromophores. ..... 91
**Figure 5.2** Spectral characterization of new BFP variants.. ..... 96
**Figure 5.3** Photobleaching curves for the new blue-fluorescing FPs. ..... 102
**Figure 5.4** New blue-fluorescing FPs expressed in live cells. ..... 103
**Figure 5.5** Live cell imaging of EBFP2 fusion vectors. ..... 103
**Figure 6.1** Sequence alignment of wild-type avGFP, EGFP, T-Sapphire, mAmetrine, and mKalama1. ..... 117
**Figure 6.2** Characterization of mAmetrine. ..... 118

**Figure 6.3** Corrected photobleaching curves for FPs. ..... 119
**Figure 6.4** Fluorescence emission spectra for a series of analogous FRET constructs in live cells. ..... 120
**Figure 6.5** Fluorescence excitation and emission spectra of (A) mAmetrine and tdTomato; (B) mTFP1 and mCitrine. ..... 121
**Figure 6.6** Four-color widefield imaging of an adherent HeLa cell expressing mAmetrine, mTFP1, EYFP, and tdTomato in targeted fusion constructs. ..... 122
**Figure 6.7** Caspase-3 biosensors based on dual FRET pairs. ..... 123
**Figure 6.8** Live cell imaging with dual FRET pairs (I). ..... 124
**Figure 6.9** Live cell imaging with dual FRET pairs (II). ..... 125
**Figure 6.10** Live cell imaging with dual FRET pairs (III). ..... 126
**Figure 6.11** Cytoplasmic ratios versus time for single staurosporine-treated HeLa cells expressing both a caspase-3 FRET biosensor and a control FRET construct that is not a substrate for caspase-3. ..... 127
**Figure 7.1** The schematic representaion of single FP-based $Ca^{2+}$ sensors. ..... 133
**Figure 7.2** The schematic representaion of FRET-based $Ca^{2+}$ sensors. ..... 134
**Figure 7.3** Modeled structures of (A) mAmetrine and (B) cpmAmetrine-173. ..... 142
**Figure 7.4** Primary structures of CaYangs and CaYins. ..... 144
**Figure 7.5** The $Ca^{2+}$ response of (A) CaYang1; (B) CaYin0.9; and (C) CaYin0.7. .. 144
**Figure 7.6** The $Ca^{2+}$ response of a cotransfected HeLa cell expressing ER-targeted CaYang1 and non-targeted CaYin0.9. ..... 148

# ABBREVIATIONS AND SYMBOLS

| | |
|---|---|
| $\varepsilon$ | Extinction coefficient |
| $\phi$ | Fluorescence quantum yield |
| $\lambda$ | Wavelength |
| $\lambda_{ab}$ | Absorbance wavelength |
| $\lambda_{em}$ | Fluorescence emission wavelength |
| $\lambda_{ex}$ | Fluorescence excitation wavelength |
| $\mu M$ | Micromolar ($10^{-6}$ mole per liter) |
| $\tau$ | Fluorescence lifetime |
| 3-D | 3-dimemsional |
| amFP486 | *Anemonia majano* cyan fluorescent protein |
| avGFP | *Aequorea victoria* green fluorescent protein |
| BFP | Blue fluorescent protein |
| CaM | Calmodulin |
| CFP | Cyan fluorescent protein |
| cFP484 | *Clavularia sp.* cyan fluorescent protein |
| ClavFP | *Clavularia sp.* cyan fluorescent protein |
| cpEGFP | Circularly permutated enhanced green fluorescent protein |
| cpFP | Circularly permutated fluorescent protein |
| cpGFP | Circularly permutated green fluorescent protein |
| cpmAmetrine | Circularly permutated mAmetrine protein |
| cpVenus | Circularly permutated Venus protein |
| cpYFP | Circularly permutated yellow fluorescent protein |
| DAPI | 4',6-diamidino-2-phenylinde |
| DMEM | Dulbecco's modified Eagle's medium |
| DNA | Deoxyribonucleic acid |
| dsFP583 | *Discosoma sp.* red fluorescent protein |
| DsRed | *Discosoma sp.* red fluorescent protein |
| EBFP | Enhanced blue fluorescent protein |
| ECFP | Enhanced cyan fluorescent protein |

| | |
|---|---|
| *E. Coli* | *Escherichia coli* |
| EDT | Ethane dithiol |
| EGFP | Enhanced green fluorescent protein |
| EP-PCR | Error-prone polymerase chain reaction |
| ER | Endoplasmic reticulum, cell compartment |
| ESPT | Excited state proton transfer |
| FACS | Fluorescence activated cell sorter/sorting |
| FITC | Fluorescein isothiocyanate |
| FlAsH | 4',5'-bis(1,3,2,-dithioarsolan-2-yl)-fluorescein |
| FMN | Flavin mononucleotide |
| FP | Fluorescent protein |
| FRET | Förster (or fluorescence) resonance energy transfer |
| GFP | Green fluorescent protein |
| HBSS | Hank's balanced salt solution |
| HeLa | Immortal cell line derived from Henrietta Lacks cervical cancer cells |
| LB | Luria-Bertani media |
| M | molar (mole per liter) |
| mECFP | Monomeric enhanced cyan fluorescent protein |
| Mit | Mitochondrion, cell compartment |
| mRFP | Monomeric red fluorescent protein |
| mTFP | Monomeric teal fluorescent protein |
| NADH | Nicotinamide adenine dinucleotide, reduced form |
| Ni-NTA | $Ni^{2+}$-nitrilotriacetate |
| NLS | Nuclear localization sequence |
| Nuc | Nucleus, cell compartment |
| OptiMEM | Modified Eagle's minimum essential medium, reduced serum |
| PA-GFP | Photoactivatable green fluorescent protein |
| PBS | Phosphate buffered saline |
| PCR | Polymerase chain reaction |
| $R_0$ | Förster radius |
| ReAsH | 4',5'-Bis(1,3,2-dithioarsolan-2-yl)-resorufin |

| | |
|---|---|
| RFP | Red fluorescent protein |
| rpm | Revolutions per minute |
| SDS-PAGE | Sodium dodecyl sulfate polyacrylamide gel electrophoresis |
| SHM | Somatic hypermutation |
| StEP | Staggered extension process |
| tdTomato | Tandem dimeric red fluorescent protein variant |
| TBS | Tris buffered saline |
| TFP | Teal fluorescent protein |
| UV | Ultraviolet light |
| Vis | Visible light |
| YC | Yellow Cameleon |
| YFP | Yellow fluorescent protein |

# CHAPTER 1:

# PROTEIN ENGINEERING AND ITS APPLICATION TO FLUORESCENT PROTEINS

## 1.1 INTRODUCTION

The remarkable progress in the development of fluorescence-related techniques (including fluorescence microscopy) in the past few decades has enabled great advances in biomedical research. This progress has taken the form of both instrument development and fluorophore development.

In respect to fluorophores, between synthetic dyes, fluorescent nanoparticles, and fluorescent proteins (FPs), there is a daunting arsenal of technologies currently available to researchers in the biological sciences [1, 2]. Consequently, when it comes to determining which is the most suitable technology to employ for a particular *in vitro* experiment, a researcher should consider the numerous pros and cons of each type of probes (e.g. with respect to the available colors, size, photostability, etc.) before deciding on the best course of action. However, when it comes to the study of protein dynamics and biochemical events in live cells there is a singular desirable feature that renders all other considerations essentially mute: only FP technology enables the facile and relatively non-invasive introduction of genetically encoded fluorescence [1, 2].

This thesis describes engineering of new FPs and FP-based biosensors that facilitate live cell imaging. In this first chapter, the topics of protein engineering, physics of fluorescence, and FP technology are reviewed.

## 1.2 PROTEIN ENGINEERING

Proteins are linear macromolecules generally made from just the 20 common amino acids. The side chains of the 20 amino acids provide the relatively limited selection of chemical functional groups found in proteins. Even with this limited selection of available functional groups, proteins have seemingly unlimited structural and functional diversity. The resolution of this paradox is, of course, well understood to result from the extremely large amount of diversity that results from simply combining the 20 common amino acids in different linear arrangements. For example, there are $20^{100}$ possible protein sequences for a 100-residue protein. Because of this enormous diversity, proteins are able to carry out the structural, mechanical and enzymatic functions associated with almost every process within cells [3].

Although there has been tremendous progress in developing a detailed understanding of protein structure and function, we have not yet developed robust methods for *de novo* design of proteins [4]. Although some very impressive progress has been made in this area in recent years [5, 6], researchers interested in protein engineering normally work with proteins that already exist in nature. Modifications of these proteins can sometimes be guided by computational design or chemical intuition, but the most powerful methods are those that mimic the process of natural evolution by natural selection.

The concept of "evolution by natural selection" was first introduced by Charles Darwin to describe the fact that individuals with a heritable trait that provides a reproductive advantage are more likely to produce offspring than individuals who lack the trait [7]. Natural selection is directionless, in the sense that it does not favour any particular 'type' of trait beyond the fact that the trait provides a reproductive advantage in the wild. In contrast, from the beginnings of human history, humans have been involved in 'unnatural' selection of animals and plants for traits that are agriculturally desirable. This process can be termed 'directed evolution'. For example, grains with bigger size were used as seeds for the next generation. It simply resulted in improved grain yields, although the science behind the selection was not known at that time.

While the discussion in the previous paragraph deals with the evolution of organisms, the same concepts can be applied to single proteins. A key development that enabled 'directed protein evolution' was the development of site-directed mutagenesis in the late 1970s [8]. Since then, the progress on organic synthesis of nucleotides, the molecular biology (e.g. the polymerase chain reaction) and protein x-ray crystallography, has brought laboratory evolution to be a routine technique. The ease of nucleotide synthesis and mutagenesis permits virtually unlimited genetic modification. The increasing available protein structures coupled with the computational methods also promise to extend our predictive capability from protein primary structures to protein 3-dimensional (3-D) structures and protein functions.

'Protein engineering', the phrase describing the laboratory evolution of proteins, was first introduced in 1984 when Wilkinson et al. evolved a new tyrosyl-transfer RNA synthetase with increased enzyme-substrate affinity [9]. Some recent applications of

protein engineering have provided many valuable tools for a variety of research applications. For example, antibodies have been evolved to catalyze organic reactions [10], and proteases have been engineered to be active in stringent conditions [11].

The general strategies of protein evolution are classified into two broad categories: rational design and directed evolution.

### 1.2.1 Structure-based rational design

Rational design relies on detailed knowledge of the proteins 3-D structure and site-directed mutagenesis. Usually, the investigators use available structures to determine the residues crucial for protein activities, e.g. the residues close to enzymatic active sites, or residues directly catalyzing reactions. Sometimes, but not always, the potential mutations are first evaluated computationally. Then the potential residues are targeted for mutagenesis. The mutants are then further characterized for targeted activities.

Site-directed mutagenesis is usually inexpensive and technically easy. However, the structures of a large portion of the proteins are unavailable, and even when it is available, the effects of mutations on protein function are not easily predictable [12]. The rationally-introduced mutations are often detrimental rather than beneficial even though there has been some successful examples [13]. Structure-based site-directed mutagenesis is more widely used to tackle biochemical problems (e.g. the mechanism of an enzymatic reaction). Its power for protein evolution is usually limited unless it is combined with directed protein evolution as described below.

### 1.2.2 Directed protein evolution

Directed evolution is a method mimicking the natural selection process [12]. A typical experiment usually includes several rounds of repeating steps of diversification and selection or screening [14]. In the diversification step, the gene of interest is altered randomly to create a library of gene variants. The gene library is then screened for the desired properties or selected by surviving ability. The mutants with optimal desired properties are identified and isolated for the next step. Then the DNA of the improved mutants could be amplified for gene sequencing or subjected into the next round of directed evolution. Usually the process is carried out for several rounds. The winners of

the previous round are diversified in the following round to create the library. In the whole process, the beneficial mutations are accumulative.

With respect to directed evolution, the term 'selection' is generally reserved for processes that are based on survival of the most 'fit' variants. The term 'screening' is generally reserved for processes that are based on certain property other than survival. On basis of this property, the experimenter must make a decision about which variant will be declared the 'winner' and serve as the template for the next generation. There is some ambiguity in these terms however, since a variant identified by screening will survive, while the undesirable variants will perish in the autoclave.

The success of directed evolution is critically dependent on the gene diversification step: the bigger the size of the created library is, the higher chance to find the one with desired property [12]. There are many different strategies developed for creating the genetic complexity of the library. The simplest method is random point mutagenesis, e.g. error prone polymerase chain reaction (EP-PCR) [15]. In this method, the gene of the template is usually amplified by polymerase chain reaction (PCR) under conditions favouring poor fidelity, such as using a high-error-rate polymerase, or using a high-error-rate buffering condition. The error rate of reaction can be generally adjusted. The upper limit of library size is constrained by the number of variants that can be screened in practice (discussed below). The lower limit of library size is constrained by the fact that beneficial mutations are rare and a large fraction of the library consists of non-functional or crippled variants. In the process of random mutagenesis, useful mutations are accumulated linearly in every step [12]. In contrast, shuffling the genes of several parental templates by molecular biology, a process known as DNA shuffling, is a combinatorial mutagenesis and has been testified to produce better diversity [16]. Akin to natural sexual recombination, DNA shuffling recombines the mutations from individual genes. The advantage increases exponentially with the numbers of parents that can be recombined.

One example combining random mutagenesis and DNA shuffling is shown as **Figure 1.1** [17]. In this case, the template is randomized by error-prone PCR and followed by screening the library. Two or more improved variants are then recombined by DNA shuffling. DNA shuffling involves the digestion of the DNA of improved

variants by DNase I into random fragments, and those fragments are reassembled into a full-length gene by primerless PCR. Two fragments with sequence homology prime on each other, and recombination occurs when fragments from one copy of a gene anneal to fragments from another copy, causing a crossover event. Then the full-length products are amplified with terminal primers. The generated library is screened and the improved mutant is identified, and carried into the next round.

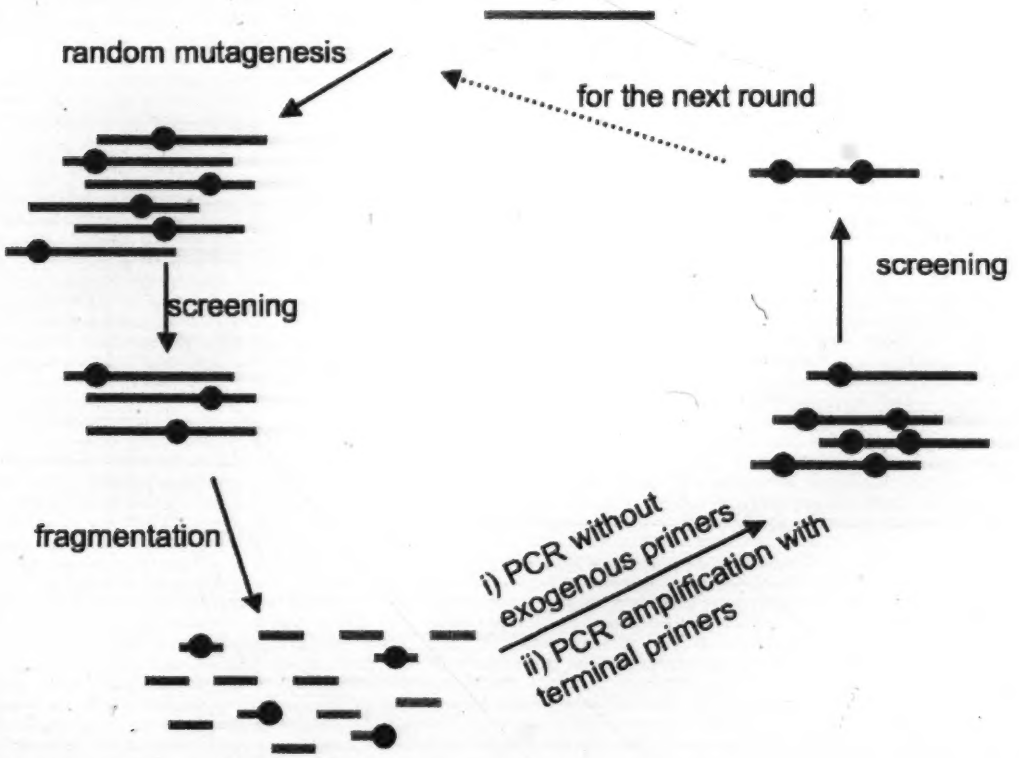


**Figure 1.1** An example of directed evolution. Random mutagenesis followed by screening and recombining improved variants, allows combination of useful mutations and elimination of deleterious mutations. (Redrawn and modified from [17])

Since the introduction of DNA shuffling by Stemmer in 1994 [18], many other combinatorial diversification strategies have been developed, such as the staggered extension process (StEP) method and the ITCHY/SCRATCHY method [13, 16]. In addition to these molecular biology based methods, other approaches such as chemical mutagenesis, UV irradiation and mutator strains could also be used for diversification

[19]. Recently the Tsien group reported an example of using iterative somatic hypermutation to evolve far-red FPs [20].

Another important factor for directed evolution is the ability to screen or select. Under current technology level, the size of mutant library is limited to $10^4$-$10^6$ and not all desired properties could be easily screened for [21]. For high throughput screening, the desired properties should be read out as a noticeable 'signal', such as survival, binding efficiency, or fluorescence. Those parameters are not only readable, but also can be used as a means to physically separate the desirable variants from the undesirable ones. For instance, the cells with different fluorescence spectra can be isolated by fluorescence activated cell sorter (FACS) [21].

The advantage of directed evolution techniques is that this approach doesn't require structural information to achieve the results [12]. The whole process mimics Darwinian evolution — random mutagenesis, recombination and selection (screening). Improved properties or even new properties could be obtained after extensive searching in the iterative evolution process [22].

### 1.2.3 Semi-rational engineering

Rational design and directed evolution techniques are not mutually exclusive. For example, the site-directed mutagenesis could be carried out between rounds of directed evolution. It has also been demonstrated recently that when combining information gained from structure analysis, the capability of directed evolution has been greatly expanded [12]. Saturated or semi-saturated site-directed mutagenesis of 'hot spots' identified by structure analysis could be applied as the diversification steps of directed evolution. What's more, overlap PCR strategy could be used to generate libraries simultaneously targeting several positions [23]. The generated libraries targeting at the 'hot spots' could be screened or selected and the whole process constitutes a round of directed evolution.

## 1.3 FLUORESCENCE AND FLUORESCENCE MICROSCOPY

In the past two decades, fluorescence techniques (including fluorescence microscopy) have undergone remarkable advances and are now fundamental to modern biological research. Because of the high sensitivity, fluorescence techniques are generally

preferred to expensive and difficult handling radioactive isotopes for most biochemical applications [24].

### 1.3.1 Fluorescence

Luminescence occurs when a substance emits light from an electronically excited state. The phenomenon can be further subdivided into two groups depending on the mechanism: fluorescence or phosphorescence. Although our ancestors noticed the phenomenon of luminescence in living organisms (bioluminescence) several thousands of years ago [25], the scientific description of luminescence didn't appear until the mid-19th century. Fluorescence of quinine, the first fluorophore, was reported by Sir John Herschel in 1845 [26]. This was followed by a description of Stokes Shift by Sir George Gabriel Stokes [27]. The theory of the fundamental fluorescence mechanism was proposed later by Professor Jablonski [28]. Today we still use the diagrams named after Professor Jablonski to illustrate the mechanisms of luminescence.

After a molecule is excited from the ground state to an electronically excited state (usually both are singlet states in which the electrons in the orbital are paired with opposite spins), there are several possible pathways to undergo in the following steps. Usually the molecule has been excited to a high vibration level of electronically excited state, and then it rapidly relaxes to the lowest vibration level of $S_1$ (**Figure 1.2**). This process occurs within $10^{-12}$ s or less and is called 'internal conversion'. Then high-energy electrons could relax to the ground state by non-radiative relaxation (e.g. solvent quenching) or by emitting photons that are referred to as fluorescence. Sometimes molecules in $S_1$ state could also undergo a spin conversion, a process called 'intersystem crossing', into a triplet state $T_1$. Photon emission from $T_1$ (if there is any) is termed phosphorescence. Phosphorescence is generally shifted to longer wavelength (lower energy) than fluorescence because $T_1$ is usually in lower energy than $S_1$. The lifetime of fluorescence is in the order of $10^{-8}$ s, which is much shorter than phosphorescence, because the direct transition from a triplet excited state to the singlet ground state is kinetically unfavored by the quantum-mechanical selection rules [24].

Because internal conversion is usually involved when the molecules are excited to high vibration levels of electronically excited states, the energy of fluorescence emission

light is lower than the energy of excitation light. So fluorescence emission is at longer wavelength compared to excitation. Sir George Gabriel Stokes first observed this phenomenon in 1852 and the wavelength shift between the excitation and emission was named after him as 'Stokes shift' [27].

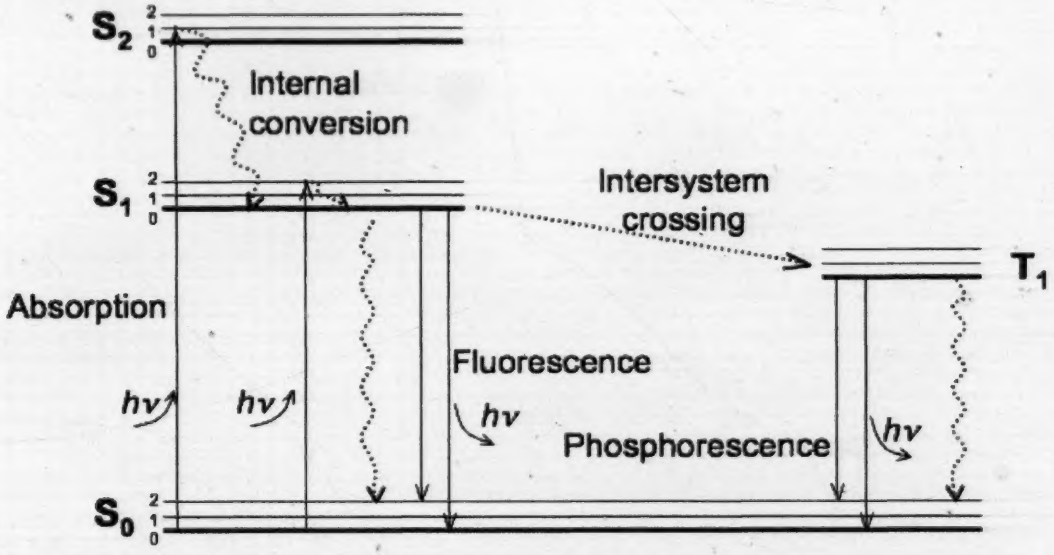


**Figure 1.2** Jablonski diagram. The solid arrows show the absorption or emission of photons. The dashed arrows show non-radiative process. (Redrawn and modified from [29])

Typically the fluorescent molecules, or referred to as fluorophores, are rigid aromatic molecules. The rigidity of molecules is important because the thermovibration and rotation of the molecule (or other non-radiative relaxations) are competing with the photon emitting process.

The intensity of the fluorescence is, of course, dependent on the concentration of the fluorophore. Two other parameters, termed extinction coefficient ($\varepsilon$) and quantum yield ($\phi$), are used to describe the intrinsic brightness of a fluorophore and are independent of concentration. Extinction coefficient, also referred to as molar absorptivity, is a measure of how strongly a chemical species absorbs light at a given wavelength. Fluorescence quantum yield is the ratio of the number of photons emitted to the number of photons absorbed. The intrinsic brightness of a fluorophore is often

defined as the product of extinction coefficient and quantum yield ($brightness = \varepsilon \times \phi$) [24].

### 1.3.2 Photobleaching

At the single molecule level, it is often observed that a single dye molecule enters a dark state after emitting a certain number of photons. For a bulk fluorophore solution, it is also noticeable that fluorescence fades during excitation. This process is referred to as 'photobleaching'. The ability of a dye to resist photobleaching is referred to as its 'photostability'. The photostability of a particular fluorophore constrains the available time period to observe fluorescence, so it is one of the most important features of a fluorophore [24].

When considering photobleaching in the most general sense, two different processes could be occurring: reversible photobleaching and irreversible photobleaching. In the first case, the fluorescent molecule is able to be switched on/off. Usually the reversible photobleaching involves reversible structural or chemical changes between fluorescent and dark states, although the detailed mechanism could be different case by case. The irreversible photobleaching usually is a dye photolysis process and involves the irreversible photochemical modification of the dye. Sometimes photobleaching is a mixture of both pathways: both reversible and irreversible photobleaching contribute to the fading of the dye [29].

The mechanism of irreversible photobleaching is very complex and usually dependent on the light intensity and molecular environment. It is generally understood that singlet oxygen ($^1O_2$) is probably involved: the dye in the triplet state ($T_1$) crossed from the singlet excited state ($S_1$) (**Figure 1.2**) interacts with oxygen according such that $T_1 + {}^3O_2 \rightarrow S_0 + {}^1O_2$. Singlet oxygen is highly reactive and damages dyes by free radical pathways. The generated products are complex and difficult to characterize [29].

### 1.3.3 Fluorescence resonance energy transfer

Another process that can occur when the fluorophore is in its excited state is fluorescence resonance energy transfer (FRET) to an acceptor dye. For FRET to occur, the acceptor fluorophore must be close in spatial proximity, and the absorption spectrum

of the acceptor must overlap with the emission spectrum of the donor fluorophore. Energy of the excited donor is passed to the acceptor, and promotes the acceptor to the excited state. This is a dipole-dipole coupling process and there is no intermediate photon irradiation in FRET. The acceptor emits if it is fluorescent, in a process often referred to as sensitized emission. However, the acceptor could also be a nonfluorescent chromophore in which case the donor is quenched but no sensitized emission occurs. This energy transfer mechanism is also termed as Förster resonance energy transfer, named after the German scientist Theodor Förster [30].

The extent of energy transfer is determined by several factors, such as the distance between the donor and acceptor, the extent of spectral overlap, and the dipole orientations of the two. Usually FRET efficiency is used to quantify the extent of energy transfer, which is defined as the fraction of energy transfer event occurring per donor excitation event. It could be calculated by measuring the fluorescence intensities of the donor with acceptor ($F_D'$) and without acceptor ($F_D$):

$$\text{FRET efficiency } E = 1 - F_D'/F_D.$$

The distance between the donor and acceptor when FRET efficiency is 50% is called the Förster radius ($R_0$). FRET efficiency depends on the donor/acceptor distance ($r$) with an inverse 6th power law (**Figure 1.3**):

$$E = 1/[1+(r/R_0)^6].$$

The Förster distance is dependent on the dipole orientations and spectral overlap integral ($J$):

$$R_0 = (8.8\times10^{23}\kappa^2 n^{-4}\phi_0 J)^{1/6}\text{ Å},$$

where $\kappa^2$ is the dipole orientation factor, $n$ is the refractive index of the medium, $\phi_0$ is the quantum yield of the donor in the absence of the acceptor. When donor and acceptor are freely rotating and randomly oriented to each other, $\kappa^2$=2/3. The spectral overlap integral is defined as

$$J = \int f_D(\lambda)\cdot\varepsilon_A(\lambda)\cdot\lambda^4\cdot d\lambda \text{ cm}^3\text{M}^{-1},$$

where $f_D$ is the normalized donor emission spectrum, $\varepsilon_A$ is the acceptor molar extinction coefficient in $\text{M}^{-1}\text{cm}^{-1}$, $\lambda$ is the wavelength in unit of cm. For most dyes, FRET occurs at distances less than 100 Å (with typical $R_0$ of 20 – 70 Å) [24].

Because FRET efficiency is highly dependent on the dye distance (**Figure 1.3**) and FRET occurs in the distance proximate to the size range of proteins, FRET is widely used as a spectroscopic ruler to measure the distance between fluorophores [24].

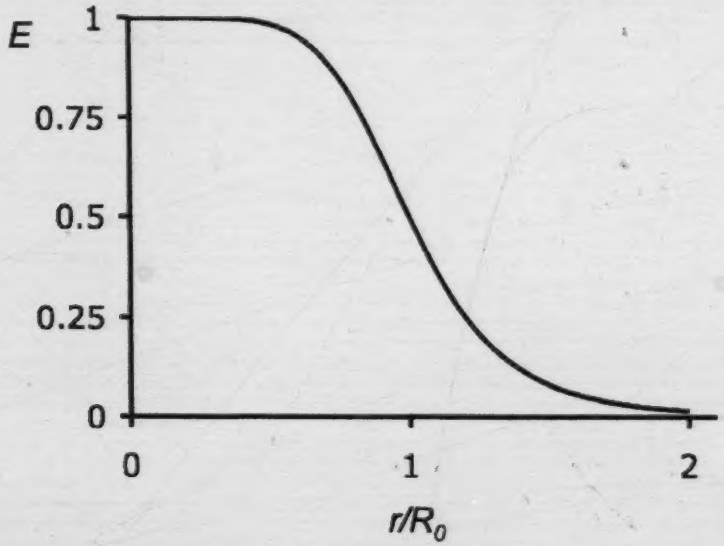


**Figure 1.3** FRET efficiency ($E$) is highly dependent on the distance ($r$) between donor and acceptor. The x-axis is the ratio of the distance between donor and acceptor to Förster radius. The y-axis is the FRET efficiency.

### 1.3.4 Fluorescence lifetime

Fluorescence lifetime is defined to describe the average time the fluorophore spends on a whole excitation and emission cycle. Because the time the molecule resides in the excited state $S_1$ is much longer than other steps (**Figure 1.2**), fluorescence lifetime is nearly equal to the lifetime of the excited state [24]. The fluorescence lifetime is highly sensitive to the environment. For example, the presence of quenchers would dramatically decrease the fluorescence lifetime. For this reason, fluorescence lifetime provides information that is unavailable from direct fluorescence intensity measurements. Akin to intensity, lifetime could work as an additional dimension of measurable information for spectroscopy and microscopy applications.

Another important application is to measure FRET efficiency by the lifetime method. The FRET efficiency can be defined by the fluorescence lifetime with acceptor ($\tau'$) and without the acceptor ($\tau$): $E = 1 - \tau'/\tau$. The measurement of FRET efficiency by

the lifetime method has several advantages. The primary advantage is that lifetime is independent of the intensity or concentration of the fluorophore. Therefore those factors complicating intensity approaches do not influence the lifetime approach. However, lifetime measurements present a more significant technical challenge, and the necessary instrumentation is usually less accessible.

### 1.3.5 Spectrofluorometer

Fluorescence intensities and the spectral profiles are recorded by instruments known as spectrofluorometers or fluorescence spectrometers. The first practical spectrofluorometer appeared in the 1950s [24]. **Figure 1.4** shows a simplified layout of a spectrofluorometer. The light from the light source of the instrument (e.g. a Xe lamp) passes an excitation monochromator that selects the excitation wavelength, and then enters the sample. The fluorescence emitting from the sample is directionless but only the light perpendicular to the excitation is recorded by placing an emission monochromator and detector aligned by 90° to the excitation light pathway. By scanning the excitation or emission monochromator, the fluorescence excitation or emission spectra are recorded, respectively.

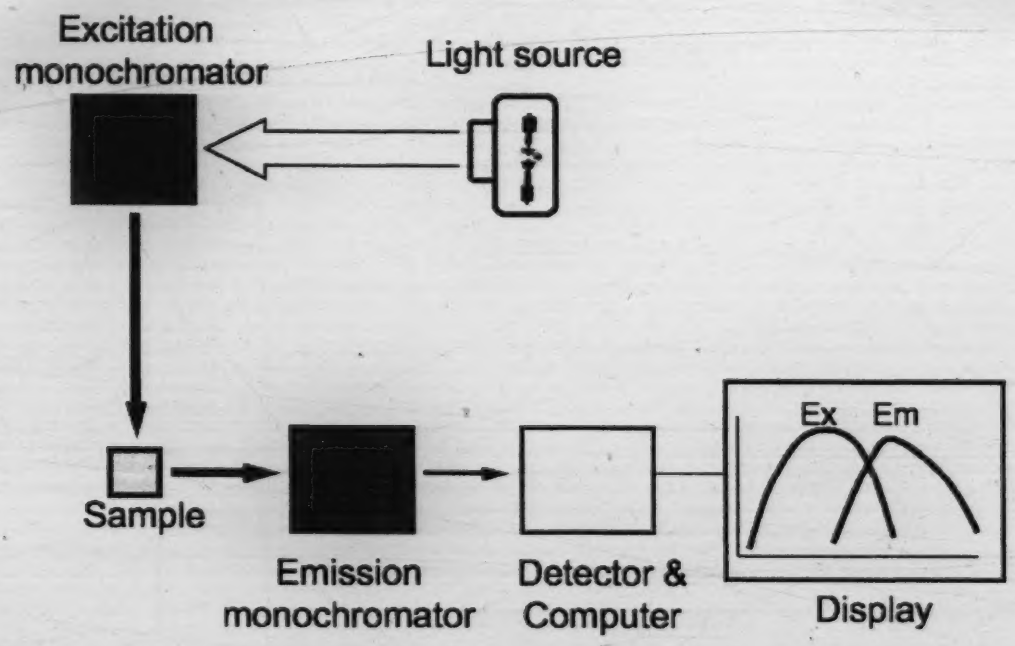


**Figure 1.4** A general schematic of a spectrofluorometer with 90° geometry.

For an ideal instrument, the excitation spectrum should represent the relative emission at each excited wavelength with equal excitation intensity. Similarly the emission spectrum should represent the photon emission rate at each wavelength. In reality, the intensities of light source over the wavelengths are not the same and the responses of the instrument are not identical over the wavelengths as well. So excitation and emission spectra should be corrected to present the real fluorophore fluorescence profiles.

Microplate readers equipped with monochromators are available for measuring fluorescence spectra in high throughput applications. The samples are contained in multi-well plates, and the plate readers record the fluorescence rapidly on numerous samples with somewhat reduced spectral resolution.

### 1.3.6 Fluorescence microscopy

Microscopy techniques have been a valuable tool in life sciences and other fields since around 1600 when the first compound microscope was probably invented by Zacharias Janssen [29]. Microscopy has been, of course, a routine technique for visualizing small objects, such as the living cells and cell compartments. By combining the use of fluorescence with light microscopy, researchers developed a way to acquire more information and produce images with higher contrast. The principle of fluorescence microscopy was shown by Köhler at the beginning of the 20th century, and it has started to become a powerful tool since ~1970. The first laser scanning confocal microscope was constructed in 1982 by Carl Zeiss, Inc [29]. More recently, technical developments including new instruments such as disk-scanning confocal system and the newly available fluorescent dyes including FPs have further advanced fluorescent microscopy to be a more accessible technique in biological research labs and clinical labs [29].

Epi-fluorescence microscopy also called wide-field fluorescence microscopy is the least expensive and most widely used fluorescence microscopic technique. **Figure 1.5A** shows a simplified light pathway for an inverted wide-field microscope. Typically the light from the light source (e.g. Hg lamp or Xe lamp) is first filtered by the excitation filter and then strikes the dichroic beamspliter. The beamspliter reflects the light passing through the excitation filter, so the reflected light reaches the sample after passing an

objective lens, and then excites the fluorophores in the sample. The fluorescence emitting from the sample is directionless and in lower energy than the excitation light due to the Stokes shift. It is designed that the fluorescence passing through the objective could pass the dichroic beamsplitter because it has a longer wavelength (**Figure 1.5B**). The emitted light with the longer wavelength reaches the eyepiece, detector or camera after passing another emission filter. Wide-field fluorescence microscope allows the acquisition of fluorescence images although a significant amount of light comes from out-of-focus planes. Combining it with deconvolution technology provides higher quality pictures, and allows 3-D reconstruction. Also taking advantage of pinholes, the laser scanning confocal microscopy produces images with less out-of-focus light. The out-of-focus light could be further reduced by multiphoton fluorescence microscopy. The details about those advanced technologies are beyond the scope of this chapter and are not discussed here.

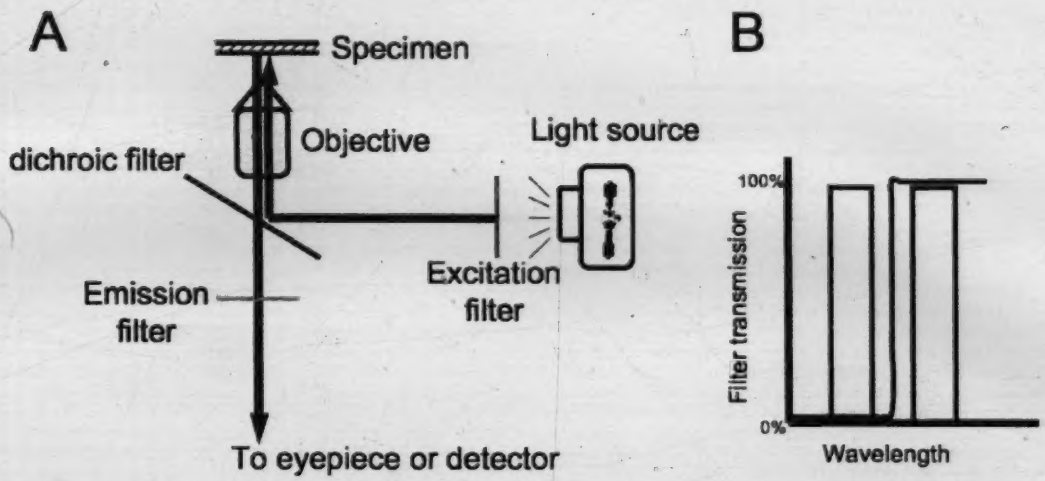


**Figure 1.5** (A) A simplified light pathway for an inverted wide-field microscope. (B) Schematic transmission profiles for an ideal pair of excitation filter (blue), dichroic filter (black) and emission filter (green).

The resolution of a focusing (far-field) light microscopy is limited by the phenomenon of light diffraction. The best resolution for conventional light microscopy is about 400 nm, a scale much bigger than the typical protein size. Recently, several groups proposed strategies to gain super resolution images with tens of nanometre resolution. Some of those techniques involve the use of photoactivatible or photoswitchable FPs [31, 32].

## 1.4 FLUOROPHORES

As described above, the development of improved instrumentation was critically important for advancing the role of fluorescent microscopy in bioimaging. On the 'other side of the coin', development of improved fluorophores has also been critical. As of today, sophisticated imaging equipment, in conjunction with different fluorophores, have demonstrated invaluable service in many thousands of bioimaging experiments.

The fluorophores can be categorized into two major groups: intrinsic natural fluorophores and extrinsic fluorophores. Intrinsic fluorophores include aromatic residues (e.g. tryptophan) of proteins, fluorescent cofactors such as reduced nicotinamide adenine dinucleotide (NADH) (**Figure 1.6**) and flavin mononucleotide (FMN), chlorophyll and other fluorescent molecules. Of course, some specific types of fluorescence experiments can only be done using intrinsic fluorophores. However, intrinsic fluorophores are not amenable to many types of bioimaging experiments. Researchers would also like to image the location and concentration of the vast majority of biomolecules that do not have a distinct fluorescent signal. It is for this reason that extrinsic fluorophores are required.

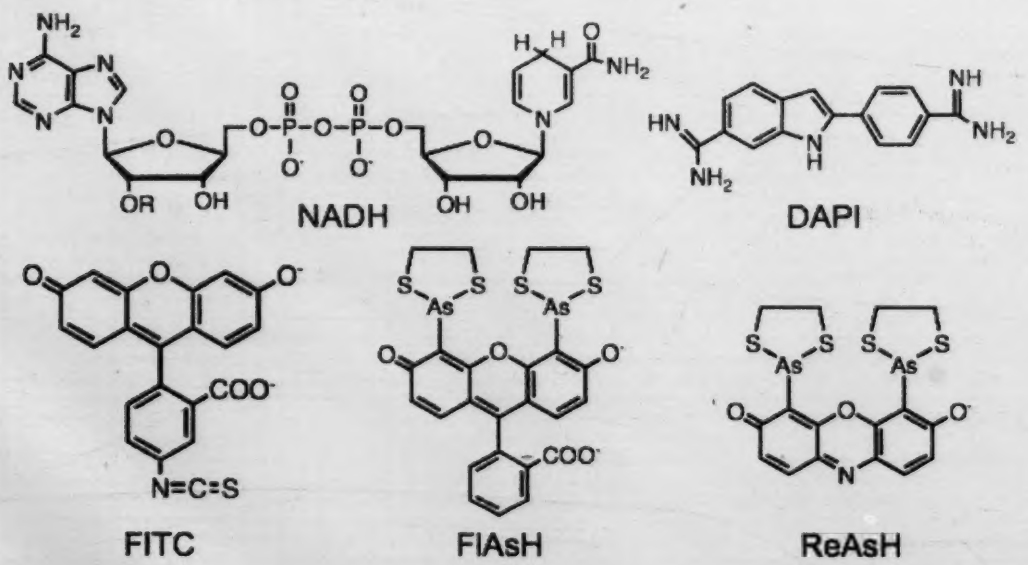


**Figure 1.6** Structures of some intrinsic and extrinsic fluorophores. Fluorophores are shown in color perspectives of their respective fluorescence. FlAsH and ReAsH are nonfluorescent in the form drawn above.

Many extrinsic fluorophores have been developed for a variety of applications. For example, 4',6-diamidino-2-phenylindole (DAPI) (**Figure 1.6**) is routinely used to stain DNA because it binds strongly into the minor groove of DNA. In more general situations, fluorescein, rhodamine, cyanine dyes and other organic dye molecules are routinely used. Those organic dye molecules have extended conjugation and usually rigid structures, so they have high quantum yields. In addition to organic dyes, semiconductor nanoparticles (also known as quantum dots) have found use in some bioimaging studies.

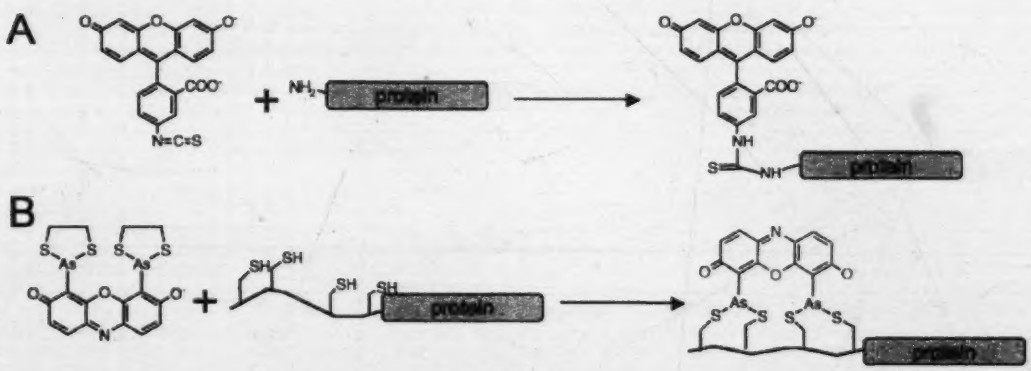


**Figure 1.7** Labeling proteins with extrinsic fluorophores. (A). FITC reacts with the primary amine of the protein. (B). Nonfluorescent ReAsH-EDT reacts with the tetracysteine tag and turns to a highly fluorescent form.

Synthetic organic dyes or quantum dots are required to be conjugated to target molecules, usually proteins in most applications. Many chemical strategies have been developed. For example, the fluorescein-derived molecule fluorescein isothiocyanate (FITC, **Figure 1.6**) reacts with an amine by forming a covalent bond (**Figure 1.7A**). This reaction has selectivity to primary amines over other functional groups. However, it has no selectivity regarding a specific protein because all solvent exposed primary amines are, more or less, equally reactive. In recent years, some labelling methods with improved molecular selectivity have been developed, for example, expressing the target protein with a tag that has high affinity to the fluorophore, or using an enzyme to catalyze the formation of covalent bonds with the fluorophore [33]. One of the most successful examples is the tetracysteine tag that reacts with 4',5'-bis(1,3,2,-dithioarsolan-2-yl)-fluorescein (FlAsH) and 4',5'-Bis(1,3,2-dithioarsolan-2-yl)-resorufin (ReAsH) (**Figure 1.6** and **Figure 1.7B**) [34, 35]. The dye molecules, FlAsH or ReAsH, are nonfluorescent

in the ethane dithiol (EDT) bound form. They react with the tetracysteine tag of expressed proteins, and turn into highly fluorescent forms. To date, many labelling methods have been developed, but almost all are laborious and technically challenging.

Synthetic organic dyes, quantum dots, and FPs (to be discussed in the next session), are three major groups of extrinsic fluorophores. They all have advantages and disadvantages. Organic dyes have more choices of colors, but are limited by the availability of labelling methods. Quantum dots have high photostability, but they are multivalent, potentially toxic and are much larger. The fluorescent protein technique is more widely accepted by the biologist community because of the ease of use, but also limited in some circumstances that will be discussed in the following text.

## 1.5 FLUORESCENT PROTEINS AND EVOLUTION

### 1.5.1 *Aequorea victoria* green fluorescent protein

In 1962 a Princeton University researcher by the name of Osamu Shimomura reported on the purification and characterization of the protein responsible for the bioluminescence of *Aequorea* jellyfish. Shimomura had painstakingly harvested many thousands of jellyfish, cut off their bioluminescent organs with scissors and squeezed the proteins from the tissue wrapped in a handkerchief: a procedure that produced a solution known aptly as 'squeezate'. From this squeezate Shimomura isolated the bioluminescent protein aequorin: a tremendous accomplishment in its own right. In a footnote within the manuscript describing this work, he mentions the presence of another curious protein in squeezate that was not bioluminescent but rather fluorescent [36]:

'*A protein giving solutions that look slightly greenish in sunlight though only yellowish under tungsten lights, and exhibiting a very bright, greenish fluorescence in the ultraviolet of a Mineralite, has also been isolated from squeezates.*'

Shimomura could not have anticipated that with this second protein, known as *Aequorea victoria* green FP (avGFP), would emerge in the mid 1990s as a powerful tool for life science research. Today avGFP is used in thousands of labs around the world as a non-obtrusive genetically encoded marker that enables an untold number of otherwise unimaginable applications [37]. Some of the more common applications include: tracking and imaging fusion proteins in live cells; fluorescence imaging in transgenic tissue and

animals; sensing of intracellular enzyme activities; and imaging of transplanted tumors in rodent models of cancer.

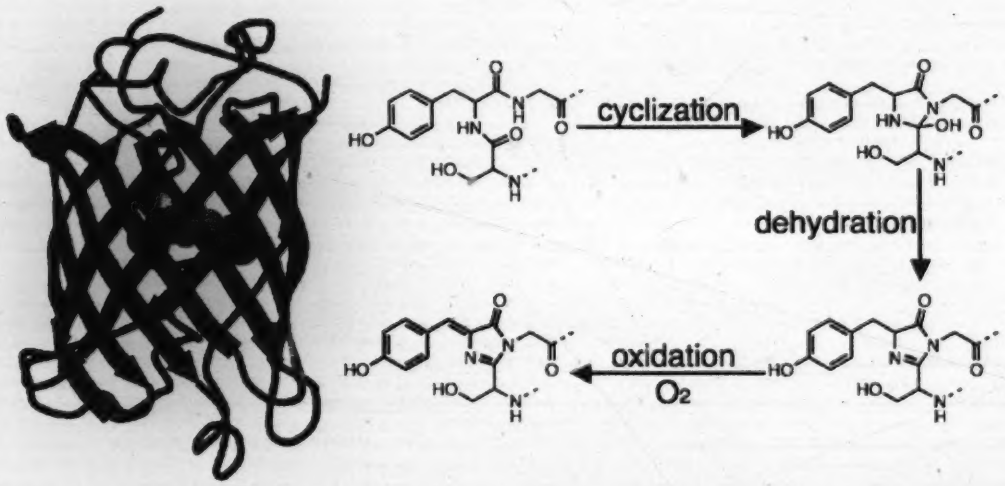


**Figure 1.8** avGFP structure and a proposed mechanism of chromophore formation. The left is the avGFP x-ray structure [38]. The yellow-shielded structure (in space filling representation) is the mature chromophore. The right shows a possible pathway of the chromophore formation from the Ser65-Tyr66-Gly67 peptide sequence.

Not only is avGFP one of the most utilitarian proteins known to science, it is also one of the most aesthetically pleasing. From the macroscopic perspective, solutions of avGFP have a pleasant greenish hue as was accurately described by Shimomura. However, it is at the molecular level that avGFP is most fetching (**Figure 1.8**). avGFP is composed of 238 amino acids arranged in an 11-stranded β-sheet that is wrapped into an attractive pseudosymmetric cylinder [38]. Given that this structure is somewhat squat, it is often referred to as a β-can. Located near the center of the can is the heart of avGFP: the visible wavelength fluorophore that makes this protein so unique. Unlike other proteins, such as hemoglobin, that are colored due to the presence of a bound non-protein chromophore, avGFP is self sufficient to generate its intrinsic chromophore from its own polypeptide sequence. That is, the protein requires no other jellyfish-specific proteins or factors for it to undergo the post-translational modifications (a process referred to as maturation) leading to formation of the mature chromophore. In the presence of molecular oxygen, expression of the avGFP gene in a variety of organisms, ranging from bacteria to plants to mammals, will result in the formation of green fluorescing cells

and/or tissues. It is this functional autonomy that makes avGFP so exceptionally useful as a tool in life science research.

For the wild type avGFP, the three sequential amino acids forming the chromophore are Ser65, Tyr66 and Gly67. One of the proposed mechanisms (**Figure 1.8**) [37] shows the first step is a cyclization process; the N of Gly67 attacks the carbonyl of Ser65 and a five-member ring is formed. Then one molecule of water is released to form a double bond. The last step is the oxidation by molecular oxygen forming the extended conjugation of mature chromophore. The residues of the β-barrel catalyze all steps. Only the three sequential amino acids alone are not sufficient to form a chromophore.

One might expect that there is relatively little scientific advance to be made by simply expressing avGFP in various cell types and thereby rendering them green fluorescent. Indeed, this is not exactly the type of application that has driven the explosive growth in the popularity of avGFP for life science research. The single most important and most common application of avGFP is in the study of fusion-protein localization, dynamics, and function in live cells. Investigators interested in the biological role of a certain protein can fuse the gene encoding that protein to the gene encoding avGFP. This fusion is done in such away the protein product will be expressed as a single polypeptide, creating a covalent link between the protein of interest and the avGFP. A plasmid containing the chimeric gene under control of a suitable promoter is then used to transfect mammalian cells. The transfected cells integrate the DNA into their own chromosomes and express the chimeric gene, as they would any other gene in their genome, to produce the protein of interest fused to the fluorescent label that is avGFP. In the ideal situation, the protein of interest dictates the localization and dynamics of the fusion protein and the avGFP tag is a non-perturbing bystander. Through the use of time-lapse fluorescence microscopy or one of a growing number of variations on this technique, one can create movies that reveal the intracellular spatiotemporal dynamics of the protein of interest. To confirm that the avGFP is not disrupting the normal localization of the protein of interest, researchers often stain the cells with labeled antibodies against the endogenous protein of interest and compare the results to that obtained with the avGFP tag. Needless to say, the major advantage of the avGFP based approach relative to traditional immunohistochemistry is that it enables researchers to

investigate protein dynamics in living cells and tissue and is not limited to static localization of proteins in dead and fixed tissue.

### 1.5.2 Unnatural colors and enhanced mutants of avGFP

By itself, avGFP was a wonderful gift from Nature to the scientific community. However, in several regards the wild-type protein is sub-optimal with respect to the quite 'unnatural' applications in which it is typically used. For example, the wild-type protein has evolved to fold and undergo the chromophore-forming reaction most efficiently in the cool temperatures of the ocean waters. When transplanted to tissue culture or a living organism it is often expected to perform these same tasks at a balmy 37 °C; a process which it could accomplish only inefficiently. Fortunately, avGFP is remarkably amenable to protein engineering by genetic modification and this process can be used for the discovery of variants with improved properties. Accordingly, one of the first and most significant improvements in the properties of avGFP was the engineering of variants that matured much more efficiently at 37 °C.

Another drawback of avGFP is that it was originally available in just the one fluorescent color that *Aequorea* had generously provided. However, this limitation was also soon overcome through the efforts of protein engineers, most notably Professor Roger Y. Tsien of the University of California San Diego, who was primarily responsible for the development of blue, cyan, enhanced green, and yellow versions of folding enhanced GFP [37]. This small palette of color variants, known as BFP, CFP, EGFP, and YFP, respectively (the 4 leftmost members in **Figure 1.9**) [39-41], greatly expanded the range of possible applications of the growing family of FP variants.

**Figure 1.9** The fluorescent protein color palette. Shown is a composite of several images with excitation ranging from 400-600 nm.

The wild-type avGFP exists with a mixture of neutral and ionized chromophores in the ground state (**Figure 1.10AB**). Regardless which form is excited, the chromophore fluoresces from an ionized form. Dual excitation peaks and fast photobleaching are the most unsatisfactory properties of avGFP. Enhanced green fluorescent protein (EGFP) was created by introducing a S65T mutation that stabilizes the ionized chromophore in both the ground state and excited state (**Figure 1.10B**) [40]. EGFP has a single excitation peak and improved photostability. Replacing the tyrosine forming the avGFP chromophore with a histidine or tryptophan created BFP and CFP (**Figure 1.10CD**). However, these histidine- and tryptophan-derived chromophores are of less extended conjugation and higher energy than the ionized tyrosine-derived chromophore. Therefore the spectra are blue shifted. The more red-shifted YFP was created by introducing a tyrosine mutation on the β-barrel (**Figure 1.10E**) [41]. This tyrosine stacks with the chromophore through the π-π interaction shifting the spectra to longer wavelength.

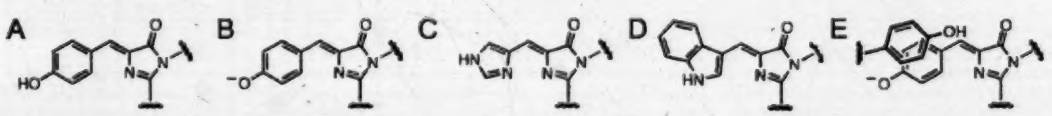


**Figure 1.10** The chromophore structure of (A) wild-type avGFP in the ground state (major); (B) wild-type avGFP in the ground state (minor), or wild-type GFP in the excited state, or EGFP in the both states; (C) BFP; (D) CFP; and E) YFP.

Besides the mutations mentioned above that contribute major spectral shifts, many other mutations were also simultaneously introduced to rescue the fluorescence or improve other properties of proteins (e.g. folding efficiency). For example, a S65G mutation is also necessary in YFP. The fluorescence of a FP is determined by both the chromophore structure and the environment (the β-barrel) imposed upon the chromophore by the surrounding residues.

The initial color-transited mutants have only a few mutations compared to wild type avGFP, so there was significant room to improve the initial variants by carrying out protein evolution process. Because the evolution history of the blue, cyan, and green variants will be extensively discussed in the following chapters, it is not reiterated here. The original YFP photobleaches very fast and is highly pH sensitive. It was partially improved by the development of Citrine [42] and Venus [43]. However, the

photostability is still its Achilles' heel, so an improved monomeric yellow FP with high brightness, photostability and pH resistance is still needed. Also the reports on cyan species of photobleached YFP raise more concerns of FRET measurements using a YFP photobleaching strategy [44, 45].

The availability of a selection of FP colors enabled simultaneous imaging of multiple different fusion proteins in live cells to identify protein pairs that did, or did not, colocalize to specific intracellular compartments. This selection of colors also enabled researchers to begin to ask whether two proteins were physically interacting (or at least within a distance of less than 10 nm of each other). Such questions cannot be answered by the observation of colocalization since the theoretical resolution limit of conventional optical imaging with visible light is limited to several hundred nanometers. To obtain information on the proximity of 2 proteins in live cells and with better than 10-nm resolution, investigators exploit the phenomenon of FRET. Although the physical basis of FRET requires a good deal of theory to explain properly, it manifests itself in quite simple and practical manner. If two fluorophores are close enough together in space, the higher energy fluorophore passes its excited state energy to the lower energy fluorophore that will then emit a photon at its characteristic fluorescence wavelength. In the case of avGFP variants, the CFP (higher energy donor) and YFP (lower energy acceptor) pair is widely used for FRET-based detection of protein-protein proximity's and interactions in live cells. By exciting CFP with blue light and imaging of the ratio of yellow to cyan fluorescence with band pass filters, FRET efficiency between proteins can be easily and quantitatively measured using widely available epifluorescence microscopy equipment.

### 1.5.3 *Anthozoa* FPs

A major breakthrough in the field of FPs occurred with the discovery of FPs in non-bioluminescent *Anthozoa* coral species [46]. In late 1999 it was reported, by Professor Sergey A. Lukyanov of the Russian Academy of Science, that coral is a source of homologues of avGFP with hues ranging from cyan all the way to red [46]. To date, a wide spectrum of FPs has been cloned from non-jellyfish organisms. However, they usually suffer from some degree of the obligatory quaternary structures: several subunits resembling the avGFP form the quaternary structures.

Clearly the coral had figured out how to create more colors than the protein engineers were able to do! Coral FPs have a variety of chromophore structures. Green variants usually have the ionized tyrosine-derived chromophores that are the same as EGFP. Also coral could blue shift this chromophore spectrally to cyan through more subtle mechanisms than completely changing the structure of the chromophore as in *Aequorea*-derived CFP (e.g. electrostatic interactions in cFP484, **Figure 1.11A**, that is further investigated and discussed in **Chapter 2** and **Chapter 4**).

The FP family derived from avGFP only includes variants spectrally encompassing blue to yellow. Despite the best efforts of protein engineers, variants with only a modest red-shift (i.e. YFP) had been engineered from avGFP. The search for further red-emitting FP has long been the goal for live-cell and whole animal imaging, primarily due to the requirement for probes in this spectral region in multicolor imaging experiments as well as the fact that longer excitation wavelengths generate less phototoxicity and can probe deeper into biological tissues.

ZsYellow (originally referred to as zFP538) is a yellow FP that was discovered in the *Anthozoa* button polyp *Zoanthus* during a search in reef corals for naturally occurring GFP analogs emitting fluorescence in longer wavelength regions [46-48]. This protein is ~10 nm red-shifted compared to *Aequorea* YFP. The fluorescence emission spectrum of ZsYellow is peaked at 538 nm. Further investigation showed that it has a unique chromophore structure (**Figure 1.11B**). A lysine residue is involved in the formation of a non-aromatic 6-member ring. The resulted chromophore has more extended conjugation compared to the chromophore of EGFP. ZsYellow is a tetramer.

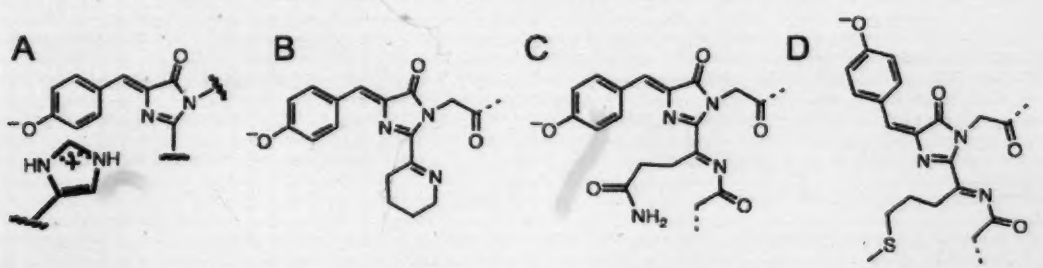


**Figure 1.11** The chromophore structures of (A) cFP484; (B) ZsYellow; (C) DsRed; and (D) eqFP611.

A red fluorescent protein (RFP) from *Discosoma* coral, *Discosoma* RFP (or DsRed) was also discovered [46]. The DsRed fluorophore is similar in structure to that found in native green fluorescent protein, but is modified through the oxidation of a second backbone bond to extend the conjugated system (**Figure 1.11C**). DsRed is also an obligate tetramer [49].

As was originally done with the *Aequorea* GFP, coral FPs have now been subjected to extensive engineering for brighter fluorescence and shifted hues. DsRed has been a particularly fruitful source of improved variants. The tetrameric structure of DsRed is a detriment and there are many examples in which fusion to a tetrameric RFP drastically perturbs the localization of the protein of interest. Fortunately this obstacle was eventually overcome by the use of extensive protein engineering to convert the tetrameric *Discosoma* RFP to a monomeric RFP known as mRFP1. The construction of truly monomeric variants, as well as monomers from the proteins in other *Anthozoa* species, has proven to be a difficult task [23]. A total of 33 amino acid alterations to the DsRed sequence were required for the creation of the first-generation monomeric red FP (termed mRFP1) [23]. However, this derivative exhibits significantly reduced fluorescence emission compared to the native protein and photobleaches very quickly, rendering it much less optimized than analogous green and yellow FPs. Further directed evolution of mRFP1 with selection for brighter and wavelength-shifted variants eventually produced the mFruit series of monomeric yellow, orange, red and far-red FPs (the 7 rightmost samples in **Figure 1.9**), named in honor of common fruits that bear colors similar to their respective fluorescence emission spectral profiles [50]. Typically, the chromophore-forming residues, Q66 and Y67 (homologues positions 65 and 66 in avGFP), were targeted for mutagenesis, and color-transited or enhanced variants were searched for. Further evolution was carried out to improve the properties of each color. Differently the two far-red mutants, mRaspberry and mPlum were produced through a method combining iterative somatic hypermutation (SHM) and FACS [20]. Certain variants of resulted 'mFruit' FPs feature increased extinction coefficients, quantum yields, or photostability, although no single variant has already been optimized by all criteria.

Besides DsRed, there have been many other red and far-red FPs cloned so far. As an example, eqFP611, was isolated from the sea anemone *Entacmaea quadricolor*. Site-

directed mutagenesis efforts have yielded dimeric variants of eqFP611 [51]. The unique chromophore of eqFP611 (**Figure 1.11D**), adopts a coplanar but trans conformation within the interior of the β-barrel. It is a significantly different conformation in comparison to the chromophore conformation observed in GFP and DsRed. Another far-red FP with the longest emission wavelength to my knowledge, termed AQ143, has also been derived from mutagenesis efforts on a chromoprotein isolated from the anemone *Actinia equine* [52]. The excitation and emission maxima of AQ143 are 595 nm and 655 nm, respectively, and its brightness is comparable to mPlum [20]. The photostability of this protein has not been reported and it forms an obligate tetramer.

Recently the Russian scientists, Chudakov and his co-workers, also monomerized and evolved new red and far-red FPs from eqFP578, a dimeric FP cloned from the sea anemone *Entacmaea quadricolor*. The corresponding monomers are named as TagRFP and mKate respectively [53, 54]. Both two proteins have higher intrinsic fluorescence brightness because of enhanced quantum yields. However, the improvement observed when expressed in live cells is modest in comparison to corresponding 'mFruits' variants, probably because of poorer folding efficiency.

Plasmid DNA containing the genes for each of the mFruit variants is now commercially available from Clontech Laboratories, Inc. of Mountain View, California. A variety of other commercial vendors are now offering engineered coral FPs of a wide variety of colors including, but not limited to: Evrogen of Moscow, Russia; MBL International of Woburn, Massachusetts; and Allele Biotechnology of San Diego, California. Most of the original *Aequorea*-derived colors are now available from Invitrogen of Carlsbad, California, though many of more recently reported and further improved versions are typically distributed by the lab in which they were developed or by a non-profit plasmid repository such as Addgene Inc. of Cambridge, Massachusetts.

### 1.5.4 Circularly permutated FPs

Circular permutation is a method to manipulate the primary sequence of a protein, and provides alternative N- and C- termini, so it offers new possible ways to create fusion proteins. Generally speaking, the original N- and C- termini of the protein are fused together by a linker, and new N- and C- termini are created somewhere else within the

protein. Usually the function of the original protein is required to be retained, and the success of circular permutation is controlled by and could be predicted from some empirical rules: first, the original N- and C- termini should be close and the linker should be floppy, so the disturbance to the original protein is minimized and its folding is not completely affected; second, the original protein should be robust enough and the new N- and C- termini should be in a place tolerant to the disturbance; third, additional protein evolution could be applied to rescue the function of the circularly permutated variants.

FPs have rigid β-barrel structures. In 1999 twenty circularly permutated variants of GFP were created and tested for fluorescence and thermostability by S. Topell et. al. [63]. Several positions tolerant for circular permutation were identified. Similar work has been done for EGFP and YFP to create fluorescent circular permutation of the original sequences (abbreviated as cpEGFP and cpYFP) [64, 65].

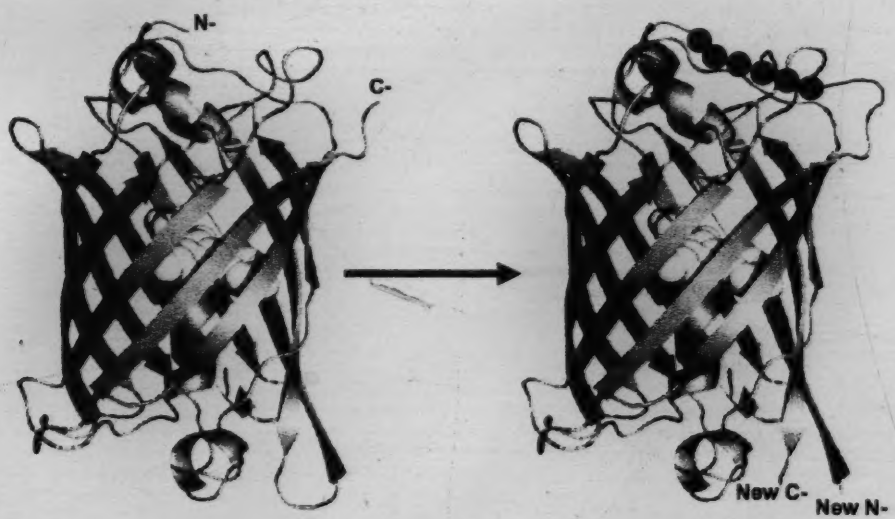


**Figure 1.12** An illustration of creating a circularly permutated variant of a FP. The original N- and C- termini are jointed by a floppy linker (the gray dots), and the new N- and C- termini are created somewhere else with the protein.

The circularly permutated variants of FPs (cpFPs) (**Figure 1.12**) provide several advantages than the original proteins in certain cases. First, the new termini of cpFPs could be closer to the chromophore therefore the change of the fusion protein could be transferred to the fluorescent protein more sensitively. This is a mechanism to use FPs to report the 'signals' transferred from the fusion proteins. For example, cpGFP and cpYFP

variants were fused with calcium binding domains to create calcium sensors, G-CaMP [66] and PeriCams [65]. Second, FRET is a dipole-dipole coupling interaction, so cpFPs provide additional dipole moment when fused with other FPs in FRET experiments. There have been many examples that cpYFP and its enhanced variant cpVenus provide enhanced dynamic ranges in FRET-based calcium sensors Cameleons (to be discussed in **Section 1.5.6** and **Chapter 7**) [67].

### 1.5.5 Standard applications of FPs

The simplest application of FPs is to express the FP gene itself in live cells in order to 'mark' the transfected cells. This type of experiment is useful when doing cotransfection experiments or cell sorting type applications. The single FP gene can also be placed under the control of a gene promoter of interest. When the promoter is turned 'on', more FP is present in the cell and thus the activity of the promoter can be monitored. A greater variety of biological experiments are possible using FPs that are fused with a protein of interest. Accordingly, the localization or dynamics of that protein could be imaged and analyzed. In a single experiment, FPs with different hues could be used. However, fluorescence hues of FPs are confined to a relatively narrow region of the electromagnetic spectrum (essentially the visible wavelengths) due to protein-imposed restrictions on the possible manipulations of the chromophore structure and environment. This limitation is exacerbated by the relatively broad excitation and emission peaks of FPs, which further restricts the number of colors that can be distinguished with bandpass filters on a widefield microscope. With currently available FPs, imaging of up to four distinct colors (e.g. blue and green or cyan and yellow, orange, and far-red) is technically possible on a filter based system [68]. Imaging of six distinct colors has been achieved using a single laser line for excitation and spectral unmixing of the emission [69].

### 1.5.6 FRET applications of FPs

FRET is the transfer of excitation energy from a higher energy (more blue-shifted) donor fluorophore to a lower energy (more red-shifted) acceptor chromophore. Because the process happens in range of nanometres and is highly dependent on distance, a FRET pair of fluorophores can act as a nanoscale ruler that enables their interchromophore distance to be accurately determined in either a spectroscopic or imaging modality. So

FRET is routinely used to detect protein-protein interactions in live cells. FRET does not require the acceptor to be fluorescent, but if it is, sensitized emission from the acceptor will occur. The ratio of acceptor to donor fluorescence is typically used as a surrogate for FRET efficiency in live cell imaging. The BFP-EGFP couple was the first pair of engineered FPs that had the appropriate overlap of donor fluorescence and acceptor absorbance to allow their use as a FRET pair [37]. This pair was soon superseded by the still popular CFP-YFP couple, which has been used in vast majority of FRET-based probes to date.

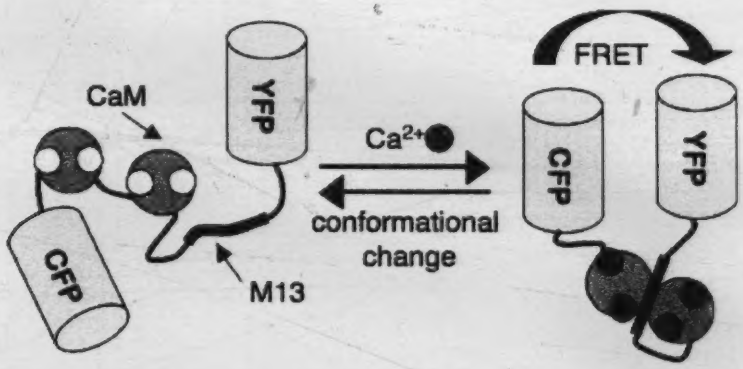


**Figure 1.13** The representative structure of Cameleon. Calmodulin and M13 were inserted between a FRET donor (CFP) and acceptor (YFP). The calcium concentration changes trigger the FRET efficiency changes between the FRET pair.

The engineering of various colors of monomeric FPs have been but one of many recent highlights in the fast moving field of FP research. For example, major effort within the FP field has been invested in the engineering of biosensors that change their fluorescence intensity, or fluorescence color, in response to an external stimulus. One approach to the development of such biosensors is to exploit FRET, by sandwiching a 'sensing' domain (that is, a region of protein that undergoes a conformational change when bound to a particular target molecule or when post-translationally modified by an enzyme) between donor and acceptor FPs. Some notable examples of such biosensors include ones that detect $Ca^{2+}$ [70], kinase activity [71], and histone methylation [72]. The $Ca^{2+}$ sensor Cameleons were created by inserting the $Ca^{2+}$-binding protein calmodulin (CaM) and a CaM-binding peptide M13, between the fluorescent protein donor and acceptor (e.g. CFP and YFP) (**Figure 1.13**). When the CaM binds calcium, it also binds

the M13 peptide. This conformation change changes the distance and dipole orientations of CFP and YFP. Therefore the FRET efficiency changes reflect the calcium concentration changes [70].

## 1.6 THE SCOPE OF THE THESIS

Despite the popularity and versatility of FP technology, there are still many areas in which FPs are lacking and in need of improvement. Much work has already gone into the development of various colors of FPs. A few members in the 'toolbox' are of special importance, but considerably less optimal than others. The goal of the work here was to develop improved variants for those less optimal members, and provide new FP tools for some novel applications.

**Chapter 2** describes the development of a new monomeric teal fluorescent protein (mTFP1) for fluorescence imaging. While ECFP has stood the test off time in multicolor labeling applications and as the preferred FRET donor to YFP, its spectral properties limit its utility in some applications: ECFP is relatively dim, and has broad excitation and emission peaks. These problems have prompted me to engineer a new monomeric CFP with improved spectroscopic properties. As the starting template in the directed evolution process, *Clavularia* FP484 (a.k.a. cFP484 or ClavCFP) has been monomerized and optimized to create mTFP1 which is a favourable alternative to existing CFP. This work has been published as a full paper in *Biochemical Journal* [73].

**Chapter 3** describes the characterization of a photoswitchable FP, mTFP0.7. In the directed evolution process of mTFP1, it was noticed that some variants underwent fast and reversible photoswitching. One mutant, designated as mTFP0.7, was subjected to further characterization. Further more, the x-ray crystal structures of both isomers were solved in collaboration with Prof. S.J. Remington. Some important structural features of mTFP0.7 are also discussed in this chapter. The data in this chapter have been disclosed in papers published in *Proceedings of the National Academy of Sciences of the U.S.A.* and *Proceedings of SPIE* [61, 74].

**Chapter 4** describes the factors determining the color of mTFP1 and the live cell imaging application of itself and its color-transited variants. The mTFP1 chromophore has the same extension of conjugation as EGFP. However the fluorescence of mTFP1 is

blue shifted. The mechanism of the blue shifting was investigated. Also mWasabi, a green version of mTFP1 was further evolved and evaluated for live cell imaging. This work has been published as a full paper in *BMC Biology* [75].

**Chapter 5** describes the development of improved blue FPs by exploring different chromophore structures. EBFP, the GFP variant the tyrosine of whose chromophore is replaced by histidine, is relatively dim and photobleaches exceptionally fast. EBFP can be used as a FRET donor for EGFP but those drawbacks limit its usage. In order to find better BFP alternatives, several chromophore structures have been explored and different variants have been created and compared. This work has been published as a full paper in *Biochemistry* [76].

**Chapter 6** describes the development of compatible FRET pairs that can be imaged in the same cell. In the process of searching BFPs, I was fortunate to discover a violet-excitable yellow-fluorescing variant. This protein was further improved and named as mAmetrine. I have shown that the combination of mAmetrine, mTFP1, and two other FPs from the FP 'toolbox' provides two compatible FRET pairs that can be imaged in the same cell. These new FRET pairs have been used to monitor caspase activation in apoptotic cells. The manuscript describing this work has been published in *Nature Methods* [77].

**Chapter 7** describes the ongoing and unpublished work to further extend the usage of the dual FRET pairs. To achieve this, different calcium sensors have been created and compared in order to provide tools enabling simultaneous calcium imaging in two cell compartments.

In **Chapter 8** is provided a summary of all work and an outlook for future developments in this field.

# CHAPTER 2:

# DIRECTED EVOLUTION OF A MONOMERIC, BRIGHT, AND PHOTOSTABLE VERSION OF CLAVULARIA CYAN FLUORESCENT PROTEIN

The research described in this chapter, together with other x-ray crystallography data by J. Nathan Henderson and S. James Remington at the University of Oregon has been published in *Biochemical Journal* [73].

## 2.1 INTRODUCTION

FPs, including mutants of avGFP [37] and its numerous homologues from *Anthozoa* corals [46, 78], have enabled fluorescence imaging of recombinant fusion proteins to become a popular and widely accessible technique in cell biology research [79, 80]. The defining feature of FPs is their remarkable ability to autonomously generate a visible wavelength fluorophore within the confines of their distinctive β-barrel structures [38, 81]. Chromophore formation in wild-type avGFP is a stepwise process that converts a sequence of 3 amino acids (Ser65, Tyr66, and Gly67) into a unique conjugated system that extends from the side chain of Tyr66 to a 5-membered heterocycle formed from main chain atoms [82]. The steric, electrostatic, and hydrogen-bonding environment imposed upon the chromophore by the surrounding residues strongly influences the fluorescence properties. This dependence has allowed researchers to engineer avGFP variants with altered colors, brightness, and photostability [37]. For example, in wild-type avGFP the ground-state chromophore exists as an equilibrating mixture of the neutral phenol with maximal absorbance at 395 nm and the anionic phenolate with maximal absorbance at 475 nm [83]. Efforts to engineer variants with the ground-state equilibrium shifted towards either the anionic or protonated form of the chromophore have been highly successful and have resulted in popular green fluorescent variants (emission peak at ~510 nm) such as EGFP [84] and Sapphire [39], respectively. Another particularly useful class of variants that have resulted from protein engineering efforts are the avGFP-derived YFPs that are defined by the Thr203Tyr mutation, an anionic phenolate tyrosine-derived chromophore, and an emission peak that is ~20 nm red-shifted from that of EGFP [38].

An approach that has proven successful for the engineering of blue-shifted avGFP variants has been to alter the covalent structure of the chromophore through substitution of other aromatic amino acids for Tyr66. For example, replacing Tyr66 of avGFP with a tryptophan gives an indole-containing chromophore with an emission peak in the cyan region (~480 nm) of the visible spectrum [39]. Although the original Tyr66Trp mutant of

avGFP was only weakly fluorescent, efforts to improve the brightness yielded the widely used variant ECFP [41, 70] and more recently Cerulean [85] and CyPet [86]. Although ECFP has stood the test of time as a useful fluorophore for multicolor labeling and as the preferred FRET donor to a YFP acceptor, its spectral properties are suboptimal [68, 85]. Some limitations have been partially addressed in the newer variants. For example, Cerulean is 2-fold brighter than ECFP but it has decreased photostability under arc lamp illumination [68, 85]. CyPet exhibits high FRET to the YFP variant YPet [86] but wasn't optimized for expression at 37 °C [68]. Considered as a family, ECFP and its descendents are limited by fluorescence brightness that is less than 50% of the popular YFP variant Citrine [68]. In addition, variants with tryptophan-derived chromophores have a very broad fluorescence emission with a full width at half maximum (FWHM) of approximately 60 nm (**Figure 2.1A**). Other popular fluorescent proteins with tyrosine-derived chromophores (e.g. EGFP and Citrine) have single-peaked and narrower emission spectra with FWHM of approximately 31 nm.

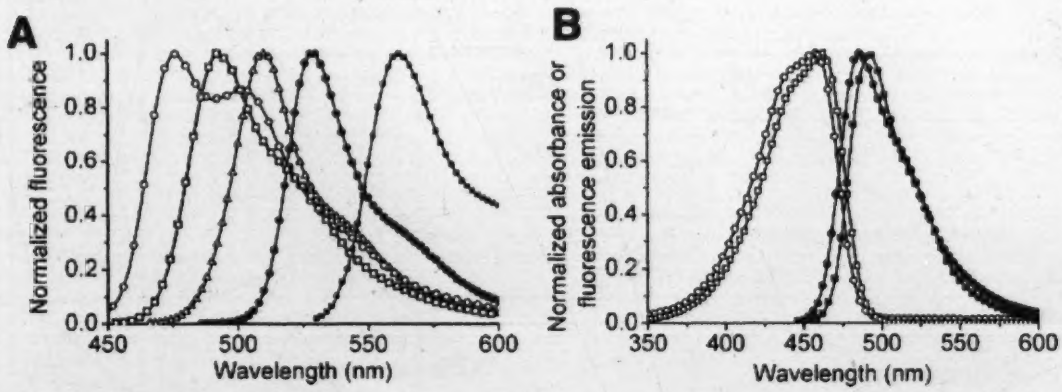


**Figure 2.1** Absorbance and fluorescence emission spectra of a selection of FPs. (A) Fluorescence emission spectra of mCerulean (○) [85, 87], mTFP1 (□), EGFP (△), Citrine (●) [42], and mOrange (■) [50]. (B) Absorbance (open symbols) and fluorescence emission (filled symbols) spectra of dTFP0.2 (○, ●) and mTFP1 (□, ■).

The limitations of the existing CFPs with tryptophan-derived chromophores could be due to intrinsic properties of the chromophore structure. Furthermore, it was reasoned that a new fluorescent protein with a tyrosine-derived chromophore and a fluorescence emission in the cyan region could serve as a superior alternative to the existing CFPs. A number of candidate FPs that fit these general criteria have been cloned from organisms

of the phylum Cnidaria in recent years. These proteins include: amFP486 from *Anemonia majano* [46]; dsFP483 and the very similar DstC1 from *Discosoma striata* [46, 88]; cFP484 from *Clavularia sp.* [46]; mcCFP and the very similar mc5 from *Montastrea cavernosa* [89, 90]; PdaC1 from *Pocillopora damicornis* [88]; anm1GFP1 from an unidentified Anthomedusae [91]; and MiCy from *Acropora* sp. [92]. An engineered variant of tetrameric amFP486 known as AmCyan1 (Clontech), and wild-type MiCy (MBL International), are commercially available. The naturally occurring CFPs have emission maxima ranging from 477-495 nm, quantum yields ranging from 0.24-0.90, and extinction coefficients ranging from 24,000-75,000 $M^{-1}cm^{-1}$. Despite these promising attributes, the natural CFPs are limited by the fact that they all have quaternary structure ranging from tight dimers in the case of anm1GFP1 and MiCy to obligate trimers or tetramers for all other *Anthozoa* CFPs reported to date.

While oligomerization of an FP is not particularly relevant to its use as a reporter of gene expression, it can often perturb the proper localization fusion proteins, particularly when the protein-of-interest is an oligomer itself [23, 93-95]. The most effective approach for overcoming the problem of FP oligomerization is to use a combination of rational protein engineering and directed evolution to create useful non-oligomerizing variants. Such an approach has been applied to a growing number of FPs including: a red FP from *Discosoma sp.* [23]; a GFP from *Galaxeidae* [96]; an orange FP from the *Fungia concinna* [92]; green-to-red photoconvertable FPs from both *Lobophyllia hemprichii* [97] and *Dendronephthya sp.* [98]; a photoactivatable GFP from *Pectiniidae* [60]; and a chromoprotein from *Montipora sp.* to create a red FP with a large Stokes shift [69]. For avGFP and its variants, a single point mutation, Ala206Lys, is sufficient to abolish the weak dimerization [99]. The application of a monomeric version of MiCy had appeared in the literature [69] but no details on the engineering or properties of this protein had yet been published.

In this chapter the engineering, optimization, and structural characterization of a monomeric variant of cFP484 from *Clavularia sp.* [46] is described. The directed evolution of the new FP was guided by selection for blue-shift, photostability, and fluorescent brightness. Accordingly, the resulting FP has brightness and photostability that equals or exceeds that of the currently preferred FP variants [68]. It is demonstrated

that this new FP is an effective and practical FRET donor to both the YFP variant Citrine [42] and the *Discosoma* RFP-derived mOrange [50].

## 2.2 EXPERIMENTAL

### 2.2.1 General methods and materials

A synthetic gene library of *Clavularia* FP484 variants was commissioned from the DNA Technologies Unit at the NRC Plant Biotechnology Group (Saskatoon, SK). The full-length gene library was constructed by PCR-based assembly of overlapping PAGE-purified oligonucleotides that had been synthesized on a Beckman 1000M solid phase DNA synthesizer. All synthetic DNA oligonucleotides for cloning and construction of subsequent libraries were purchased from Sigma-Genosys Canada or Integrated DNA Technologies. Unless otherwise indicated, Pfu polymerase (Fermentas) was used for all PCR amplifications in the buffer supplied by the manufacturer. PCR products and products of restriction digest were routinely purified using the QIAquick PCR purification kit (Qiagen) according to the manufacturers protocols. Restriction enzymes were purchased from either Invitrogen or New England Biolabs. The cDNA sequences for all TFP variants and fusion constructs was confirmed by dye terminator cycle sequencing using the DYEnamic ET kit (Amersham Biosciences). Sequencing reactions were analyzed at the University of Alberta Molecular Biology Service Unit. The proteins mECFP and mCerulean have the Ala206Lys mutation in addition to their characteristic substitutions [87, 99].

### 2.2.2 Library construction, mutagenesis, and genes encoding fusion proteins

The initial synthetic gene library was digested with Xho1 and EcoR1 and ligated into similarly digested pBAD/His B vector (Invitrogen). Subsequent libraries with saturation mutagenesis at a particular residue were constructed by either overlap-extension PCR method [23] or the Quikchange protocol (Stratagene). Randomly mutated libraries were constructed by EP-PCR as previously described [23] using Taq polymerase (New England Biolabs) under conditions optimal for 3 mutations per 1,000 bp [100]. Full-length gene libraries resulting from overlap-extension PCR or EP-PCR were digested with Xho1 and EcoR1 and ligated into similarly digested pBAD/His B.

Regardless of library assembly method, electrocompetent *Escherichia coli* (*E. coli*) strain DH10B (Invitrogen) was transformed and plated on Luria-Bertani (LB)/agar plates supplemented with ampicillin (0.1 mg/ml) and L-arabinose (0.02%). Plates were incubated for 14 h at 37 °C prior to screening.

To construct expression vectors for Cameleon variants, the gene encoding yellow Cameleon3.3 (YC3.3) was first inserted into the Xho1 and EcoR1 sites of the pBAD/His B bacterial expression vector [42]. The cDNAs encoding mECFP, mCerulean, and mTFP1 were each PCR amplified with primers that added a 5' Xho1 and a 3' Sph1 site. To maintain identical linker lengths, the 3' Sph1 site was appended immediately after the codon encoding Ala227 of mECFP and mCerulean or after the codon encoding the structurally aligned Arg220 of mTFP1. The purified PCR products were digested and ligated into the similarly digested plasmid containing the YC3.3 gene. Cameleons expressed in *E. coli* were expressed and purified as described below (**Section 2.2.4**). To create the mTFP1-YC3.3 mammalian cell expression vector, the full-length gene in pBAD/His B was PCR amplified with a 5' primer that appended a HindIII restriction site, a Kozak sequence (gccaccgccATGc, where ATG is the start codon), and the endoplasmic reticulum (ER) targeting sequence of calreticulin (MLLSVPLLLGLLGLAAAD). The 3' primer appended the ER retention signal (KDEL) followed by an EcoR1 restriction site. The PCR product was digested with HindIII/EcoR1 and ligated with appropriately digested pcDNA3 (Invitrogen).

The mOrange-mTFP1 fusion gene was created by overlap extension PCR. The gene encoding mOrange was amplified with a 5' primer that appended an Xho1 site and a 3' primer that appended the sequence for an 8 amino acid linker after residue 225. In a separate PCR reaction, the gene encoding mTFP1 was amplified with a 5' primer that added the linker sequence and a 3' primer that appended an EcoR1 site. The two purified PCR products were mixed and reamplified with the 5' primer from the mOrange reaction and the 3' primer from the mTFP1 reaction. The resulting full-length PCR product was digested with Xho1/EcoR1 and ligated into similarly digested pBAD/His B vector.

To create the mTFP1-β-actin mammalian expression plasmid, the gene encoding mTFP1 was PCR amplified with a 5' primer encoding an Nhe1 site and a 3' primer encoding an Xho1 site. The purified and digested PCR product was ligated into the

pEGFP-actin vector (Clontech) that had been previously digested with the same restriction enzymes to excise the EGFP coding sequence. To create the mTFP1-α-tubulin expression vector, an identical procedure was used to replace the EGFP gene in pEGFP-tub (Clontech) with the gene encoding mTFP1.

### 2.2.3 Library Screening

The system for imaging the fluorescence of bacterial colonies grown on 10 cm Petri dish is a custom built device that has been described in detail elsewhere [101]. Briefly, the light from a 175W xenon arc lamp (Sutter) is passed through a 436/20 nm bandpass filter (Chroma) and into a bifurcated fiber optic bundle (Newport). Light exiting the fiber optic bundle illuminates a 10 cm diameter area with an irradiance of approximately 0.04 $mW/cm^2$. For all screening up to the identification of mTFP0.6, colony fluorescence on illuminated plates was viewed through a pair of custom goggles fitted with 3mm thick GG455 glass (Chroma). When viewed through these goggles, colonies fluorescing at 480-490 nm have a distinctly 'bluish' hue and are distinguishable from 'greenish' colonies emitting at 500-510 nm. For the identification of mTFP0.7, colony fluorescence was digitally imaged with a Retiga 1300i 12-bit CCD camera (QImaging) fitted with a filter wheel (Sutter) that contains both a 480/40 nm and a 530/30 nm bandpass filter. Through the use of custom macros for Image Pro Plus (Media Cybernetics), images in both emission channels were acquired and the fluorescence intensities of all colonies were individually integrated. Colonies with high 480/530 nm intensity ratios and high brightness at 480 nm were selected for further characterization.

For the identification of mTFP0.8, mTFP0.9, and mTFP1, the screening protocol was modified in order to select for photostability. Six Royal Blue (peak emission at 455 nm) Luxeon V light emitting diodes (LEDs) (Lumileds Lighting) with narrow beam lenses (Fraen) were equipped and positioned to evenly illuminate (55 $mW/cm^2$) the 10 cm dish in the imaging system described above. Through the use of a custom serial port connection, the LEDs could be switched on and off at computer controlled intervals. An Image Pro Plus macro (Media Cybernetics) was used to automate acquisition and processing. For each plate, fluorescence images were acquired following a series of

programmed intervals of intense illumination. Using this system, I could readily identify colonies with decreased propensity to photobleach.

For all screening protocols, colonies with more intense fluorescence, high 480/530 nm intensity ratio, or decreased propensity to photobleach were picked and cultured overnight in 4 ml LB media containing ampicillin (0.1 mg/ml) and L-arabinose (0.2%). In the following day 0.1 ml of each culture was dispensed into a 96-well black clear bottom plate (Corning) and the full emission spectra of each variant were measured with a Safire2 plate reader (Tecan). Variants with the most blue-shifted and intense emission peak were used as templates in the subsequent round of library construction.

### 2.2.4 Protein purification and characterization

To prepare proteins in sufficient quantity for characterization, *E. coli* strains DH10B or LMG194 were transformed with the pBAD/His B expression vector containing the gene of interest. A single colony was used to inoculate a 4 ml culture that was allowed to grow overnight (37 °C, 225 rpm) before being diluted into 1 L of LB media containing ampicillin (0.1 mg/ml) and L-arabinose (0.2%). The culture was allowed to grow for 12 h before cells were harvested by centrifugation and lysed by French Press. Proteins were purified by Ni-NTA chromatography (Amersham). All Cameleons and mOrange-mTFP1 fusion constructs were further purified by gel filtration chromatography using a HiLoad 16/60 Superdex 75 pg column (GE Healthcare). Proteins were dialyzed into 50 mM Tris HCl, pH 7.5.

The oligomeric states of mTFP variants were determined by gel filtration chromatography on a HiLoad 16/60 Superdex 75 pg gel filtration column. Samples of the dimeric dTomato and the monomeric mCherry proteins [50] were expressed and purified as described above and used as size standards. The AKTAbasic liquid chromatography system (GE Healthcare) can monitor multiple wavelengths simultaneously. Purified TFP variants were mixed with either dTomato or mCherry and the resulting elution profiles were monitored at both 450 nm and 550 nm.

### 2.2.5 Spectroscopy

Absorption spectra were recorded on a DU-800 UV-visible spectrophotometer (Beckman). Quantum yields for TFP variants were measured using fluorescein in 10 mM

NaOH as the reference standard [102]. Extinction coefficients were measured by the alkali denaturation method [50, 103]. All emission spectra were acquired on a QuantaMaster spectrofluorometer (Photon Technology International) and have been corrected for the instrument response. The photostability of mTFP1 under xenon arc lamp illumination was determined using the method of Shaner et al. [68].

To determine the pH-dependence of the fluorescence emission of mECFP, mCerulean, and mTFP1, each protein (stock solution of 1 mg/ml in 5 mM Tris pH 7) was diluted 1:100 in a 96-well plate black clear bottom plate (Corning) containing 0.1 ml buffer (100 mM) at pH values ranging from 2 to 9. Full emission spectra at each pH were acquired with a Safire2 plate reader (Tecan). The relative fluorescence at each pH was measured at the peak wavelength.

FRET efficiencies for Cameleons and mOrange-mTFP1 fusion constructs were determined by measuring the emission spectra before and after trypsinolysis (50 μg/ml trypsin) under conditions where the linker sequence is cleaved and the fluorescent proteins remain intact. FRET efficiencies ($E$) for mECFP and mCerulean donors were calculated using the formula $E$ = 1 - (fluorescence at 475 nm before trypsinolysis / fluorescence at 475 nm after trypsinolysis). For mTFP1 donor with either a Citrine or mOrange acceptor, the fluorescence before and after trypsinolysis was measured at 490 nm.

### 2.2.6 Protein expression and imaging in HeLa cells

All DNA for mammalian cell transfection was purified by Plasmid Midi kit (Qiagen). HeLa cells were cultured in DMEM (Invitrogen) supplemented with 10% FBS (Sigma) at 37 °C. Cells in 35 mm imaging dishes were transfected with 4 μg plasmid DNA mixed with 10 μg polyethylenimine (linear, molecular weight ~25,000, Polysciences Inc.) in 0.5 ml OptiMEM (Invitrogen) and serum was added after 3 h. Approximately 14 to 24 h later the medium was exchanged for Hanks' Balanced Salt Solution (HBSS) containing no calcium chloride, magnesium chloride, magnesium sulfate, or phenol red (Invitrogen) and the cells were imaged. HeLa cells expressing mTFP1-β-actin or mTFP1-α-tubulin were imaged using a LSM510 confocal microscope (Zeiss) equipped with a 5 mW 458 nm excitation laser. HeLa cells expressing mTFP1-

YC3.3 were imaged with a Zeiss Axiovert 200M epi-fluorescence inverted microscope equipped with a xenon arc lamp and a monochrome Retiga 2000R 12-bit cooled CCD camera (QImaging). The external excitation filter wheel, excitation shutter, and emission filter wheel are controlled through a Lambda 10-3 controller (Sutter). Only dichroic mirrors are housed in the motorized reflector turret. The QED InVivo software package (Media Cybernetics) is used for automated computer control of all microscope hardware and for quantitative image analysis.

## 2.3 RESULTS AND DISCUSSION

### 2.3.1 Design of a synthetic gene library encoding dimeric variants of cFP484

At the time this project was initiated, the only reported homologues of avGFP with tyrosine-derived chromophores and emission peaks between ~480-490 nm were cFP484, amFP486, and dsFP483 [46]. These CFPs each have emission peak shapes and fluorescence brightness comparable to avGFP but are tetramers and therefore unsuitable for use as non-perturbing genetic fusion partners. A sequence alignment of these 3 proteins (**Figure 2.2**) revealed that of the 227 structurally aligned residues, there are 78 residues that are conserved in all 3 proteins and an additional 91 residues that are conserved in 2 of the 3. Considering only those positions of two-thirds conservation, cFP484 was determined as the variant with unique residues at 19%, dsFP483 at 34%, and amFP486 at 47% of the positions. Thus, of these 3 proteins, cFP484 is the least divergent from a hypothetical 'consensus' sequence. In addition, of these 3 wild-type proteins, cFP484 has been reported to have the highest fluorescence brightness and the fewest cysteine residues [46]. In consideration of these factors the cFP484 amino acid sequence was chosen as the starting point for the directed evolution process.

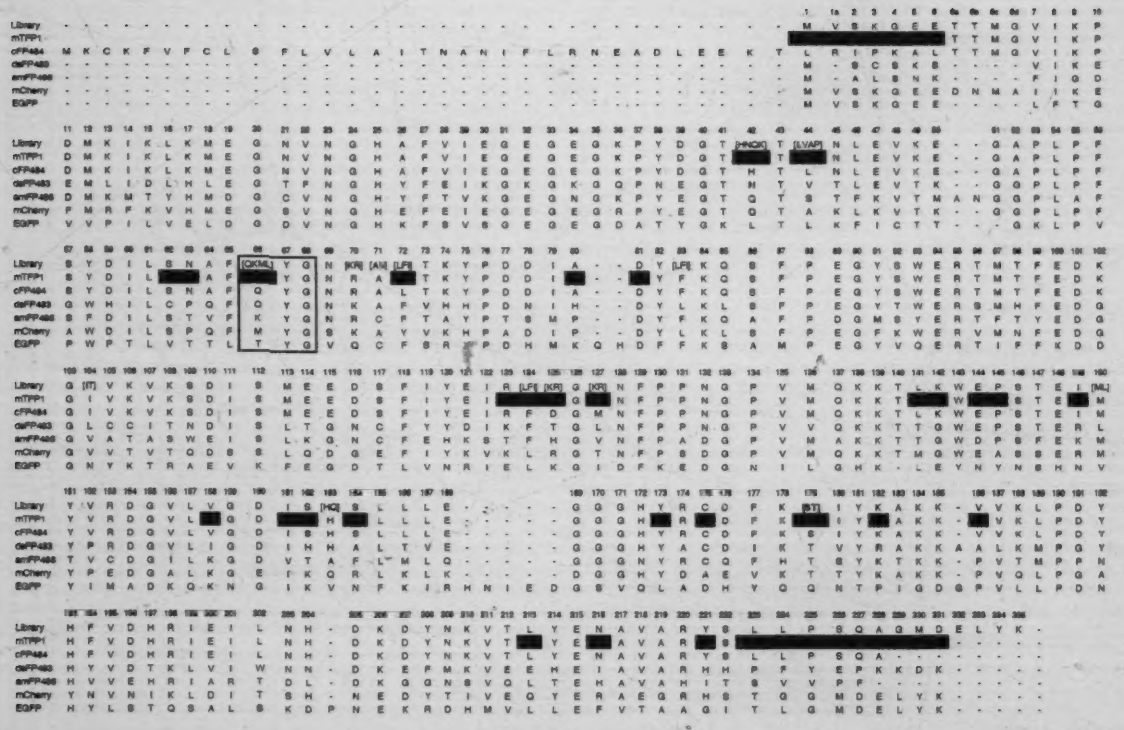

**Figure 2.2** Protein sequence alignments of mTFP1, coral CFPs, and homologues. The aligned sequences are the designed synthetic gene library, mTFP1, cFP484 from *Clavularia sp.* (Genbank accession AAF03374), dsFP483 from *Discosoma striata* (Genbank accession AAF03370), amFP486 from *Anemonia majano* (Genbank accession Q9U6Y6), mCherry derived from *Discosoma striata* dsFP583 (Genbank accession AAV52164), and EGFP derived from *Aequorea* GFP (from Clontech vector pEGFP) [46, 50]. Residues shaded cyan are changes or point mutations that are present in mTFP1. Residues 66, 67, and 68 (enclosed in black box) are the precursors of the chromophore. The rationale behind the design of the gene library is summarized in **Table 2.1**. Numbering is consistent with DsRed and its monomeric variants that have no internal insertions or deletions relative to cFP484.

**Table 2.1** Rationale for design of the synthetic dimeric gene library of cFP484.

| Residue number | Mutation | Codon[a] | Rationale |
|---|---|---|---|
| His42 | His, Asn, Gln, Lys | MAS | Mutations beneficial to tetrameric DsRed variants [104]. Not conserved in coral CFPs. |
| Leu44 | Leu, Val, Ala, Pro | SYC | Mutations beneficial to tetrameric DsRed variants [104]. Not conserved in coral CFPs. |
| Gln66 (residue of chromophore) | Gln, Lys, Met, Leu | MWG | Mutations beneficial to *Aequorea* GFP [40] and monomeric RFPs [50]. Lys or Gln present in coral CFPs. |
| Arg70 | Lys, Arg | ARG | Mutations beneficial to monomeric RFPs [23]. Lys or Arg present in coral CFPs. |
| Ala71 | Ala,Val | GYC | Mutations beneficial to monomeric RFPs [23]. Ala or Cys present in coral CFPs. |
| Leu72 | Leu, Phe, Ile | HTC | Phe in 2 coral CFPs and Leu in 1 coral CFP. |
| Phe83 | Leu, Phe, Ile | HTC | Mutations beneficial to monomeric RFPs [23, 50]. Phe in 2 coral CFPs and Leu in 1 coral CFP. |
| Ile104 | Ile,Thr | AYC | May disrupt A-B interface interactions |
| Phe124 | Leu, Phe, Ile | HTC | Mutations beneficial to dimeric RFPs [23]. Strict conservation in coral CFPs. |
| Asp125 | Lys,Arg | ARG | Likely to disrupt A-B interface interactions. |
| Met127 | Lys, Arg | ARG | Likely to disrupt A-B interface interactions. |
| Met150 | Met, Leu | MTG | Mutations beneficial to monomeric RFPs [23]. Met in 2 coral CFPs and Leu in 1 coral CFP. |
| His163 | His, Gln | CAS | Mutations beneficial to dimeric and monomeric RFPs [23, 50]. His in 2 coral CFPs and Ala in 1 coral CFP. |
| Ser179 | Ser, Thr | WCC | Mutations beneficial to dimeric RFPs [23]. Thr in 2 coral CFPs and Ser in 1 coral CFP. |

[a]Single letter codes for bases are as follows: A = adenosine, C = cytidine, G = guanosine, T = thymidine, H = A or C or T, M = A or C, R = A or G, S = C or G, W = A or T, and Y = C or T.

At that time, no crystal structure of cFP484 or one of its cyan homologues was available. Therefore the DsRed crystal structure was used to model the cFP484. The gene library with a theoretical diversity of ~$5 \cdot 10^5$ cFP484 variants (**Figure 2.2** and **Table 2.1**) was rationally designed and synthesized. Important features of the library included: mammalian codon usage; deletion of 40 non-homologous residues from the N-terminus; addition of the 7 N-terminal and 7 C-terminal residues of avGFP; semi-degenerate codons encoding potential 'tetramer-breaking' mutations at 3 external positions; and semi-degenerate codons encoding potential 'rescuing' mutations at 11 internal positions. Sequencing of random clones revealed that 12% of the genes had mutations only at desired positions and thus the true library diversity, including unintentional errors introduced during synthesis, was ~$4 \cdot 10^6$ variants.

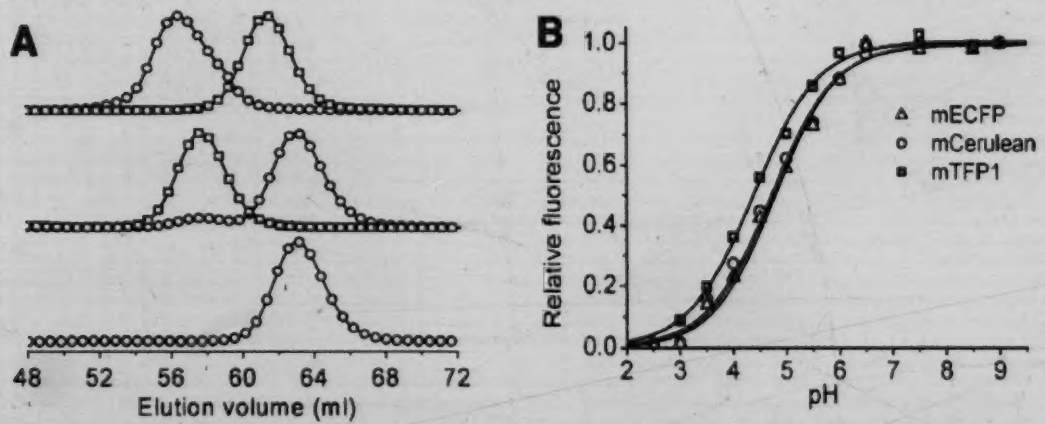


**Figure 2.3** Characterization of oligomeric structure and pH sensitivity of mTFP1. (A) Gel filtration chromatography elution profile of dTFP0.2 and mTFP1. Detection is at either 450 nm (○) or 550 nm (□). The upper profile is a coinjection of dTFP0.2 and monomeric mCherry [50], the middle profile is dimeric dTomato [50] and mTFP1, and the lower profile is mTFP1 alone. Earlier generations of mTFP had elution times identical to mTFP1 (data not shown). The small 450 nm peak at the dimer elution volume in the middle profile is due to the weak absorbance of dTomato at this wavelength. (B) pH-Dependence of the fluorescence emission of mCerulean (○), mTFP1 (□), and mECFP (△).

### 2.3.2 Directed evolution of a monomeric teal fluorescent protein

The synthetic gene library was used to transform *E. coli* and colonies were screened for fluorescence. Fluorescent colonies represented ~0.5% of all colonies and were approximately equally divided between colonies that fluoresced at ~490 nm (cyan) and colonies that fluoresced at ~510 nm (green). The cyan/green dichotomy in the initial library was attributed to the designed Arg/Lys degeneracy at position 70. Of all sequenced variants, the Arg70Lys mutation was consistently found in those that fluoresced green but never in those that fluoresced cyan. As will be discussed below, Arg70 is involved in interactions that have since been proposed to be critical for blue-shifting the fluorescence [105]. The most brightly cyan fluorescent protein identified after extensive screening of the initial library was a dimer with 8 mutations relative to wild type and an emission peak at 486 nm. It was named 'teal fluorescent protein' (TFP), with a preceding 'd' for dimeric or 'm' for monomeric, and a succeeding numerical identifier, to identify new variants described herein. Following this convention, the dimeric protein identified in the initial screen is dTFP0.1 and the 170% brighter version resulting from one round of directed evolution is dTFP0.2 (**Figure 2.1B**, **Table 2.2**, and **Table 2.3**). Substitution of dimer interface residues Ser162 and Ser164 with lysines produced a monomeric version (**Figure 2.3A**), mTFP0.3, which retained only 15% of the brightness of its dimeric precursor. After multiple successive rounds of screening libraries, generated by random or saturation mutagenesis, for variants with improved brightness and high 480/530 nm emission ratio (**Table 2.2**), I arrived at mTFP0.7 that has fluorescence brightness equivalent to mCerulean (**Table 2.3**). However, when I attempted to image an mTFP0.7-β-actin fusion in live HeLa cells by confocal microscopy, I discovered that the fluorescent signal rapidly bleached upon illumination with the 458 nm laser. Further investigation with purified protein revealed that the apparently bleached protein spontaneously recovered its fluorescence over the course of several minutes. The detailed investigation of the intriguing photochromic properties of mTFP0.7 is described in **Chapter 3**.

*In vitro* characterization of purified mTFP1 revealed it to be slightly red-shifted (excitation peak at 462 nm and emission peak at 492 nm) from cFP484 (**Table 2.3**) and thus the new color classification of teal rather than cyan is appropriate. A quantum yield

of 0.85 and an extinction coefficient of 64,000 $M^{-1}cm^{-1}$ makes mTFP1 comparable in brightness to the popular YFP variants mCitrine [42] and Venus [43] and one of the brightest monomeric FPs of any color [68]. The fluorescence of mTFP1 is insensitive to physiologically relevant changes in pH (**Figure 2.3**).

**Table 2.2** Mutations in dimeric and monomeric TFP variants.

| Variant | Library construction strategies | Mutations |
|---|---|---|
| dTFP0.1 | See **Table 2.1**. | Inside: H42N, L44V, L72F, F124L, M150L, S179T<br>A-B interface: D125K, M127K |
| dTFP0.2 | 2 generations of random mutagenesis. | Inside: D81N<br>Outside: S226P |
| mTFP0.3 | Site-directed mutagenesis at 162 and 164.<br>Saturation mutagenesis at 163. | A-C interface: S162K, S164K |
| mTFP0.4 | Saturation mutagenesis at 66.<br>Semi-saturation mutagenesis at 175. | Inside: Q66C, C175V |
| mTFP0.5 | 3 generations of random mutagenesis. | Inside: S62T, C66G<br>Outside: A80P, N216S<br>A-B interface: K127E, K182R |
| mTFP0.6 | Saturation mutagenesis at 66+163, 66+197.<br>Semi-saturation mutagenesis at 66+147, 66+213. | Inside: G66A, L213V<br>Outside: S2N<br>Replace 223-228 with TG |
| mTFP0.7 | 2 generations of random mutagenesis. | Inside: V44I, Y173H<br>Outside: V186A<br>A-B interface: R123H<br>Mutate: N2S |
| mTFP0.8 | Semi-saturation mutagenesis at 62, 63, 64, 65, and 66 with screening for photostability. | Inside: N63T |
| mTFP0.9 | Semi-saturation mutagenesis at 142, 144, 145, 149, 150, and 161 with screening for photostability. | Inside: L150M (reversion to wt), I161V<br>Outside: K142G<br>A-C interface: E144D, P145A, I149R |
| mTFP1 | 2 generations of random mutagenesis with screening for photostability. | Outside: L141T, V158K, Y221N, G224D |

To determine the photostability of mTFP1, photobleaching experiments were done on droplets of purified protein suspended in mineral oil following the protocol of Shaner et al. [68] This method is designed to approximate the conditions of a typical wide-field microscopy experiment while rigorously accounting for differences in the spectral properties of the FP as well as the optical properties of the microscope. Using this method, the time for bleaching from an initial emission rate of 1,000 photons/sec/molecule down to 500 photons/sec/molecule ($t_{1/2}$) was determined to be 163 s when 10% neutral density (ND) filters were used. With no ND filters the $t_{1/2}$ was 110 s for mTFP1. For the sake of comparison, the $t_{1/2}$ for Cerulean with 10% ND filters is 36 s and the $t_{1/2}$ for EGFP with no ND filters is 174 s [68]. As previously noted [68], Cerulean displays an illumination intensity-dependent fast bleaching component that can decrease the intensity to 70% of its initial value within the first few seconds of imaging under typical conditions ([68] and Figure 2.4). No fast bleaching component was observed for mTFP1.

**Table 2.3** Fluorescent properties of CFPs and TFPs.

| Protein | $\lambda_{ab}$ (nm) | $\lambda_{em}$ (nm) | $\varepsilon^{a}*10^{-3}$ ($mM^{-1}cm^{-1}$) | $\phi^{b}$ | Brightness[c] ($mM^{-1}cm^{-1}$) | pKa | Photostability[d] | Cameleon FRET efficiency (+/- $Ca^{2+}$) | |
|---|---|---|---|---|---|---|---|---|---|
| | | | | | | | | - | + |
| cFP484[e] | 456 | 484 | 35.3 | 0.48 | 17 | ND[f] | ND | ND | ND |
| dTFP0.1 | 456 | 485 | 42 | 0.63 | 26 | ND | < 1 | ND | ND |
| dTFP0.2 | 456 | 486 | 60 | 0.68 | 41 | ND | < 1 | ND | ND |
| mTFP0.3 | 458 | 488 | 19 | 0.31 | 6 | ND | < 1 | ND | ND |
| mTFP0.7 | 453 | 488 | 60 | 0.50 | 30 | 4.0 | < 1 | ND | ND |
| mTFP1 | 462 | 492 | 64 | 0.85 | 54 | 4.3 | 163[g]/110[h] | 39% | 49% |
| mECFP | 433/451[i] | 475/504[i] | 33/30[i] | 0.41 | 13/12[i] | 4.7 | 64[h,j] | 26% | 39% |
| mCerulean | 433/451[i] | 475/503[i] | 43/37[i] | 0.64 | 27/24[i] | 4.7 | 36[g,j] | 30% | 41% |
| EGFP[j] | 488 | 507 | 56 | 0.60 | 34 | 6 | 174[h,j] | ND | ND |

[a]Extinction coefficient. [b]Quantum yield. [c]Product of φ and $\varepsilon*10^{-3}$. Values for common FP variants have been previously tabulated [68]. [d]Time to bleach from an initial emission rate of 1000 photons/s to 500 photons/s. [e]Values from ref. [46]. [f]Not determined. [g]Measured with 10% neutral density filters. [h]Measured with no neutral density filters. [i]Values for both 'humps' of mECFP and mCerulean are provided. [j]Values from ref. [68].

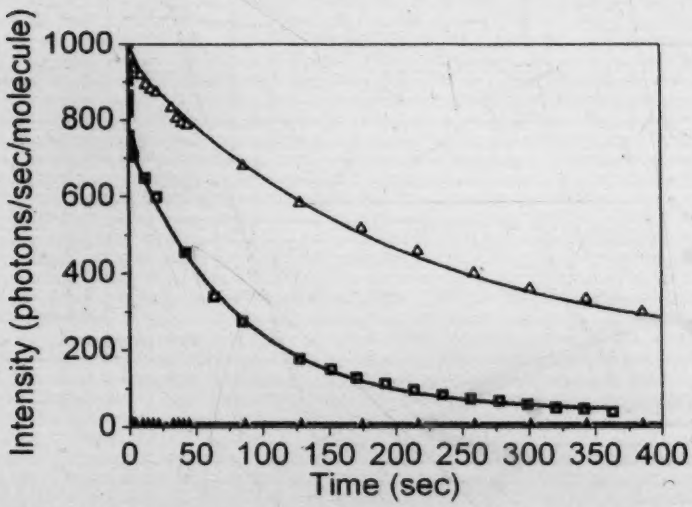


**Figure 2.4** Fluorescence photobleaching of mTFP1 (red triangle), mCerulean (blue square) and mTFP0.7 (green triangle) under epi-fluorescence microscope. The curves were scaled to 1000 photons/molecule/second initially.

### 2.3.3 Structural analysis of mTFP1

mTFP1 was crystallized and its structure was solved by J. Nathan Henderson and S. James Remington. As one would predict on the basis of sequence homology, the fold of mTFP1 is the typical "β-can" motif that is characteristic of avGFP and it homologues [38]. A comparison to structures in the Protein Data Bank using DALI [106] and DALILITE [107] revealed EosFP (PDB ID 1ZUX [108]) and dsFP583 (also known as DsRed, PDB IDs 1G7K [49] and 1GGX [109]) to be the closest structural homologues of mTFP1. EosFP has 66% sequence identity and a 0.6 Å root mean square deviation (RMSD) over 213 aligned C-alpha atoms, while dsFP583 has 55% sequence identity and a 0.7 Å RMSD over 212 aligned C-alpha atoms. The structural alignment is only slightly worse for amFP486 (PDB ID 2A46 [105]), with which mTFP1 has 51% sequence identity and a 0.9 Å RMSD over 213 aligned C-alpha atoms. The one striking difference between the structure mTFP1 and those EosFP, dsFP583, and amFP486 is the intermolecular interactions observed in the crystal lattice. Shown in **Figure 2.5A** is the monomer of mTFP1 surrounded by the closest subunits within the crystal lattice. The distance and orientations of these surrounding subunits is quite distinct from that observed for the subunits of the biologically relevant tetramers observed in the crystal structures of other

*Anthozoa* FPs such as amFP486 (**Figure 2.5B**). The crystal packing observed for mTFP1 is consistent with the fact that this protein was rationally engineered to be a monomer in solution. It is interesting to note that the 6 (3 unique interactions and their symmetrical counterparts) of the most intimate crystal contacts involve surface histidine, glutamic acid, and aspartic acid residues bridged by zinc ions. This observation is consistent with the requirement for zinc acetate in the crystallization buffer.

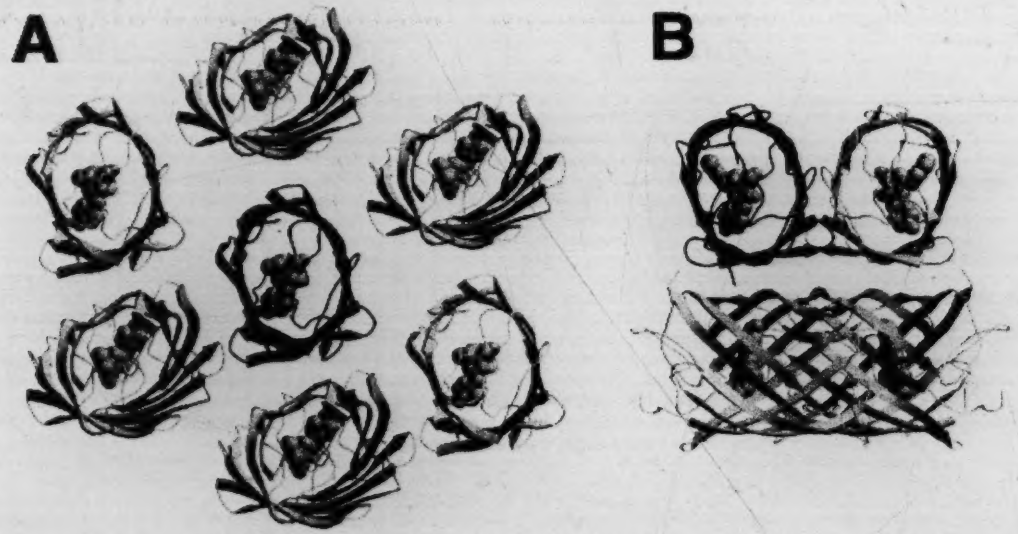


**Figure 2.5** Crystal packing of mTFP1 and amFP486 (A) Shown in dark grey cartoon representation is the asymmetric unit of mTFP1 (a single polypeptide) crystallized in the monoclinic space group C2. Also shown are the proximal copies of the protein (light grey cartoon) as generated using crystallographic symmetry operations. As expected for a monomeric variant, none of the proximal protein subunits pack in orientations similar to those typically observed in *Anthozoa* FPs such as the highly homologous amFP486 [105] shown in (B). (B) For amFP486 crystallized in the tetragonal space group $I4_122$ (PDB ID 2A46), the asymmetric unit contains a single polypeptide (dark grey cartoon) which is shown in the same orientation as mTFP1 in (A) [105]. The additional 3 subunits (light grey cartoon) of the tightly packed tetrameric biological unit were generated using the crystallographic symmetry operations.

Shown in **Figure 2.6A** and **Figure 2.6B** are the locations of all mutations at residues with side chains directed towards either the outside or the inside of the protein structure, respectively. Considering only those mutations on the surface of mTFP1 (**Figure 2.6A**) and comparing to the subunit orientation in amFP486 (**Figure 2.5B**), it is

apparent that the mutations cluster in the former protein-protein interfaces. While four of these external mutations were rationally introduced to disrupt the intermolecular interactions at the interface (residues 125, 127, 162, and 164), seven others (residues 123, 141, 158, 182, 186, 216, and 221) were discovered through random mutagenesis and screening. As shown in **Figure 2.6B**, beneficial internal mutations tend to be located in the midsection of mTFP1. With only one exception, individual internal mutations provided only incremental improvements in either the brightness or photostability of the protein, suggesting that the effects were due to slight changes in the side chain packing and internal hydrogen bond network. One particularly dramatic consequence for a single point mutation was the large increase in photostability observed for the Asn63Thr mutation that differentiates mTFP0.8 from mTFP0.7. Residue 63 is positioned directly below the chromophore when viewed as in **Figure 2.6C**. The mechanism of reversible photobleaching of mTFP0.7 is further discussed in **Chapter 3**. It is likely that this mutation improves photostability by inhibiting the cis-trans chromophore photoisomerization.

The molecular environment of the chromophore is very similar to that observed in amFP486 [105]. In particular, the four residues (Arg70, Glu148, His197, Glu214) of the critical quadrupole salt bridge network are conserved both in identity and in conformation (**Figure 2.6C**). This quadrupole salt-bridge network has been proposed to be responsible for maintaining a positive charge on His197 that may in turn limit charge transfer in the excited state and thereby give rise to the blue-shift [105]. One major difference in the chromophore environment is the presence of His163 (aligns with an alanine in amFP486) that hydrogen bonds to the phenolate oxygen of the chromophore through the imidazole side chain (**Figure 2.6C**). Interestingly, one of the surface mutations identified during selection for photostability, Glu144Asp, is hydrogen-bonded to the imidazole side chain of His163 (**Figure 2.6C**). A glutamic acid at this position (as in the wild-type protein) would probably be unable to adapt a conformation that would allow formation of a similar hydrogen bond. In amFP486 a water molecule substitutes for the imidazole side chain of His163 and makes a similar hydrogen bond to the chromophore.

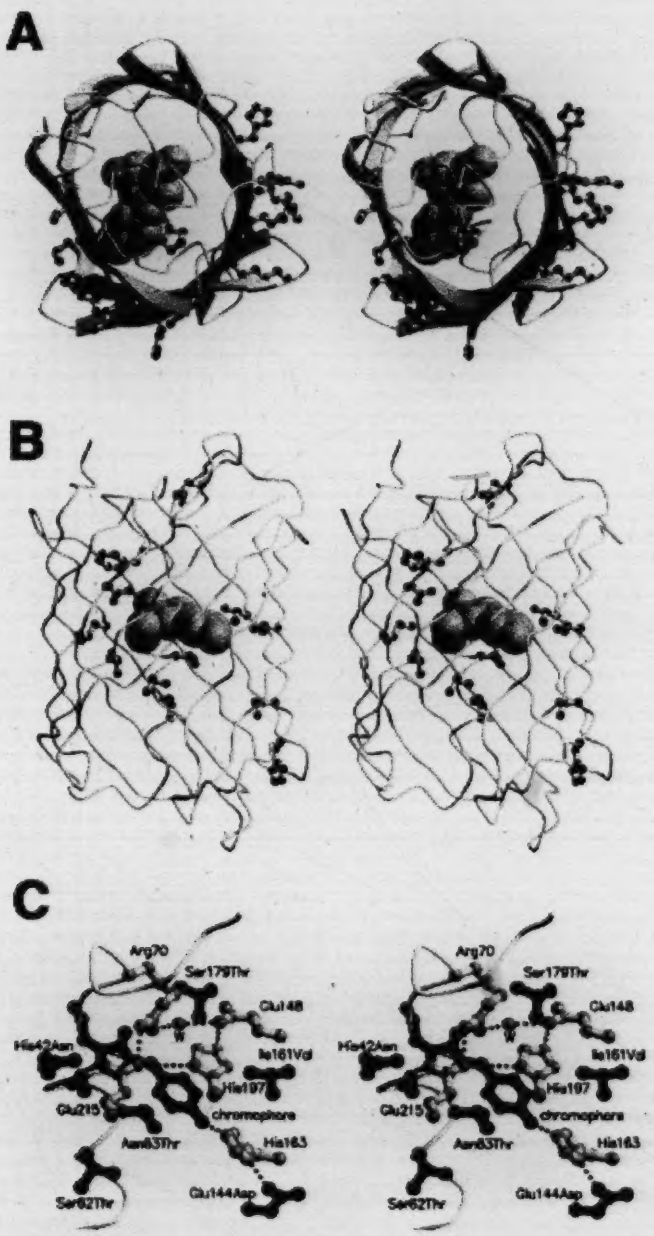


**Figure 2.6** Location of beneficial mutations in mTFP1 (A) Stereoview of mTFP1 with the polypeptide backbone in cartoon representation and the chromophore in space filling representation. All residues with fully solvent exposed side chains that are mutated relative to the wild-type cFP484 are shown in ball-and-stick representation. The protein is viewed from the same orientation as the single asymmetric unit shown in **Figure 2.5A** and **Figure 2.5B**. By comparison with the amFP486 structure shown in **Figure 2.5B**, it is

apparent that the external mutations are clustered in the former protein-protein interfaces of the tetrameric wild-type protein. (B) Stereoview of mTFP1 with all residues that are directed towards the interior of the β-barrel and mutated relative to cFP484 shown in ball-and-stick representation. (C) Stereoview of the chromophore region of mTFP1 showing the chromophore (black bonds with grey atoms), all mutations in the immediate vicinity of the chromophore (gray bonds with black atoms), and a selection of residues (i.e. the quadrupole salt bridge network and His163) that were not mutated but are discussed in the text (white bonds with grey atoms).

A surprising aspect of the mTFP1 structure is that the chromophore is extremely nonplanar with a CA-CB dihedral 'tilt' of 12.7° and a CB-CG dihedral 'twist' of -14.3°. Such distortions from planarity have previously been observed for non-fluorescent 'dark' states of certain photoswitchable fluorescent proteins [110]. However, for a protein as brightly fluorescent as mTFP1 the observation of such distortion is unexpected and apparently inconsistent. Possible explanations for this distorted structure are that it is either an artifact of crystallization or a population averaged mixture of an extremely twisted nonfluorescent chromophore and a planar fluorescent chromophore. Arguing against the first possibility is the fact that the chromophore is completely buried within the β-can structure and crystal contacts with nearby surface residues do not appear to be causing major distortions of the protein main-chain atoms. Arguing against the second possibility is the fact that there is no significant residual electron density in the immediate vicinity of the chromophore and thus no evidence of alternate conformations. Further high-resolution structural studies will be required to address this interesting observation.

### 2.3.4 mTFP1 as a FRET donor to mCitrine and mOrange

To assess mTFP1's suitability as a FRET donor to mCitrine, analogous versions of yellow Cameleon3.3 (YC3.3) [70] containing either mECFP, mCerulean, or mTFP1 were constructed and their FRET efficiency in the absence and presence of $Ca^{2+}$ was determined (**Table 2.3** and **Figure 2.7A**). All three versions of YC3.3 exhibited similar increases in FRET efficiency upon $Ca^{2+}$-binding, but the mTFP1-YC3.3 version was notable for its significantly higher efficiencies in both the $Ca^{2+}$-bound and $Ca^{2+}$-free states. The trend in experimental FRET efficiencies, mECFP < mCerulean < mTFP1, is consistent with our calculated $R_o$ values of 5.0 nm for mECFP, 5.3 nm for mCerulean,

and 5.7 nm for mTFP1. It is important to note that the original YC3.3 contained ECFP and had been optimized for maximum FRET difference between the $Ca^{2+}$-bound and $Ca^{2+}$-free states. It is therefore unsurprising that switching to an mTFP1 donor (with a different dipole orientation and increased $R_o$ value) results in a slightly decreased dynamic range. This is almost certainly because the protein was empirically optimized [70, 111] for interfluorophore distance changes centered on the $R_o$ of ECFP (where there is the strongest dependence of FRET efficiency on distance). If mTFP1-YC3.3 were to be subject to similar systematic optimization, I am confident that the dynamic range could be significantly improved.

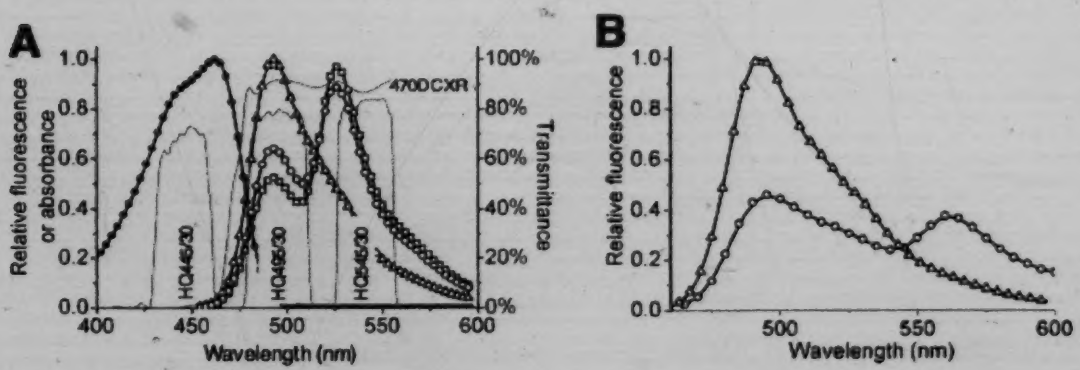


**Figure 2.7** mTFP1 as a FRET donor to a YFP or mOrange acceptor (A) Shown is the *in vitro* emission spectra of mTFP1-YC3.3 [70] with no $Ca^{2+}$ (○), 10 mM $Ca^{2+}$ (□), and no FRET (△). To obtain the 'no FRET' spectrum, the linker between the two fluorescent proteins was digested with trypsin under conditions where the fluorescent proteins remain intact. Shown in gray lines is a plot of % transmittance vs. wavelength for the custom filter set used for imaging of mTFP1-YFP FRET to produce the data shown in **Figure 2.9**. Filters are designated with Chroma Technology Corp. part numbers. (B) Shown is the in vitro emission spectra for an mTFP1-mOrange fusion protein before (○), and after (△), proteolysis of the linker peptide.

The calculated $R_o$ value (5.7 nm) for mTFP1-mOrange FRET suggested to us that this new monomeric FP pair could compare favorably with the previously reported dimeric MiCy-mKO FRET pair [92]. To experimentally validate mTFP1 as a FRET donor to mOrange, mTFP1 and mOrange were genetically fused with an 8 amino acid linker. The emission spectra for the purified fusion protein before and after trypsinolysis of the linker is shown in **Figure 2.7B**. The experimental FRET efficiency was calculated

to be 53.6%. Relative to EGFP, mTFP1 is a superior FRET donor to mOrange because it is brighter (**Table 2.3**) and can be excited at or near its blue-shifted absorbance peak of 462 nm without significant cross excitation of mOrange. It remains to be seen how mTFP1 and mMiCy will compare in this regard [69].

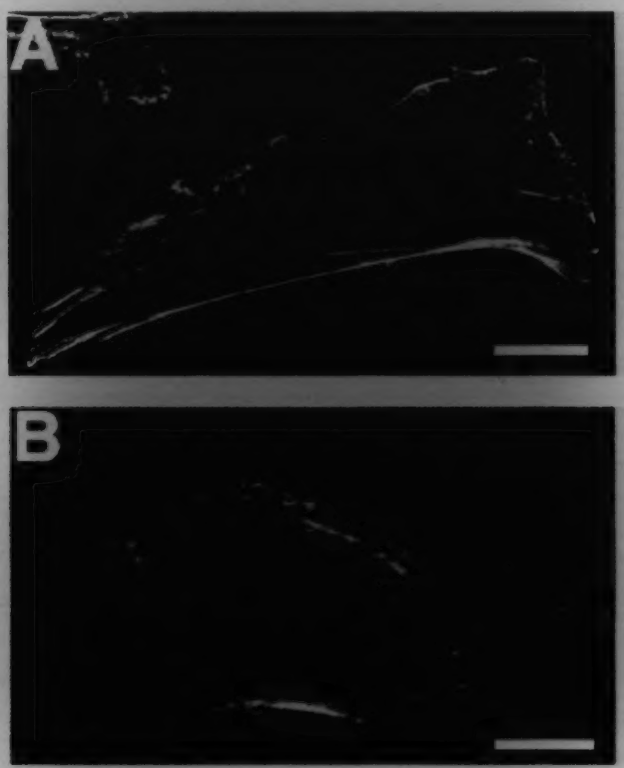


**Figure 2.8** Localization of mTFP1 fusion proteins in live HeLa cells. Confocal fluorescence images of HeLa cells expressing either mTFP1-β-actin (A) or mTFP1-α-tubulin (B). Scale bar = 10 μm in both images.

### 2.3.5 Live cell imaging of mTFP1 fusions and FRET reporters

To determine if mTFP1 was suitable for use as non-perturbing fusion partner, I expressed mTFP1-β-actin (**Figure 2.8A**) and mTFP1-α-tubulin (**Figure 2.8B**) fusions in mammalian cells. Scanning confocal microscopy with a 458 nm laser revealed that both fusion proteins localized correctly. In stark contrast to the results with mTFP0.7-β-actin, there was no significant decrease in fluorescence intensity upon repeated image acquisitions.

Typical filter sets used to image Cerulean by epi-fluorescence microscopy are adequate but suboptimal for mTFP1. To take advantage of mTFP1's improved brightness, I recommend a 445/30 nm excitation filter, a 470 nm beamsplitter, and a 495/30 nm emission filter (**Figure 2.7A** and **Table 2.4**). This combination gives a 2.6-fold increase in fluorescent signal relative to mCerulean imaged using a standard CFP set (e.g. a 436/20 nm excitation filter, a 455 nm beamsplitter, and a 480/40 nm excitation filter). I have used the recommended set in combination with a new YFP emission filter (545/30 nm), to demonstrate that mTFP1-YC3.3 can be practically employed in live cell FRET imaging. The gene encoding mTFP1-YC3.3 was cloned into a mammalian expression vector with an N-terminal signal sequence and a C-terminal endoplasmic reticulum (ER) retention peptide [70]. FRET imaging of transiently transfected HeLa cells on an Zeiss Axiovert 200M equipped with a digital CCD camera revealed a typical pattern of ER localization and robust ratiometric responses to induced changes in the free $Ca^{2+}$ concentration (**Figure 2.9**). This result demonstrates that the spectral distinction between mTFP1 and mCitrine are sufficient for these proteins to be used as an advantageous new FRET pair that can be imaged on a standard epi-fluorescence microscope equipped with appropriate bandpass filter sets.

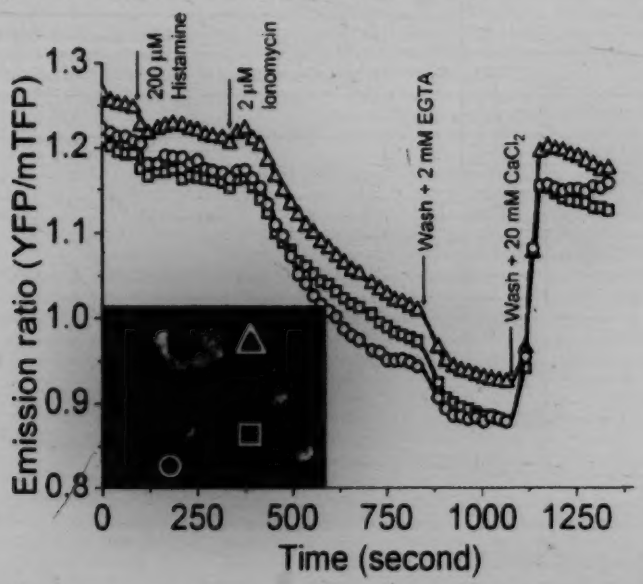


**Figure 2.9** FRET imaging of mTFP1 with a YFP acceptor. Shown is a plot of the emission ratio versus time for 3 HeLa cells (see donor fluorescence image in the inset) expressing mTFP1-YC3.3 targeted to the endoplasmic reticulum. Images in both the

donor and acceptor emission channels were acquired every 5 seconds with identical exposure times (300 ms) and 10% neutral density filters. Histamine (200 μM) or ionomycin (2 μM) were added at the indicated time points.

**Table 2.4** Experimentally determined relative fluorescence intensities for identical concentrations of mTFP1, mCerulean, and mCitrine imaged on an epi-fluorescence microscope with xenon arc lamp illumination.

| Protein | Excitation filter[a] | Beamsplitter[a] | Intensity relative to mCerulean imaged with a HQ436/20 excitation filter and D480/40 emission filter[a] | |
|---|---|---|---|---|
| | | | D480/40 | HQ495/30 |
| mTFP1 | D436/20 | 455DCLP | 1.3 | 1.5 |
| | HQ445/30 | 470DCXR | ND[b] | 2.6 |
| mCerulean | D436/20 | 455DCLP | 1.0 | 0.8 |
| | HQ445/30 | 470DCXR | ND[b] | 1.3 |

| Protein | Excitation filter[a] | Beamsplitter[a] | TFP or CFP emission filter[a] | Relative intensity passed by YFP emission filter[a,c] | |
|---|---|---|---|---|---|
| | | | | HQ535/30 | HQ545/30 |
| mTFP1 | D436/20 | 455DCLP | HQ495/30 | 0.39 | 0.30 |
| | HQ445/30 | 470DCXR | HQ495/30 | 0.39 | 0.30 |
| mCerulean | D436/20 | 455DCLP | D480/40 | 0.35 | 0.30 |
| | HQ445/30 | 470DCXR | HQ495/30 | 0.41 | 0.34 |
| mCitrine | HQ500/20 | Q515LP | ND[b] | 1 | 0.91 |
| | D436/20 | 455DCLP | ND[b] | 0.12 | 0.07 |
| | HQ445/30 | 470DCXR | ND[b] | 0.15 | 0.09 |

[a]All filters and beamsplitters were purchased from Chroma Technology Corp. Filters are designated with Chroma part numbers. [b]Not determined. [c]For mTFP1 and mCerulean, intensities are relative to the intensity in the indicated TFP or CFP emission channel. For mCitrine, all intensities are relative to the intensity obtained with a HQ500/20 excitation filter and HQ535/30 emission filter.

## 2.4 CONCLUSIONS

Using a combination of rational protein engineering and directed evolution I have created a new monomeric FP, dubbed mTFP1, that harbors an anionic phenolate-type chromophore chemically identical to that of EGFP. As such, the blue-shifted mTFP1 is the beneficiary of the narrow peak shape, high brightness, and high photostability properties that are empirically associated with the EGFP chromophore [68]. A recurring theme in the history of FP engineering is that, given the plethora of applications for which FPs are suitable research tools, no new variant makes all others redundant [50, 68, 80]. With this in mind, I readily acknowledge that the properties of mTFP1 make it a

superior fluorophore for some, but not all, applications. Applications for which mTFP1 offers a clear advantage over existing alternatives include intra- and inter-molecular FRET with a yellow or orange acceptor FP and dual color imaging in combination with an orange or red FP. For dual color imaging in combination with a YFP, mTFP1 could provide a brighter fluorescent signal than existing *Aequorea*-derived CFPs but the bleedthrough into the acceptor emission channel may be only slightly better (or possibly worse) depending on the specific filter combination in place.

In conclusion, relative to monomeric alternatives of similar color, mTFP1 has a number of favorable attributes that will allow practical FRET imaging at significantly lower intracellular protein concentrations, higher light intensities, and for greater duration than is currently possible. These advantages make mTFP1 an excellent complement to the existing selection of monomeric fluorescent proteins recommended for use in fluorescence imaging [68]. In a recent report from the group of Richard N. Day at the University of Virginia, the use of mTFP1 for imaging in live cells has been independently reevaluated [112]. The authors state that mTFP1 has "*increased brightness, optimized excitation using the standard 458 nm laser line, increased photostability and improved spectral overlap with Venus*" and it may improve "*the detection of interactions involving proteins that are difficult to express or that need to be produced at low levers in cells*", thus providing further support for the conclusions in this chapter.

# CHAPTER 3:

# CHROMOPHORE CIS-TRANS PHOTOISOMERIZATION: CHARACTERIZATION OF THE REVERSIBLY PHOTOSWITCHABLE VARIANT mTFP0.7

The research described in this chapter has been reported in *Proceedings of SPIE* [74]. Other related data acquired by x-ray crystallographers, J. Nathan Henderson and S. James Remington at the University of Oregon, were not detailed in this chapter, however, could be found in the paper in *Proc. Natl. Acad. Sci. USA* [61].

## 3.1 INTRODUCTION

Osamu Shimomura is credited with discovering GFP in 1961 when he was isolating aequorin, a calcium-dependent bioluminescent protein from the *Aequorea victoria* jellyfish collected from the sea [36]. Several decades had to pass before efforts to develop GFP as a genetically encoded tracer molecule were seriously pursued. The initial breakthrough in this regard was the cloning of the gene by Prasher in 1992 [113]. Within just two more years the first reports of GFP expression in organisms other than jellyfish, including *E. Coli* and *C. elegans*, started to appear [114, 115]. However, it was soon realized that wild-type GFP is sub-optimal for live cell imaging due to drawbacks such as dual excitation peaks and poor folding efficiency. Fortunately improved variants of GFP, including the variant known EGFP, were soon reported [37]. In addition, mutants with new colors such as blue (BFP), cyan (CFP) and yellow (YFP) followed soon after [39, 41]. Another landmark development in the history of FPs was the discovery of GFP-like proteins in corals by Lukyanov [46]. Among the first reported coral FPs was the tetrameric red fluorescent protein known as *Discosoma* Red or DsRed (also known as dsFP583). A handful of monomeric proteins with emission wavelengths ranging from yellow to far-red (known as the "mFruit" series) have been engineered from DsRed [20, 50].

A relatively recent development in the field of FPs is the discovery of variants that can be switched 'on' or 'off' or converted to a new color by irradiation with specific wavelengths of light [116]. The term "optical highlighters" has been used to describe those FPs. Optical highlighters can become fluorescent from a nonfluorescent state reversibly or irreversibly, or change their color of fluorescence after illumination by a certain wavelength of light. They are usually termed photoswitchable, photoactivatable, or photoconvertable FPs.

The first useful optical highlighter designed specifically for photoactivation studies is a variant of avGFP, termed PA-GFP. This photoactivatable version of avGFP was developed by substitution of histidine for threonine at position 203 (T203H) [57]. It has negligible absorbance in the region between 450-550 nm. After photoactivation with violet light (~405 nm), the absorption maximum at 504 nm increases approximately 100-fold. The activation light could turn on a subpopulation of PA-GFP in a cell. Therefore it is a very useful tool for investigation of protein dynamics.

Some FPs can be turned "on" or "off, by simply changing the illumination wavelength. This phenomenon has been initially observed in the wild-type and several derivatives of avGFP at the single molecule level, and described as molecular 'blinking' [58, 59]. A recent study reported that Dronpa, a mutant of a GFP-like fluorescent protein cloned from a coral *Pectiniidae*, underwent on/off photoswitching in both batch of protein or single molecular level [60, 118]. When irradiated at 488 nm, Dronpa emits fluorescence with a maximum at 518 nm from a deprotonated chromohpore the same as EGFP. When illuminated at 488 nm, Dronpa is starting to be driven to the protonated species that is nonfluorescent. The rate of this process is light-intensity dependent. The dark state has a 390-nm absorption peak and readily converted back to the original fluorescent deprotonated state with illumination at 405 nm. The protein Dronpa represents a class of FPs that undergo reversible photoswitching.

Optical highlighters represent perhaps the most promising approach to the *in vivo* investigation of protein dynamics [55] and have recently become useful for high-resolution microscopy techniques that break the classical diffraction barrier [32, 62].

## 3.2 EXPERIMENTAL

### 3.2.1 General methods

All general molecular biology were carried out as previously described in **Section 2.2**. The cDNA sequences for all FP variants and fusion constructs were confirmed by dye terminator cycle sequencing using the DYEnamic ET kit (Amersham Biosciences). Sequencing reactions were analyzed at the University of Alberta Molecular Biology Service Unit. All filters for fluorescence screening and imaging were purchased from Chroma Technology (Rockingham, VT).

### 3.2.2 Protein purification

The proteins were purified as in **Section 2.2**. *E. coli* strain LMG194 was transformed with the pBAD/His B expression vector containing the FP gene of interest. A single colony was used to inoculate a 4 ml culture that was allowed to grow overnight (37 °C, 225 rpm) before being diluted into 1 L of LB medium containing ampicillin (0.1 mg/ml) and L-arabinose (0.2%). The culture was allowed to grow for 5 h before cells were harvested by centrifugation and lysed by French Press or sonification. Proteins were purified by Ni-NTA chromatography (Amersham).

### 3.2.3 Absorption measurements

Absorption spectra of mTFP0.7 were recorded on a DU-800 UV-visible spectrophotometer. Fresh protein purified by the method described above was diluted into PBS and contained in a 50 µl measuring cuvette. The absorption spectrum measured instantly was considered as in the fluorescent state. Then six Royal Blue (peak emission at 455 nm) Luxeon V LEDs (light emitting diodes) (Lumileds Lighting) with narrow beam lenses (Fraen) were used to illuminate the protein in the cuvette for 15 min after laying mineral oil on top of the solution to prevent evaporation. Then the cuvette was quickly moved into the spectrophotometer and the spectrum recorded was considered as in the dark state.

### 3.2.4 Kinetics

On a clean plastic surface, 5 µl protein of mTFP0.7 was added as a drop, followed by laying 20 µl mineral oil to prevent evaporation. The LEDs described above were used to bleach the protein drop. The intensity of light was adjusted to 6 $mW/cm^2$, 3.3 $mW/cm^2$, 2 $mW/cm^2$ or 1 $mW/cm^2$ by connecting different numbers of LEDs or changing the distances between LEDs and the protein drop. Much weaker light (~ 0.04 $mW/cm^2$) bandpass-filtered from a Xe-arc lamp was used to record the fluorescence. The LEDs could be switched on and off at computer-controlled intervals. An Image Pro Plus macro (Media Cybernetics) was used to automate acquisition and processing. For each measurement, fluorescence images were acquired following a series of programmed intervals of intense illumination.

To measure the temperature dependence of fluorescence recovery of mTFP0.7, a glass well bathed by a temperature-controllable water circulating system was used. 500 μl protein solution was contained in the well for 15 min at a certain temperature, followed by illuminating the solution by LEDs for 15 min. Same system described above was used to record the fluorescence recovery of the solution.

All curves were fitted by OriginLab 7.0 to derive the rates of reactions.

## 3.3 RESULTS AND DISCUSSION

### 3.3.1 Photophysical characterization of mTFP0.7

In the previous Chapter, I described the evolution of a new monomeric teal fluorescent protein (mTFP1) and the test of it for live cell imaging and other applications. In the evolution process, I derived a variant mTFP0.7 with high fluorescence brightness (**Table 2.3**). However, when I attempted to image an mTFP0.7-β-actin fusion in live HeLa cells by confocal microscopy, I discovered that the fluorescent signal rapidly disappeared upon illumination with the 458 nm laser. The fluorescence bleached so quickly that the acquisition of even a single image was unsuccessful. Upon careful investigation of this phenomenon, I found that mTFP0.7 underwent a light-induced reversible transition from the fluorescent state to a 'bleached' state. That is, the cyan fluorescent state diminished when illuminating the sample with 458 nm light, but was slowly and spontaneously replenished in the dark. To characterize the two states, I measured the UV-vis absorbance of the same protein solution in both states (**Figure 3.2A**). The freshly purified 'bright' state of the protein absorbs lights with a 453 nm peak while the 'dark' state with the absorption maximum at 376 nm. When exiting the 'dark' protein at 376 nm, the protein shows no detectable fluorescence. Previous studies of GFP chromophores have demonstrated that the protonated form of GFP absorbs at maximally 395 nm. I suspected that the 376 nm-absorbing 'dark' state of mTFP1 corresponds to a protonated chromophore state and the photobleaching of mTFP0.7 involves a protonation event. Another phenomenon I noticed was the bleached protein took about 30 minutes to relax back to the initial fluorescent state in the room temperature (the speed of the recovery could be enhanced by light from 395 nm LEDs). Because of the relatively slow rate of recovery, certainly much slower than expected for a simple deprotonation event, I

speculated that there should be additional molecular rearrangments or reactions involved. A reasonable hypothesis was that the photobleaching (and recovery) were associated with cis-trans isomerization about the double bond between what was formerly the Cα-Cβ of Tyr67. In a subsequent collaboration with S. James Remington of the University of Oregon, the X-ray crystal structures of mTFP0.7 in both the 'bright' and 'dark' states were determined [61]. The crystal structures clearly supported the cis-trans isomerization hypothesis (**Figure 3.1**). In addition, the hydrogen bonding of the chromophore phenol oxygen and the hydrophobicity of the chromophore environment correlated with my previous protonation/deprotonation proposal. That is, the chromophore was protonated in the 'dark' trans state and deprotonated in the 'bright' cis state.

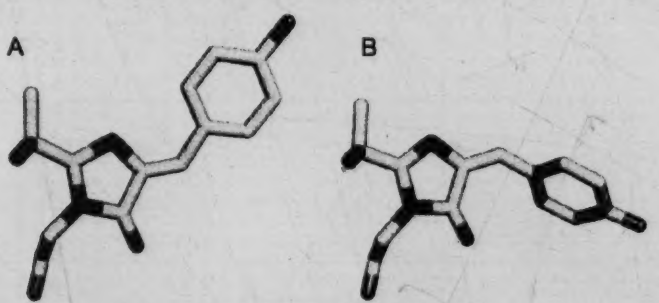


**Figure 3.1** The chromophore structures of mTFP0.7 in (A) fluorescent state and (B) dark state. The structures were drawn from PDB 2OTB and 2OTE.

In order to further characterize the isomerization process, I measured the kinetics of bleaching and recovery by imaging the fluorescent changes of protein drops under mineral oil. The intensity of light used to bleach the protein was controlled by connecting different numbers of LEDs or changing the distances between LEDs and samples. Less intense light filtered from a Xe-arc lamp was used to record the fluorescence. The bleaching curves under 6 $mW/cm^2$, 3.3 $mW/cm^2$, 2 $mW/cm^2$ and 1 $mW/cm^2$ were recorded respectively (**Figure 3.2B**). The recovery processes for each protein drop bleached by different light intensities were recorded as well. Under the measured light intensity range, the recovery processes showed little kinetic difference. But the rates of bleaching reaction were strongly dependent on the intensity of light. Both the fluorescence loss and recovery could be fitted as first order reaction. When plotting the rates of fluorescence loss with the light intensities, strong linear correlation was shown (**Figure 3.2C**). The detailed mathematical analysis showed the half-life of the bleaching

reaction to be 66 seconds per $mW/cm^2$ when illuminated with the Royal Blue (peak emission at 455 nm) Luxeon V LEDs. Those numbers could only be used to estimate the rate of reaction under light intensity ranging in $mW/cm^2$, because the light effect is most likely to be non-linear in much higher light intensity condition, e.g. > 1 $W/cm^2$.

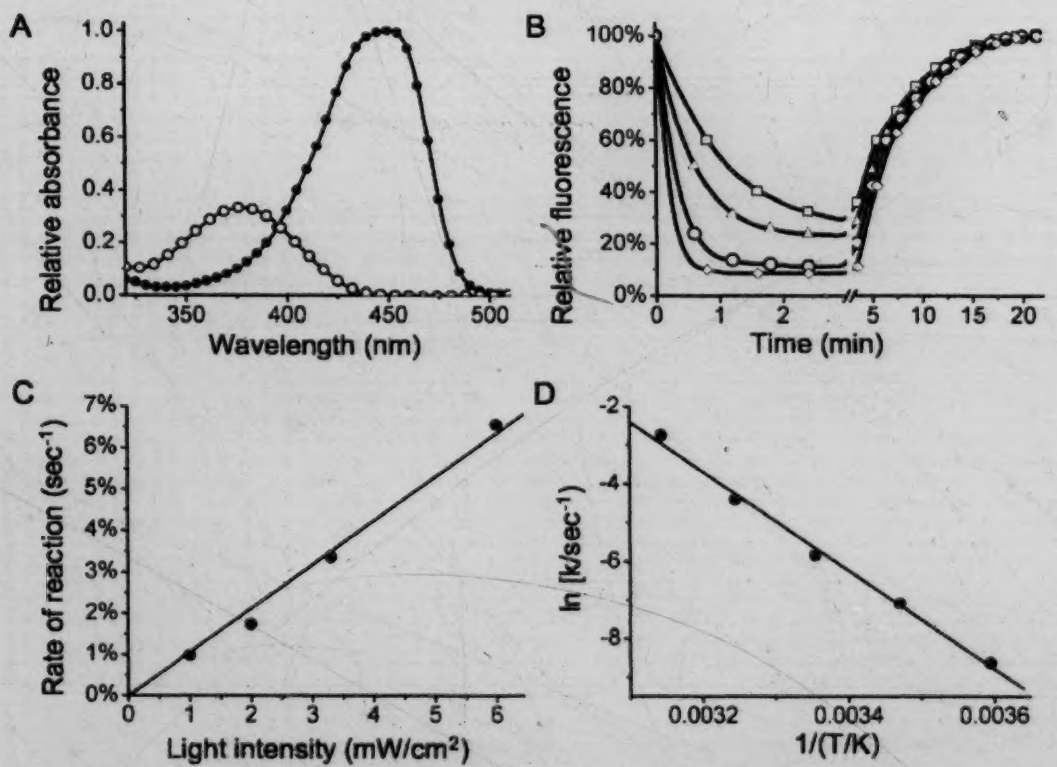


**Figure 3.2** (A) The absorbance of mTFP0.7 in the fluorescent state and dark state. (B) The fluorescence loss of mTFP0.7 under different light intensities (from top to bottom: 1, 3, 3.3 and 6 $mW/cm^2$) and the respective recovery. (C) The dependence of the rates of fluorescence loss of mTFP0.7 on light intensities. (Linear fit: y = 1.06% x, R=0.994) (D) The Arrhenius plot of the fluorescence recovery of mTFP0.7. (Linear fit: y = -12757x + 37.147, R = 0.997)

To characterize the fluorescence recovery reaction, a bleached solution was incubated at a variety of temperatures and the fluorescence was recorded over time. The resulting curves were fitted as first order reactions in OriginLab 7.0. The rates of reaction showed strong dependence on temperature (**Table 3.1**). For example, the half-life of the reaction is 300× longer at 5 °C than at 45 °C. The rates of reaction were calculated by fitting the curves and are shown in **Table 3.1**. Using the rates of reaction and the

corresponding temperatures, the activation energy of the trans-cis isomerization was identified as ~ 106 kJ/mol (**Figure 3.2D**). The energy barrier for mTFP0.7 trans-cis relaxation is significantly higher than the barrier of ~71 kJ/mol determined for the KFP cis-trans relaxation [119]. Correspondingly the KFP cis-trans relaxation (half-life to be ~ 70 s at room temperature) is much faster than mTFP0.7 trans-cis isomerization [119].

**Table 3.1** The kinetics of the fluorescence recovery of mTFP0.7 at different temperatures

| Temperature | Rate of reaction **k** ($sec^{-1}$) | Half-life $t_{1/2}$ (min) | lnk | 1/T |
|---|---|---|---|---|
| 5 °C | 1.80E-04 | 64.2 | -8.62 | 0.0036 |
| 15 °C | 8.40E-04 | 13.7 | -7.08 | 0.0035 |
| 25 °C | 2.91E-03 | 4.0 | -5.84 | 0.0034 |
| 35 °C | 1.23E-02 | 0.9 | -4.40 | 0.0032 |
| 45 °C | 6.43E-02 | 0.2 | -2.74 | 0.0031 |

### 3.3.2 Prospects for use of mTFP0.7 in live cell imaging

mTFP0.7 undergoes fast photobleaching that limits its use in a conventional microscope. However, like Dronpa and its mutants, mTFP0.7 may find application in some specialized experiments [60, 120]. For example, simultaneous 400 nm and 458 nm irradiation of mTFP0.7 might produce significant fluorescence by keeping a significant population of the molecules in the 'bright' state. This approach could be used to spatially limit the volume of excited fluorophores, providing some of the advantages of two-photon excitation, such as improved spatial resolution (z-axis) and optical sectioning in confocal microscopy. Further more, this protein could be applied for other super resolution microscopy techniques, such as RESOLFT [31] and PALM [32].

## 3.4 CONCLUSIONS

mTFP1, a valuable addition to the fluorescent protein 'toolbox', is the brightest and most photostable fluorescent protein in its respective color class. The new reversibly photoswitchable mTFP0.7 has proven to be transiting between a fluorescent state with a cis and deprotonated chromophore, and a dark state with a trans and protonated chromophore. This mechanism might be universal for photoswitchable FPs and could also be more broadly involved in the FP photobleaching or blinking phenomena. Further

more, I expect that further development of mTFP0.7 variant may lead to yet another useful addition to the FP 'toolbox' for use in live cell imaging.

# CHAPTER 4:

# HUE-SHIFTED VARIANTS OF mTFP1: IDENTIFICATION OF THE MOLECULAR DETERMINANTS OF COLOR AND APPLICATIONS IN FLUORESCENCE IMAGING

The research described in this chapter has been reported in *BMC Biology* [75]. It should be clearly pointed out that an undergraduate Peter Wong assisted me with the directed evolution of mWasabi, and also Michael W. Davidson and Scott G. Olenych at the National High Magnetic Field Laboratory and the Florida State University, carried out the creation of most of the mammalian expression vectors and performed the confocal imaging of mWasabi and mTFP1 fusion proteins.

## 4.1 INTRODUCTION

The availability of engineered avGFP variants with altered color, where color refers to the absorbance and/or fluorescence emission spectral profiles, has been a boon to life science research [121]. Access to a wide ranging FP color palette has allowed researchers to simultaneously track multiple proteins or use fluorescence resonance energy transfer (FRET) to detect protein-protein interactions in a live cell [79]. Fortunately, avGFP has been a fertile source of new colors of FPs. The main classes of color variants derived from avGFP include those that are blue fluorescent [76], cyan fluorescent [85], cyan-excitable green fluorescent [40], UV-excitable green fluorescent [122], and yellow fluorescent [41]. Coral is also an abundant source of FPs [46, 123] and in recent years this treasure-trove, which includes variants with fluorescent hues ranging from cyan to far-red, has yielded a number of exciting new variants [50, 56, 116]. For example, in **Chapter 2** I have described the engineering of a codon optimized and monomeric version of cFP484, a tetrameric cyan FP (CFP) from *Clavularia* coral [46]. The resulting protein, known as monomeric teal FP (mTFP1), has an anionic tyrosine-derived chromophore that is chemically identical to that of EGFP (**Figure 4.1A**). However, the absorbance and fluorescence emission maxima of mTFP1 (emission maximum = 492 nm) are blue shifted by ~15 nm relative to EGFP (emission maximum = 507 nm) due to numerous amino acid differences in the chromophore-containing cavity [73, 105] (compare **Figure 4.2A** and **Figure 4.2C** and see Figure **Figure 4.3A**). I have demonstrated that mTFP1 is a favorable alternative to avGFP-derived CFPs with tryptophan-derived chromophores such as enhanced CFP (ECFP) or Cerulean [85]. The specific advantages of mTFP1 include a narrower and single-peaked emission spectrum, improved brightness and photostability, and a single exponential lifetime decay [73].

In this Chapter I report on the efforts to engineer a series of new colors of mTFP1-derived FPs through the use of site-directed mutagenesis and random mutagenesis with library screening. This work has provided important insight into the amino acid determinants of color in mTFP1. In addition by collaboration with Michael W. Davidson a thorough assessment of mTFP1 fusion proteins has been undertaken to determine if such constructs exhibit their expected pattern of subcellular localization. Together these new results further establish mTFP1, and its suitably optimized hue-shifted variants, as useful new additions to the toolkit of FPs for cell biology research.

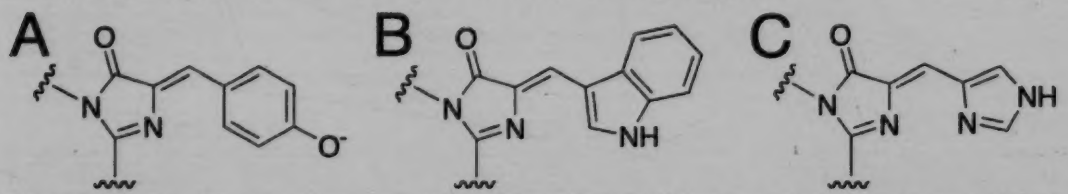


**Figure 4.1** Chromophore structures of mTFP1 and its hue-shifted variants. (A) The chromophore structure shared by EGFP, mTFP1, and mWasabi. (B) The chromophore structure shared by ECFP and the mTFP1-Y67W variant. (C) The chromophore structure shared by EBFP and the mTFP1-Y67H variant.

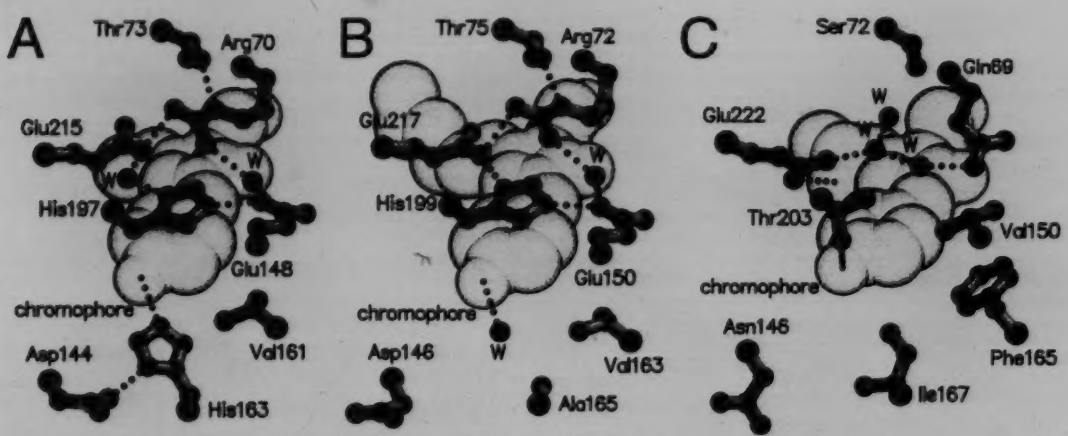


**Figure 4.2** The chromophore environment of mTFP1, amFP486, and avGFP-S65T. (A) Shown in space filling representation is the chromophore of mTFP1 (Protein data bank code 2HQK) [73]. The side chains of residues that are discussed in the text and that are in close proximity to the chromophore are shown in ball-and-stick. Hydrogen bonds are indicated with black dotted lines. Cα for each residue is represented as a black sphere. Atoms labeled 'W' are ordered water molecules. (B) The chromophore environment of amFP486 showing the residues that are structurally aligned with the residues represented in (A) (PDB code 2A46) [105]. (C) The chromophore environment of avGFP-S65T (and

EGFP) showing the residues that structurally align with those represented in (A) (PDB code 1EMA) [38]. avGFP-S65T and EGFP differ only by the Phe64Leu mutation which does not significantly modify the conformation of any residues shown in this figure.

## 4.2 EXPERIMENTAL

### 4.2.1 General methods

Synthetic DNA oligonucleotides for cloning and library construction were purchased from Integrated DNA Technologies (Coralville, IA). PCR products and products of restriction digests were purified by gel electrophoresis and extraction using either the GenCatch™ gel extraction kit (Epoch Biolabs, TX) or the QIAquick™ gel extraction kit (QIAGEN, Valencia, CA). Plasmid DNA was purified from overnight cultures by using either the GeneJET™ Plasmid Miniprep Kit (Fermentas, ON) or the QIAprep Spin Miniprep kit (QIAGEN, Valencia, CA). Restriction endonucleases were purchased from either Invitrogen or New England Biolabs. Dye terminator cycle sequencing using the DYEnamic ET kit (Amersham Biosciences) was used to confirm the complete cDNA sequences for all FP variants and fusion constructs. Sequencing reactions were analyzed at the University of Alberta Molecular Biology Service Unit and the Florida State University Bioanalytical and Molecular Cloning DNA Sequencing Laboratory. All filters for fluorescence screening and imaging were purchased from Chroma Technology (Rockingham, VT), Omega Filters (Brattleboro, VT) and Semrock (Rochester, NY). The nucleotide sequence of mWasabi has been deposited in the GenBank® nucleotide sequence database under accession number EU024648.

### 4.2.2 Mutagenesis and library construction

Mutagenesis was done by overlap PCR or error-prone PCR as previously described in **Section 2.2**. The PCR products were digested with Xho1 and EcoR1 and ligated into pBAD/His B vector digested with the same two enzymes (Invitrogen). The crude ligation mixture was used to transform electrocompetent *E. coli* strain DH10B (Invitrogen) which were then plated on Luria-Bertani (LB)/agar plates supplemented with ampicillin (0.1 mg/mL) and L-arabinose (0.02%). Plates were incubated for 14 h at 37 °C prior to picking individual colonies (in the case of site-directed mutagenesis for creation of blue shifted variants) or fluorescence-based library screening for red shifted variants.

### 4.2.3 Library screening

The screening system has been described previously in **Section 2.2** and will only be described here in brief. The light from a 175 W xenon-arc lamp (Sutter) was passed through a bandpass filter selecting for 460-490 nm light. The light passed into a bifurcated fiber optic bundle (Newport) positioned to illuminate a Petri dish harboring bacterial colonies. The fluorescence emission of the colonies was screened by eye using tinted plastic goggles that block light with wavelength less than 500 nm. Colonies with more intense fluorescence were picked for further investigation. Colonies of interest were cultured overnight in 4 mL LB medium containing ampicillin (0.1 mg/mL) and L-arabinose (0.2%). The following day 0.1 mL of each culture was dispensed into individual wells of a clear bottom 96-well plate (Nunc) and the full emission spectra of each variant measured with a Safire2 plate reader equipped with monochromators (Tecan). Variants with the most intense and red shifted fluorescence emission were used as templates in the subsequent round of library construction.

### 4.2.4 Protein purification and characterization

For production of protein, *E. coli* strain LMG194 was transformed with the pBAD/His B expression vector containing the FP gene of interest. A single colony was used to inoculate a 4 mL culture that was allowed to grow overnight (37 °C, 225 rpm) before being diluted into 1 L of LB medium supplemented with ampicillin and L-arabinose. The culture was grown for 12 h before cells were harvested by centrifugation and lysed by French Press. Proteins were purified by Ni-NTA chromatography (Amersham). Absorption spectra were recorded on a DU-800 UV-visible spectrophotometer (Beckman) and fluorescence excitation and emission spectra were recorded on a Safire2 plate reader. Reference standards for determining the quantum yields of blue- or green-fluorescing FP variants were quinine sulfate in 0.1 M $H_2SO_4$ or EGFP, respectively. Extinction coefficients were calculated using the protein concentration as determined by the BCA method (Pierce) and the chromophore absorbance as determined by UV-visible spectroscopy. For fluorescence pKa measurements, the protein of interest was first dialyzed into dilute buffer (5 mM Tris HCl, pH 7.5) before being diluted into a series of 200 mM phosphate and imidazole

buffers at various pH values. Fluorescence intensity was measured using a Safire2 plate reader.

### 4.2.5 Photostability measurements

For photostability measurements of green-fluorescing variants, microdroplets of either the purified protein (100 μM) or *E. coli* culture (previously transformed with the expression plasmid and induced) was mixed with mineral oil and vortexed. Approximately 5 μL of this suspension was sandwiched between a glass slide and a glass cover slip. Individual drops were identified by fluorescence microscopy and subjected to photobleaching. For all experiments, EGFP was subjected to bleaching under identical conditions and used as a reference standard.

### 4.2.6 Mammalian expression vectors

To create the Sapphire-actin and mWasabi-NLS vectors, the genes encoding Sapphire (also known as H9-40) [37, 39, 122] and mWasabi were PCR amplified with a 5' primer encoding an NheI site and a 3' primer encoding an XhoI site. The purified and digested PCR products were ligated into pEGFP-actin or pEYFP-Nucleus (Clontech), respectively, which had been previously digested with the same restriction enzymes to excise the FP coding sequence. An analogous nuclear localization construct was made for EGFP. All of the other mTFP1 and mWasabi vectors were constructed using C1 and N1 (Clontech-style) cloning vectors. The FPs were amplified with a 5' primer encoding an AgeI site and a 3' primer encoding either a BspEI (C1) or NotI (N1) site. The purified and digested PCR products were ligated into similarly digested EGFP-C1 and EGFP-N1 cloning vector backbones. To generate fusion vectors, the appropriate cloning vector and an EGFP fusion vector were digested, either sequentially or doubly, with the appropriate enzymes and ligated together after gel purification. Thus, to prepare mTFP1 and mWasabi N-terminal fusions, the following digestions were performed: human non-muscle α-actinin; EcoRI and NotI (vector source, Tom Keller, FSU); human cytochrome C oxidase subunit VIII, BamHI and NotI (mitochondria, Clontech); human zyxin, BamHI and NotI (Clare Waterman-Storer, NIH); rat α-1 connexin-43 and rat β-2 connexin-26, EcoRI and BamHI (Matthias Falk, Lehigh University); human H2B, BamHI and NotI

(George Patterson, NIH); N-terminal 81 amino acids of human β-1,4-galactosyltransferase, BamHI and NotI (Golgi, Clontech); human microtubule-associated protein EB3, BamHI and NotI (Lynne Cassimeris, Lehigh University); human vimentin, BamHI and NotI (Robert Goldman, Northwestern University); human keratin 18, EcoRI and NotI (Open Biosystems, Huntsville, AL); chicken paxillin, EcoRI and NotI (Alan Horwitz, University of Virginia); rat lysosomal membrane glycoprotein 1, AgeI and NheI (George Patterson, NIH); endoplasmic reticulum (calreticulin signal sequence and KDEL retention sequence), AgeI and EcoRI (Clontech). To prepare mTFP1 and mWasabi C-terminal fusions, the following digests were performed: human β-actin, NheI and BglII (Clontech); human α-tubulin, NheI and BglII (Clontech); human light chain clathrin, NheI and BglII (George Patterson, NIH); human lamin B1, NheI and BglII (George Patterson, NIH); human fibrillarin, AgeI and BglII (Evrogen); human vinculin, NheI and EcoRI (Open Biosystems, Huntsville, AL); peroximal targeting signal 1 (PTS1 - peroxisomes), AgeI and BspEI (Clontech); chicken protein tyrosine kinase 2, AgeI and BglII (Clare Waterman-Storer, NIH); human annexin (A4), AgeI and BspEI (Alen Piljic, EMBL, Heidelberg); human RhoB GTPase with an N-terminal c-Myc epitope tag (endosomes), AgeI and BspEI (Clontech); and the 20-amino acid farnesylation signal from c-Ha-Ras, AgeI and BspEI (membrane, Clontech). DNA for mammalian transfection was prepared by either the Plasmid Midi or Maxi kit (QIAGEN).

### 4.2.7 Live cell imaging

HeLa epithelial (CCL-2, ATCC) and Grey fox lung fibroblast (CCL-168, ATCC) cells were either cultured and transfected as previously described in **Section 2.2**, or grown in a 50:50 mixture of DMEM and Ham's F12 with 12.5% Cosmic calf serum (Hyclone) and transfected with Effectene (QIAGEN). For dual color imaging, the two expression plasmids were pre-mixed in a 1:1 ratio before transfection. Widefield live cell imaging was performed with a Zeiss Axiovert 200M microscope equipped with appropriate filter sets (Chroma), a Nikon TE-2000 inverted microscope equipped with Omega filters, or an Olympus IX71 equipped with Semrock filters. Laser scanning confocal microscopy was conducted on a Nikon C1Si and an Olympus FV1000, both equipped with argon-ion 457 and 488 nm lasers and proprietary filter sets. Spinning disk

confocal microscopy was performed on an Olympus DSU-IX81 equipped with a Lumen 200 illuminator (Prior, Boston, MA), Semrock filters, and 10-position filter wheels driven by a Lambda 10-3 controller (Sutter, Novato, CA).

Sapphire fluorescence was measured using a 375-415 nm bandpass excitation filter, a 475 nm longpass beamsplitter, and 500-550 nm bandpass emission filters. mTFP1 was imaged with a CFP filter set (96188, Nikon) or a custom set composed of a 430-460 nm bandpass excitation filter, a 475 nm longpass beamsplitter, and a 480-520 nm bandpass emission filter. EGFP and mWasabi were imaged using either a standard EGFP filter set (41017, Chroma), a QuantaMaxTM Green set (Omega), or a BrightLine GFP set (3035B, Semrock).

## 4.3 RESULTS AND DISCUSSION

### 4.3.1 Blue shifted variants of mTFP1

A series of computational studies have provided support for the idea that there is a partial transfer of charge from the phenolate moiety to the imidazolinone moiety (**Figure 4.1A**) in the excited state of the avGFP anion [58, 124]. Since the phenolate is more electron rich in the ground state than in the excited state, factors that contribute charge stabilization will tend to increase the energy barrier for charge transfer and shift the excitation and emission peaks to higher energy wavelengths (i.e. towards the blue). The crystal structures of mTFP1 [73] and amFP486 [105] (a tetrameric cyan-fluorescing FP from *Anemonia majano*) revealed that these homologous blue shifted FPs both have structurally analogous histidine imidazoles, His197 of mTFP1 and His199 of amFP486, stacked against the phenolate ring of the chromophore (**Figure 4.2A** and **Figure 4.2B**). Due to the involvement of the imidazole in a quadrupole salt bridge network (with Glu148, Glu215, and Arg70 in mTFP1; Glu150, Glu217, and Arg72 in amFP486) it is likely to have significant cationic character. A simple electrostatic interpretation of the imidazole-chromophore interaction might therefore suggest that this cationic character is helping to stabilize anionic character on the phenolate ring. Other mutagenesis-based studies have provided support for the idea that the side chain of the residue aligning with residue His163 of mTFP1 (**Figure 4.2A**), or a buried water molecule that occupies the cavity when the side chain is small (as is the case of Ala165 in amFP486 as shown in

Figure 2B), also has an important role in stabilizing anionic character on the phenolate ring [47]. Henderson et al. have proposed that the electrostatic interaction with His199 is of greater significance than the interaction with the water molecule in the residue 165 side chain cavity for causing the blue shifted emission of the amFP486 chromophore [105]. The relative importance of His197 and His163 with respect to the blue shift of the mTFP1 chromophore has not been investigated.

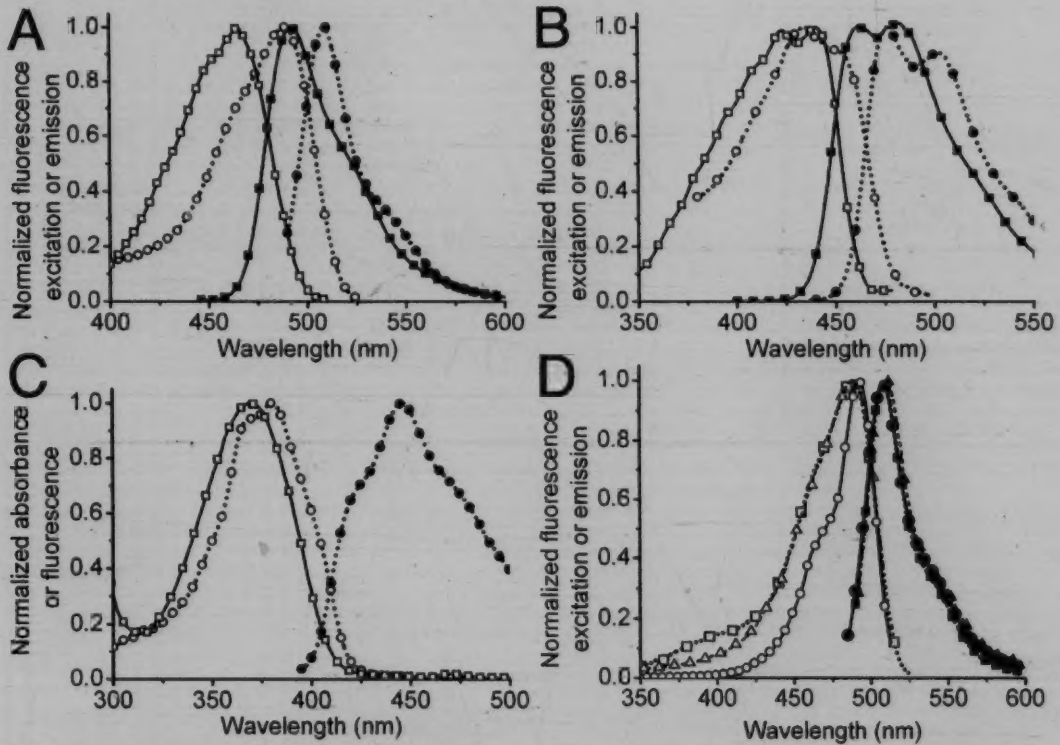


**Figure 4.3** Spectra of hue-shifted variants of mTFP1. (A) Excitation (open symbols) and emission (filled symbols) spectra of EGFP (circle) and mTFP1 (square). (B) Excitation (open symbols) and emission (filled symbols) spectra of ECFP (circle) and mTFP1-Y67W (square). (C) Excitation (open symbols) and emission (filled symbols) spectra of EBFP (circle) and the absorbance (open symbols) spectrum of the nonfluorescent mTFP1-Y67H variant (square). (D) Excitation (open symbols) and emission (filled symbols) spectra of mWasabi (circle), EGFP (square) and Emerald (triangle). Spectra were collected at 1 nm steps, but only every 5th data point is shown for clarity.

It was reasoned that if this electrostatic-based mechanism for 'fine tuning' of the emission wavelength is indeed operative in mTFP1, variants with alternative

chromophore structures, should also be blue shifted relative to their avGFP analogues. Two qualifications are that formation of the excited state still involves charge transfer to the imidazolinone ring and that significant repacking of the side chains lining the chromophore-containing cavity does not occur with the new chromophore structure. To investigate if this mechanism for blue shifting the fluorescence could be translated to alternative chromophore structures, I created the Tyr67Trp and Tyr67His mutants of mTFP1. The chromophore structures of mTFP1-Y67W and mTFP1-Y67H are chemically identical to that of avGFP-derived ECFP and EBFP, respectively (**Figure 4.1B** and **Figure 4.1C**). Accordingly, I expected that the absorbance and fluorescence emission maxima of mTFP1-Y67W and ECFP (and mTFP1-Y67H and EBFP) would be similar but not necessarily identical. If differences between the spectra of the two proteins were observed, they must be attributable to the effect of the protein environment on the chromophore.

Measuring the absorbance and emission spectra of purified mTFP1-Y67W revealed that this protein is fluorescent, exhibits the typical double-humped peaks associated with a tryptophan-derived chromophore, and is blue shifted relative to ECFP (**Figure 4.3B**). Considering the mean wavelength at half maximum intensity, the excitation and emission peaks are shifted by 13 nm and 13.5 nm, respectively. This result contrasts with a previous report in which it was demonstrated that the analogous substitution in amFP486 results in a protein that is not blue shifted relative to avGFP-derived CFP [47]. The purified mTFP1-Y67H variant exhibited no significant fluorescence, but it did have a strong absorbance peak that was blue shifted by 10.5 nm (mean wavelength at half maximum intensity relative to avGFP-derived EBFP (**Figure 4.3C**).

These results demonstrate that the protein-chromophore interactions responsible for blue shifting the absorbance and emission maxima (i.e. raising the energy of the excited state) of mTFP1 are not entirely dependent on the presence of a tyrosine-derived chromophore. In the crystal structure of mTFP1, the imidazole of His163 is observed to form a hydrogen bond with the phenolate oxygen of the chromophore (**Figure 4.2A**). An analogous interaction is not possible in the mTFP1-Y67H or mTFP1-Y67W variants. In contrast, the close stacking of the His197 imidazole against the phenolate chromophore is an interaction that could be preserved in the mTFP1-Y67W or mTFP1-Y67H variants. I

conclude that the hydrogen bond with His163 is not significant with respect to the blue shift of mTFP1 and it is either the close stacking of the His197 imidazole and/or a hydrogen bond-independent electrostatic effect of His163 that is responsible for the blue shift. Based on the interaction of His163 with the carboxylate of Asp144 (**Figure 4.2A**), it is plausible that the imidazole could have significant cationic character.

**Table 4.1** Properties of hue-shifted mTFP1 variants

| | $\lambda_{ex}$ (nm) | $\lambda_{em}$ (nm) | $\varepsilon$ ($mM^{-1}cm^{-1}$) | $\phi$ | Brightness[a] ($mM^{-1}cm^{-1}$) | pKa | Photostability[b] |
|---|---|---|---|---|---|---|---|
| mTFP1-Y67W | 424/440[c] | 461/482[c] | 13 | 0.02 | 0.3 | ND[d] | ND |
| mTFP1-Y67H | 369[e] | NA[f] | 7 | NA | NA | ND | NA |
| G1 | 487 | 503 | 43 | 0.60 | 26 | ND | ND |
| G2 | 487 | 503 | 60 | 0.65 | 39 | ND | 65 |
| G3 | 498 | 515 | 70 | 0.70 | 49 | ND | 5.5 |
| mWasabi | 493 | 509 | 70 | 0.80 | 56 | 6.5 | 93 |
| mTFP1[g] | 462 | 492 | 64 | 0.85 | 54 | 4.3 | 110 |
| EGFP[h] | 488 | 507 | 56 | 0.60 | 34 | 6.0 | 174 |

[a] Product of extinction coefficient and quantum yield. [b] Time in seconds to bleach from an initial emission rate of 1000 photons/s/molecule to 500 photons/s/molecule. [c] Values for both 'humps' are provided. [d] ND, not determined. [e] This value is the absorption maximum. No significant fluorescence was detected for mTFP1-Y67H. [f] NA, not applicable. [g] Values from [73]. [h] Values from [68].

### 4.3.2 Red shifted variants of mTFP1

A reasonable approach to dissecting the relative importance of His163 and His197 in blue shifting mTFP1 fluorescence is to examine variants in which the identity of one residue is changed through the use of site-directed mutagenesis. It has previously been shown that His199 of amFP486, which is structurally analogous to His197 of mTFP1, is stacked against the chromophore and has multiple critical roles that dictate the spectroscopic properties (**Figure 4.2B**) [105]. I expected that, in the absence of high-

resolution crystal structures, interpretation of the effects of mutation at this position would pose a significant challenge. I opted instead to focus on His163 since it is not strictly conserved between the natural cyan-fluorescing proteins and thus less likely to have multiple critical roles. I performed saturation mutagenesis of mTFP1 at position 163 and screened the library using a colony-based fluorescence imaging system. Screening revealed that the library contained both brightly cyan-fluorescing and green-fluorescing members. DNA sequencing revealed that the bright cyan-fluorescing members of the library had, as expected, a histidine at position 163 and were thus identical to mTFP1. The brightest green-fluorescing member had a methionine at position 163 and a fluorescence emission maximum at 503 nm (**Table 4.1**). The fact that the emission maximum of mTFP1-H163M is 11 nm red shifted from that of mTFP1 provides strong support for His163 contributing to the blue shift of the mTFP1 chromophore by an electrostatic mechanism. As to why methionine, as opposed to some other amino acid, was identified as the best replacement for His163, I can suggest two possible reasons. The first is that the methionine side chain could simply be the best steric fit in the cavity formerly filled by the side chain of His163. The second is that the sulphur atom of the methionine side chain may be participating in sulphur-aromatic interactions with the chromophore. Such interactions have previously been used to explain improvements in the extinction coefficient in avGFP variants [125].

So is His163 solely responsible for the blue shift of mTFP1 or does His197 also play a role? That is, does the emission maximum of 503 nm for mTFP1-H163M represent an appropriate 'reference' state for this particular chromophore structure when located in this particular chromophore cavity and in the complete absence of any blue shifting effects? Previous work suggests that the answer to the latter question is probably no, and the emission maximum of the reference state is more likely to be approximately 515 nm. One piece of evidence supporting this suggestion is that the emission maximum of amFP486-H199T is 515 nm [105]. This variant has essentially an identical chromophore cavity to mTFP1, with the obvious exception of the His199Thr replacement. The second piece of evidence in support of this suggestion is that the GFP-T203H mutant has a fluorescence emission at 517 nm when excited at 475 nm [57]. Residue Thr203 of GFP [38] is structurally aligned with His197 of mTFP1 (compare **Figure 4.2A** and **Figure**

**4.2C**), and thus GFP-T203H likely has an imidazole-chromophore stacking interaction similar to that of mTFP1 [105]. However, unlike the positively charged imidazole of His197 in mTFP1, the imidazole of His203 in GFP-T203H is expected to be in the neutral charge state.

In a later section I will describe the discovery of the Thr73Ala substitution that red shifted the fluorescence of mTFP1-K139E/H163M from 503 nm to 515 nm. However, it is appropriate to discuss the implications of this fortunate finding in the current context. In the crystal structure of mTFP1, the hydroxyl group of Thr73 is hydrogen-bonded to the guanidium group of Arg70: a key participant of the quadrupole salt-bridge network responsible for maintaining the imidazole of His197 in the positively charged state (**Figure 4.2A**). I propose that the loss of the Thr73-Arg70 hydrogen bond in the Thr73Ala mutant perturbs the salt-bridge network such that the cationic character of His197 imidazole is greatly diminished or abolished. Accordingly, the Thr73Ala mutant effectively separates the electrostatic role of His197 from its additional roles in maintaining the chromophore environment and reveals that the electrostatic effect of this residue accounts for a blue shift of at least 12 nm.

The mutagenesis-based study supports the conclusion that His163 and His197 act in concert to blue shift the fluorescence emission of the mTFP1 chromophore through an electrostatic mechanism. The contribution of both residues is effectively identical with 11 nm and 12 nm of blue shift attributed to His163 and His197 respectively. This result is essentially consistent with previous studies of amFP486 which have suggested complementary roles for His199 and the water molecule adjacent to Ala165 in achieving the blue shift [47, 105]. The crystallographic and mutational study by Henderson et al. supports the conclusion that the water molecule adjacent to Ala165 has a less significant contribution than His199 [105]. In mTFP1 the (plausibly) cationic imidazole group of His163 could contribute a significant amount of electrostatic stabilization to electron density on the phenolate ring. A similar interaction is not possible in amFP486 since a lone water molecule sits in the location occupied by the His163 imidazole of mTFP1. A caveat is that the electron density modeled as a water in the amFP486 structure could actually be a sodium ion or other cation (S. James Remington, personal communication), in which case an electrostatic contribution would be not unreasonable.

### 4.3.3 Directed evolution of the red shifted variant of mTFP1

Intrigued by the high apparent fluorescent brightness of mTFP1-H163M (hereafter designated G1), I subjected this template to directed evolution in an effort create a new green FP (GFP) variant that could potentially be useful for live cell imaging. EP-PCR was used to create libraries of genetic variants, the gene libraries were expressed in *E. coli*, and colonies were screened for bright green fluorescence. The brightest green fluorescent colony identified in the first round of screening was found to express a G1 variant with the additional mutation Lys139Met (designated G2). This variant was used as the template for a second round of library construction and screening. The brightest variant identified in the second round was found to be mTFP1-T73A/K139M/H163M (designated G3). It is interesting to note that the Thr73Ala mutation present in G3 is structurally aligned with the Ser72Ala mutation that has been reported to improve the brightness of avGFP variants [84]. No further improvements were identified during a third round of screening of randomly mutated variants based on the G3 template. In vitro characterization (**Table 4.1**) of the purified green fluorescing variants revealed that relative fluorescent brightness to be 1, 1.5, and 1.9 for G1, G2, and G3, respectively. While both G1 and G2 had fluorescence maxima at 503 nm, G3 was further red shifted to 515 nm. The implications of this result have been discussed above.

Further investigation of the G2 and G3 variants revealed that the dimmer G2 was 11.8-fold more photostable than the brighter G3 variant. In my experience mutations that improve fluorescent brightness are much more readily identified than mutants that improve photostability. For this reason I forsook the brighter G3 variant and continued optimization based on the G2 template. Saturation mutagenesis at 3 positions chosen based on their proximity to the chromophore (Ala66, Val161, and Ile199) resulted in the identification of a further improved variant containing the Ala66Ser substitution. A subsequent round of random mutagenesis resulted in the identification of the Ser216Ile substitution. Additional rounds of random mutagenesis yielded no further improvements. The end product of this process is a brightly fluorescent GFP (emission maximum = 509 nm) that is equivalent to mTFP1-A66S/K139E/H163M/S216I and has been designated mWasabi. The fluorescence emission maximum of mWasabi is intermediate between that of G1 and G3, suggesting that there has been a perturbation of the salt-bridge network. It

has been previously reported that avGFP with a Ser at residue 65 is 5 nm red shifted from avGFP with an Ala at residue 65 [40]. As observed in the avGFP-S65T structure (**Figure 4.2C**), the hydroxyl group of the Ser at residue 66 of mWasabi could potentially form a new hydrogen bond with Glu215 and partially disrupt its ability to contribute to the critical salt-bridge network.

In vitro characterization of mWasabi (**Table 4.1**) revealed that it is 1.6-fold brighter than EGFP, making it one of the brightest and most photostable FPs currently available [68]. Another notable feature of mWasabi is its very narrow excitation and emission peaks (**Figure 4.3D**) that are reminiscent of the spectrum of *Renilla* GFP [126] and monomeric Azami-Green [96]. Narrower peaks allow for more efficient excitation and gathering of emission when used in combination with bandpass filters, and reduce the degree of bleed-through in multicolor imaging.

### 4.3.4 Two color imaging with mWasabi and Sapphire

EGFP and its descendents have major absorption peaks at ~488 nm [127-129]. However, due to both the breadth of this peak and the fact that in some variants a significant fraction of the protein exists as the UV-excitable neutral chromophore, EGFP and related variants are efficiently excited with violet light (~400 nm) (**Figure 4.3D**). This residual excitation with 400 nm light can unnecessarily complicate multiple color imaging in combination with a Sapphire-type variant [37, 39, 122] or fluorescence resonance energy transfer (FRET) experiments with a BFP donor [41, 130]. In terms of fluorescence emission, mWasabi, EGFP and Emerald have almost identical emission peak shapes (**Figure 4.3D**). In contrast, the differences in their excitation spectra are pronounced, with mWasabi showing almost no excitable component below 410 nm. This suggested that mWasabi would be superior to EGFP for use in two-color imaging with Sapphire. To test this proposal, mWasabi and EGFP were fused with a nuclear localization signal (NLS) and separately co-expressed with Sapphire-β-actin in HeLa cells. As shown in **Figure 4.4**, exciting Sapphire with a typical 375-415 nm bandpass excitation filter resulted in significant EGFP fluorescence as observed in the cell nucleus. In contrast, no significant fluorescence was observed for mWasabi in the cell nucleus when Sapphire was imaged under identical conditions. This result demonstrates that

mWasabi is particularly well suited for multicolor imaging in combination with fluorophores that are excitable with violet light.

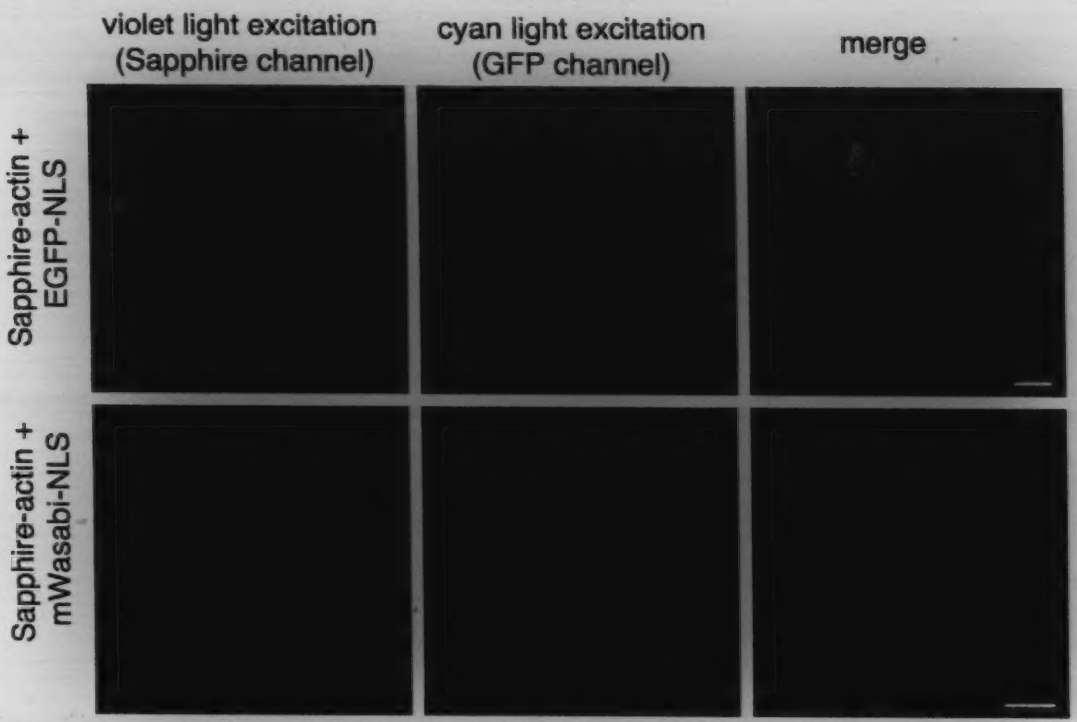


**Figure 4.4** Two color imaging with Sapphire/EGFP. Shown in the upper row of panels are HeLa cells that have been transfected with plasmids for expression of both Sapphire-actin and EGFP-NLS. Shown in the lower row of panels are identically treated HeLa cells expressing Sapphire-actin and mWasabi-NLS. Due to the residual excitation of EGFP at 400 nm, the nucleus fluoresces brightly in the Sapphire emission channel in the top row of panels. In contrast, mWasabi is not significantly excited at 400 nm and thus the nucleus is much dimmer than the actin filaments in the bottom row of panels. Scale bars represent 10 micrometers.

### 4.3.5 Imaging of mTFP1 and mWasabi fusion proteins

Both mTFP1 and its green-emitting progeny, mWasabi, are the products of an extensive process of protein engineering and directed evolution. During the development of these proteins, substantial effort was expended to find variants with the desired color, high fluorescent brightness, high folding and maturation efficiency, and high photostability. The *in vitro* characterization of these proteins confirms that I was indeed successful in engineering proteins with the desired properties. However, the ultimate goal

of this research is not to simply develop new FPs, but rather to develop FPs that will be useful tools for fluorescence imaging in living cells. To be generally useful for live cell imaging, a FP should retain its favorable properties either when fused to a variety of proteins or when targeted to a variety of subcellular compartments. In addition, the FP should not perturb the normal localization or biological function of the protein to which it is genetically fused. Such a perturbation can be caused by oligomerization of the FP: a problem that should not be relevant to monomeric FPs such as mTFP1 and mWasabi.

In **Chapter 2** I demonstrated that mTFP1 could be successfully fused with β-actin and α-tubulin protein without perturbing the native cytoskeletal structure. In this work I sought to explore the range of proteins that would tolerate fusion to mTFP1 and mWasabi by collaboration with Michael W. Davidson. A series of 22 different mTFP1 fusions (**Figure 4.5** and **Figure 4.6**) to both the C- and N-terminus of the FP were created and it was found that in all cases, the fusion proteins yielded a pattern of localization consistent with that observed for previously validated avGFP fusions. As shown in **Figure 4.6**, fusions to histone H2B and annexin A4 did not interfere with the normal cellular function of these proteins. A series of 20 similar fusions with mWasabi gave identical results (**Figure 4.7**). It is apparent that mTFP1 and mWasabi are robust and versatile fluorescent proteins that tolerate a wide variety of protein fusions and subcellular microenvironments.

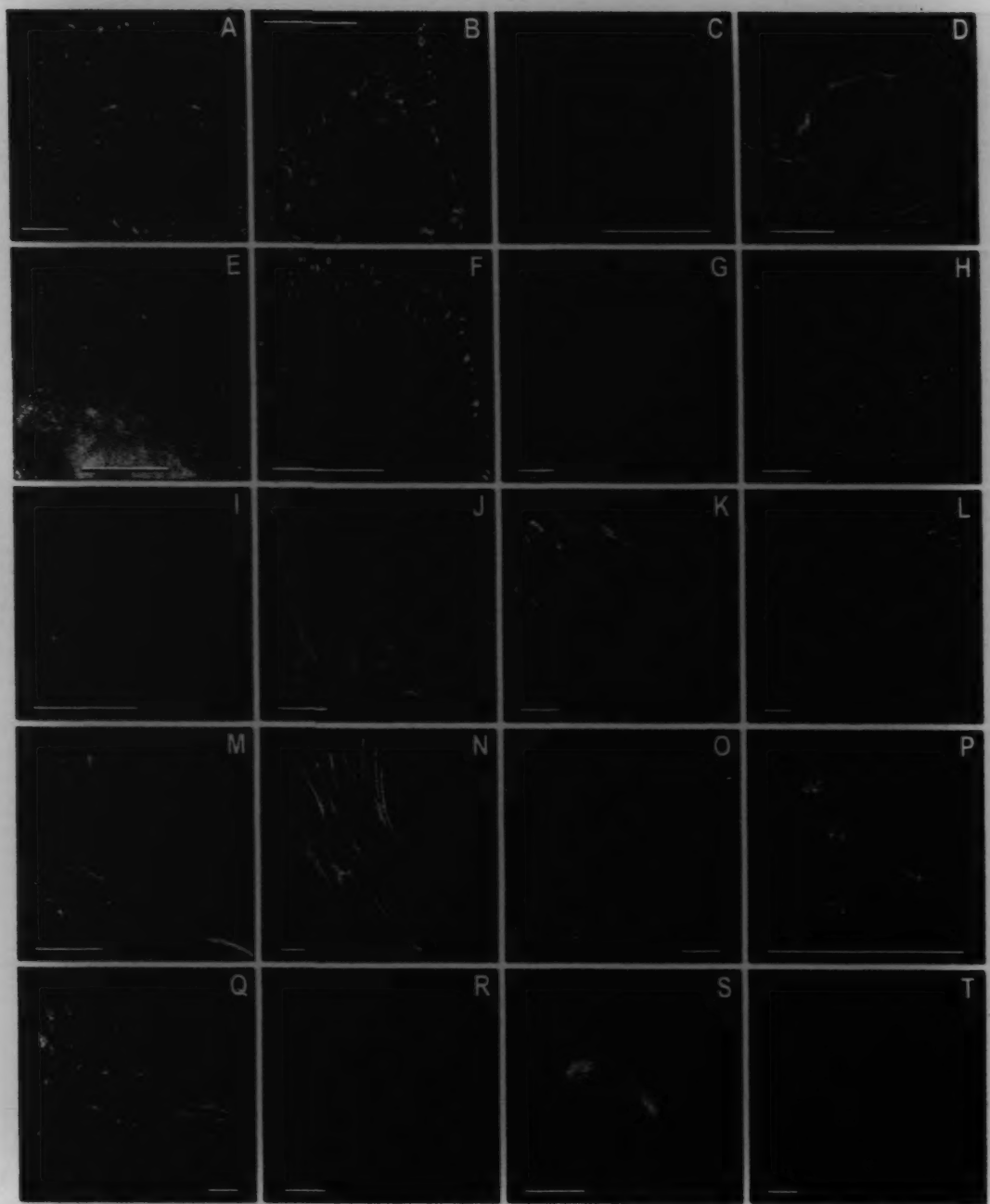


**Figure 4.5** Fluorescence imaging of mTFP1 fusion constructs. (A – K) N-terminal fusion constructs. For each fusion protein the linker amino acid length is indicated after the name of the targeted organelle or fusion protein. (A) mTFP1-α-actinin-19 (human non-muscle); (B) mTFP1-mitochondria-7 (human cytochrome C oxidase subunit VIII); (C) mTFP1-Cx43-7 (rat α-1 connexin-43); (D) mTFP1-keratin-17 (human cytokeratin 18); (E) mTFP1-endoplasmic reticulum-3 (calreticulin signal sequence (51 nucleotides)

and KDEL retention sequence); (F) mTFP1-paxillin-22 (chicken); (G) mTFP1-EB3-7 (human microtubule-associated protein; RP/EB family); (H) mTFP1-lysosomes-20 (rat lysosomal membrane glycoprotein 1); (I) mTFP1-golgi-7 (N-terminal 81 amino acids of human $\beta$-1,4-galactosyltransferase); (J) mTFP1-vimentin-7 (human); (K) mTFP1-zyxin-7 (human). (L – T) C-terminal fusion constructs. (L) mTFP1-focal adhesion kinase-5 (chicken protein tyrosine kinase 2); (M) mTFP1-lamin B1-10 (human); (N) mTFP1-$\beta$-actin-7; (O) mTFP1-clathrin light chain-15 (human); (P) mTFP1-fibrillarin-7 (human); (Q) mTFP1-vinculin-23 (human); (R) mTFP1-peroxisomes-2 (peroximal targeting signal 1; PTS1); (S) mTFP1-β-tubulin-6 (human); (T) mTFP1-farnesyl-5 (20-amino acid farnesylation signal from c-Ha-Ras). The cell line used for expressing mTFP1 fusion vectors was gray fox lung fibroblast cells (FoLu) in panels (A, G, K, N, and Q) and human cervical adenocarcinoma cells (HeLa) in the remaining panels. Scale bars represent 10 micrometers.

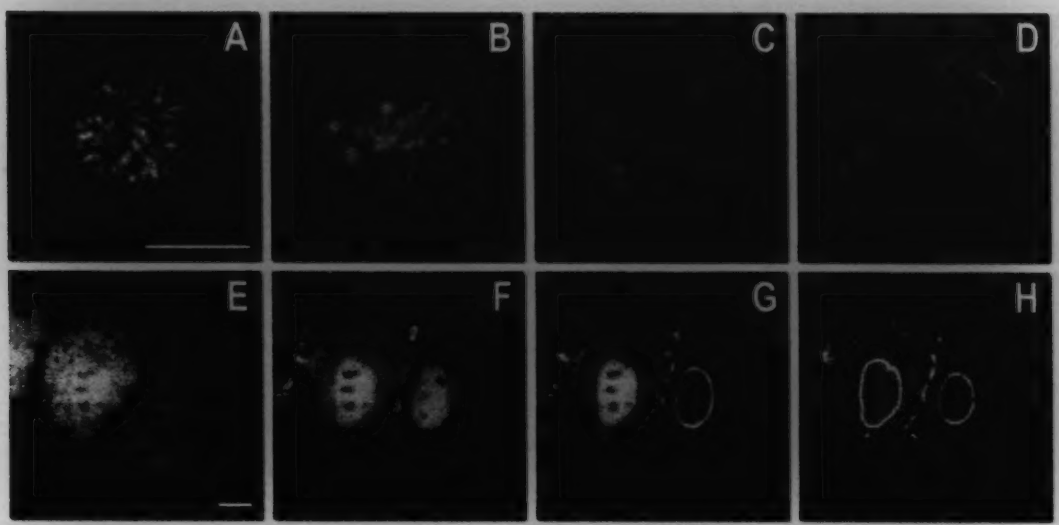


**Figure 4.6** Live cell imaging of mTFP1 fusion vectors. (A – D) Laser scanning confocal images of a single HeLa cell expressing mTFP1-H2B-6 (N-terminus; human) progressing through prophase, metaphase, anaphase, and interphase, respectively. (E - H) Spinning disk confocal images selected from a time-lapse series of HeLa cells expressing mTFP1-annexin (A4)-12 (C-terminus; human) during ionomycin-induced translocation to the plasma and nuclear membranes [131]. (E) time = 0, ionomycin added; (F) time = 5 min; (G) time = 7 min; (H) time = 9 min. Scale bars represent 10 micrometers.

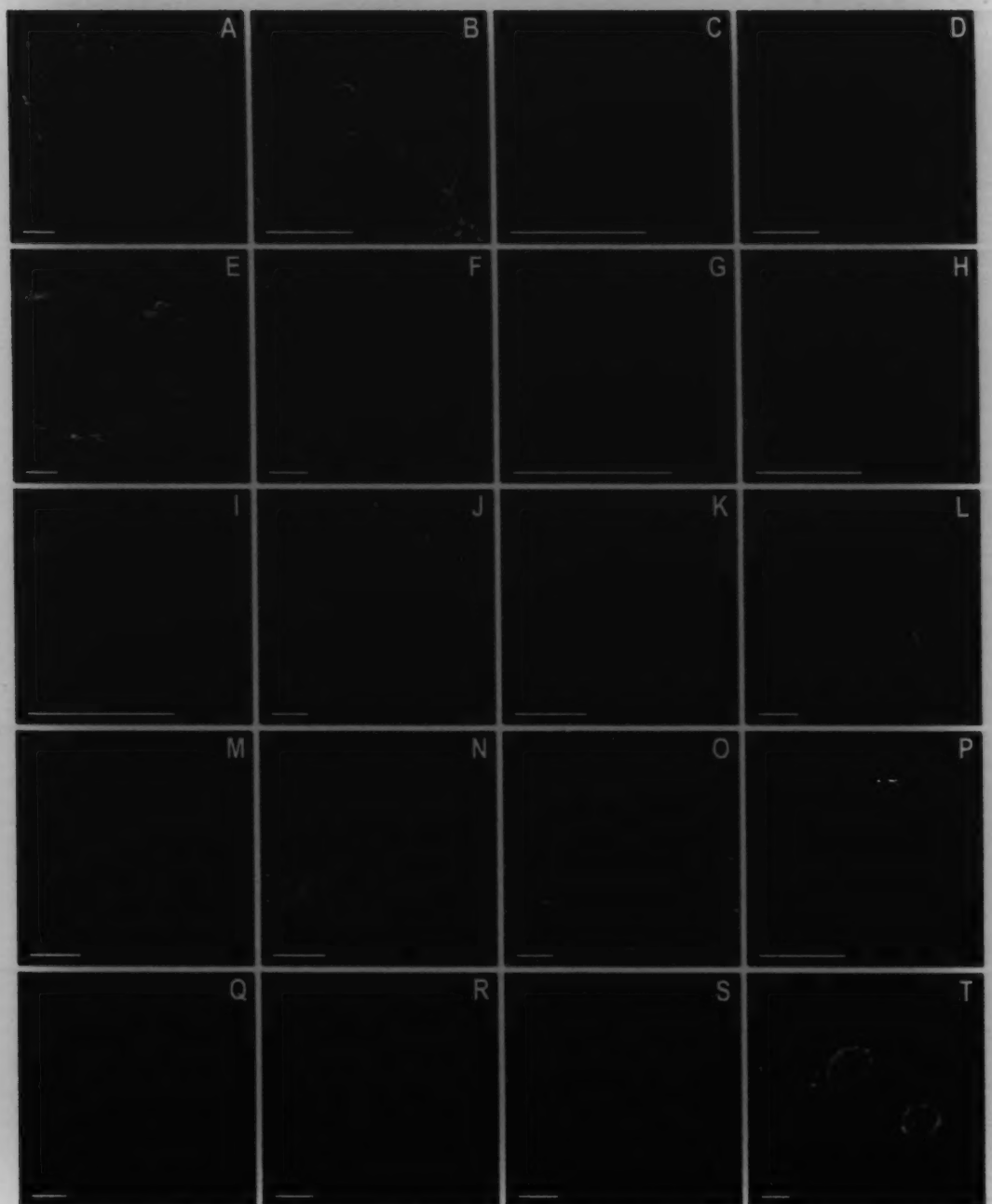


**Figure 4.7** Live cell imaging of mWasabi fusion vectors. (A – J) N-terminal fusion constructs. For each fusion protein the linker amino acid length is indicated after the name of the targeted organelle or fusion protein. (A) mWasabi-a-actinin-19 (human non-muscle); (B) mWasabi-mitochondria-7 (human cytochrome C oxidase subunit VIII); (C) mWasabi-Cx26-7 (rat b-2 connexin-26); (D) mWasabi-keratin-17 (human cytokeratin 18); (E) mWasabi-paxillin-22 (chicken); (F) mWasabi-EB3-7 (human microtubule-

associated protein; RP/EB family); (G) mWasabi-golgi-7 (N-terminal 81 amino acids of human b-1,4-galactosyltransferase); (H) mWasabi-vimentin-7 (human); (I) mWasabi-H2B-6 (human); (J) mWasabi-zyxin-7 (human). (K – T) C-terminal fusion constructs. (K) mWasabi-lamin B1-10 (human); (L) mWasabi-b-actin-7; (M) mWasabi-b-tubulin-6 (human); (N) mWasabi-clathrin light chain-15 (human); (O) mWasabi-vinculin-23 (human); (P) mWasabi-farnesyl-5 (20-amino acid farnesylation signal from c-Ha-Ras); (Q) mWasabi-focal adhesion kinase-5 (chicken protein tyrosine kinase 2); (R) mWasabi-peroxisomes-2 (peroximal targeting signal 1; PTS1); (S) mWasabi-endosomes-15 (human RhoB GTPase with an N-terminal c-Myc epitope tag); (T) mWasabi-annexin (A4)-15 (human). The cell line used for expressing mWasabi fusion vectors was gray fox lung fibroblast cells (FoLu) in panels (E and F) and human cervical adenocarcinoma cells (HeLa) in the remaining panels. Scale bars represent 10 micrometers.

## 4.4 CONCLUSIONS

In this Chapter, I have described a series of mutagenesis experiments that have provided fundamental insight into the amino acids that dictate the color of the mTFP1 chromophore. The data here supports the conclusion that His163 and His197 act in an independent and additive fashion to increase the energy of the electronic transitions responsible for absorbance and fluorescence. Although determining the precise details of the mechanism are beyond the scope of my research, the results are consistent with a previous proposal that electrostatic stabilization of charge density on the phenolate ring is a general means of achieving blue shifted emission in FPs [105].

The investigations into the amino acid determinants of the color of mTFP1 led to a series of hue-shifted variants, one of which was subjected to further engineering and directed evolution to eventually produce mWasabi. While mWasabi is an exceptionally bright and reasonably photostable GFP, I readily acknowledge that for most experiments EGFP or Emerald should remain the GFP of choice. However, there are a number of specific applications, such as two-color imaging in conjunction with a Sapphire-type variant or as a FRET acceptor with a BFP donor, where the negligible excitation of mWasabi at 400 nm provides a substantial benefit. Both mTFP1 and mWasabi are well behaved in protein chimeras, offering a bright and photostable fluorescent signal with no significant perturbation of the localization or function of the protein of interest. This

combination of desirable features firmly establishes mTFP1 and mWasabi as useful members of the FP toolkit.

# CHAPTER 5:

# EXPLORATION OF NEW CHROMOPHORE STRUCTURES LEADS TO THE IDENTIFICATION OF IMPROVED BLUE FLUORESCENT PROTEINS

The research described in this chapter has been reported in *Biochemistry* [76]. It should be clearly pointed out that Zihao Cheng created mBlueberry1 and mCherry2-Y67H, and Nathan C. Shaner together with Roger Y. Tsien at the University of California San Diego should be credited for the creation of mBlueberry2 and EBFP1.2.

## 5.1 INTRODUCTION

Certain intrinsic photophysical properties of a FP, such as quantum yield and propensity to photobleach, are necessarily determined by both the covalent structure of the chromophore (**Figure 5.1A-H**) as well as by the interactions of the chromophore with the surrounding amino acid residues. The extinction coefficient depends on these same factors as well as on the folding and chromophore maturation efficiency. A particular challenge facing protein engineers seeking bright new hues of FPs is that the key mutation for creation of a new color necessarily involves a dramatic change in the chromophore structure or environment. This dramatic change typically has severe adverse effects on the protein folding and chromophore formation efficiency. Furthermore, when the covalent structure of the chomophore has been altered by the mutation (i.e. by replacement of Tyr66 with a different aromatic amino acid, refer to **Figure 5.1**), the surrounding residues generally require optimization to once again maximize brightness. The growing number of reports in which researchers have significantly modified a FP but then optimized it for its new favorable properties could understandably leave one with the impression that all new colors of FP are readily amenable to improvement [41, 73, 132]. However, it was found that some chromophore structures (e.g. mHoneydew [50], **Figure 5.1F**) are seemingly more resistant to improvement than others (e.g. mTFP1 in **Chapter 2**). This observation led us to question whether certain suboptimal FP variants are limited by the intrinsic properties of their chromophore or by insufficient effort expended in their optimization.

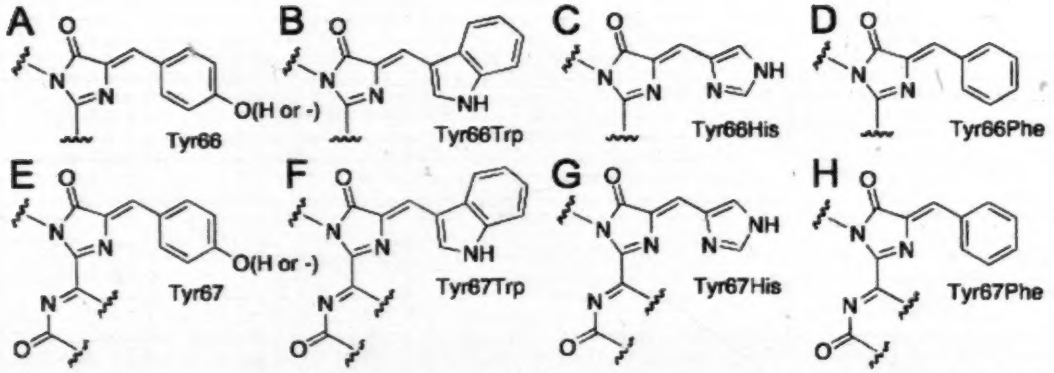


**Figure 5.1** Representative covalent structures of chromophores. (A) Wild-type GFP ground state [133] and mKalama1 (phenol), EGFP [40] and mTFP1 (phenolate); (B) ECFP [39]; (C) EBFP variants; (D) GFP-Y66F; (E) Keima ground state [69] (phenol), DsRed [134] and most mFruit variants [50] (phenolate); (F) mHoneydew [50]; (G) mCherry2-Y67His; and (H) mBlueberry variants. Although they are not represented in this figure, non-covalent interactions between the protein and the chromophore (e.g., the cationic imidazole ring of His197 in mTFP1) are also important determinants of the fluorescence hue.

A particularly interesting case study that epitomizes the challenges described in the preceding paragraph is the development of the protein now known as enhanced blue FP (EBFP). Concurrent with the first reports detailing the heterologous and functional expression of the GFP in organisms other than jellyfish [114, 115, 135], researchers were already working to create the GFP variant that would be progenitor of EBFP [39]. Introduction of the Tyr66His mutation (**Figure 5.1C**) into wild type GFP (excitation maxima at 395 and 475 nm and emission maximum at 508 nm) produced a variant with a fluorescence emission wavelength substantially blue shifted (excitation maximum at 383 nm and an emission maximum at 447 nm) from that of the wild-type protein [39]. As might be expected for such a radical change in the chromophore structure, the resulting protein had a relatively poor extinction coefficient ($\varepsilon$) of 13,500 $M^{-1}cm^{-1}$ and quantum yield ($\phi$) of 0.21. In the first reported effort to improve the brightness, screening of ~$10^4$ colonies expressing randomly mutated versions of the Tyr66His variant was sufficient for the identification of the 2-fold brighter Y66H/Y145F double mutant [41] which was designated BFP. The utility of BFP was further improved by introducing these two mutations into a codon optimized synthetic gene encoding GFP-F64L/S65T (known as

EGFP) [136]. The resulting protein, known as EBFP, remained essentially uncontested as the best available example of a blue fluorescing FP until very recently [137]. Initially, the EBFP/EGFP pair was the only option for dual color imaging and fluorescence resonance energy transfer (FRET) experiments. However, with the advent of the brighter, more photostable, and distinguishable FP hues of cyan (CFP) and yellow (YFP), there was no longer any need for researchers to tolerate the dim fluorescence and fast photobleaching of the EBFP half of the EBFP/EGFP pair. The relevance of EBFP has been further diminished by the relatively recent and explosive growth in the availability of red hues of FPs, most notably the mFruit series of variants [50]. The mFruit series provides a number of new distinguishable colors that can be paired with EGFP for 2-color imaging, or with CFP and YFP for 3-color imaging.

A bright and reasonably photostable FP with fluorescence at ~450 nm has long remained a conspicuous absence from the selection of FPs that are recommended for use in live cell imaging [68]. However, this situation appears to have changed with the recent report of Azurite, a new BFP isolated from a computationally designed library by flow cytometry [137, 138]. The photostability of Azurite is improved 40-fold relative to BFP, putting Azurite on par with some of the less photostable of the more popular and practical FPs commonly used in live cell imaging [68]. It is reasonable to expect that Azurite will find widespread use as a distinct 3$^{rd}$ color (e.g. when used in combination with EGFP and mCherry) in cytometry and fluorescence imaging applications. However, blue fluorescent variants with further improvements in both brightness and photostability would be desirable.

In the efforts to develop a superior alternative to EBFP I have investigated the potential utility of a variety of alternative blue-fluorescing FPs with chemically distinct chromophore structures. Herein I describe the creation of novel FPs including a blue-fluorescing variant of GFP with a tyrosine-derived chromophore, improved versions of EBFP and blue-fluorescing variants of *Discosoma* red FP (RFP). These efforts have resulted in the creation of variants that are both brighter and more photostable than Azurite. The usefulness of the new BFPs in fluorescence imaging applications is compared and recommendations are made.

## 5.2 EXPERIMENTAL

### 5.2.1 General Methods

All routine molecular biology procedures were carried out as previously described in **Section 2.2**. Synthetic DNA oligonucleotides for cloning and library construction were purchased from Integrated DNA Technologies (Coralville, IA USA). PCR products and products of restriction digests were routinely purified using the QIAquick PCR purification kit (Qiagen) according to the manufacturers protocols. Restriction endonucleases were purchased from either Invitrogen or New England Biolabs. The cDNA sequences for all FP variants and fusion constructs were confirmed by dye terminator cycle sequencing using the DYEnamic ET kit (Amersham Biosciences). Sequencing reactions were analyzed at the University of Alberta Molecular Biology Service Unit. All filters for fluorescence screening and imaging were purchased from Chroma Technology (Rockingham, VT USA).

### 5.2.2 Library construction and mutagenesis

Gene libraries with saturation mutagenesis at a particular residue and libraries of randomly mutated genes were constructed as previously described in **Section 2.2**. PCR products were digested with Xho1 and EcoR1 and ligated into similarly digested pBAD/His B vector (Invitrogen). Electrocompetent *E. coli* strain DH10B (Invitrogen) was transformed and plated on LB/agar plates supplemented with ampicillin (0.1 mg/ml) and L-arabinose (0.02%). Plates were incubated for 14 h at 37 °C prior to screening. To create the gene encoding Azurite [137], site-directed mutagenesis was used to introduce the T65S (reversion to wild type), V150I, and V224R mutations in EBFP.

### 5.2.3 Screening

The screening system has been described previously in **Section 2.2**. Briefly, the light from a 175W xenon-arc lamp (Sutter) is passed through a 375 nm to 415 nm bandpass filter and into a bifurcated fiber optic bundle (Newport). Light exiting the fiber optic bundle illuminates a 10 cm dish placed in a recessed holder on the bench top. Colony fluorescence was screened by imaging with a Retiga 1300i 12-bit CCD camera

(QImaging) fitted with a 440 nm to 480 nm bandpass filter. A 500 nm to 520 nm bandpass filter was used to measure GFP channel signal during ratiometric screening.

Colonies with more intense fluorescence or higher blue/green ratio were picked and cultured overnight in 4 ml LB media containing ampicillin and arabinose. The following day 0.1 ml of each culture was dispensed into a 96-well plate (Nunc) and the full emission spectra of each variant measured with a Safire2 plate reader (Tecan). Variants with the most blue-shifted and/or intense emission peak were used as templates in the subsequent round of library construction.

### 5.2.4 Protein purification

*E. coli* strain LMG194 was transformed with the pBAD/His B expression vector containing the FP gene of interest. A single colony was used to inoculate a 4 ml culture that was allowed to grow overnight (37 °C, 225 rpm) before being diluted into 1 L of LB media containing ampicillin (0.1 mg/ml) and L-arabinose (0.2%). The culture was allowed to grow for 12 h before cells were harvested by centrifugation and lysed by French Press. Proteins were purified by Ni-NTA chromatography (Amersham).

### 5.2.5 Protein characterization

Absorption spectra were recorded on a DU-800 UV-visible spectrophotometer (Beckman). A QuantaMaster spectrofluorometer (Photon Technology International) was used to acquire the fluorescent excitation and emission spectra. Quantum yields for all blue FP variants were measured using quinine sulfate in 0.1M $H_2SO_4$ as the reference standard [139]. Protein concentrations used in the calculation of extinction coefficients were determined by the BCA method (Pierce). For fluorescence pKa measurements, the protein of interest was first dialyzed into dilute buffer (5 mM Tris HCl, pH 7.5) before dilution into a series of 200 mM buffers. Fluorescent intensity was measured using a fluorescence platereader equipped with monochromators (Tecan).

Photostability measurements were performed essentially as previously described [68, 73]. Briefly, microdroplets of each blue FP were generated by vortexing the protein solution (100 μM) with mineral oil. Approximately 5 μL of this suspension were sandwiched between a glass slide and a glass cover slip. Single drops were identified at low light levels (2.5 % neutral density filters) on a wide-field microscopy equipped with

a 75W HBO lamp. Neutral density filters were removed and the protein drop was imaged with a 50 ms exposure time and without closing the shutter. Typical frame rates were 1 image/s, though it was necessary to go as fast as 3 images/s for the fast bleaching proteins and as slow as 0.03 image/second for the slow bleaching proteins. Bleaching curves were normalized to the photon emission rate of 1000 photon/s/molecule at the staring time. For all experiments, T-Sapphire [68, 140] was subjected to bleaching under identical conditions and used as a reference standard.

### 5.2.6 Live Cell Imaging

To create the nuclear localization plasmid for mammalian expression, the gene encoding each blue FP was PCR amplified with a 5' primer encoding an Nhe1 site and a 3' primer encoding an Xho1 site. The purified and digested PCR product was ligated into the pEYFP-Nuc vector (Clontech) digested with the same restriction enzymes. DNA was purified by Plasmid Midi kit (Qiagen). HeLa cells in 35 mm imaging dishes were transfected with 2 μg plasmid DNA encoding the blue FP and 2 μg pEGFP-Actin (Clontech). Cells were treated with the DNA mixed with 10 μg PEI in 0.5 ml OptiMEM (Invitrogen) and serum was added after 30 min. The next day the medium was exchanged for PBS and the cells were imaged on an Axiovert 200M (Zeiss) equipped with a 75 W xenon-arc lamp. Blue fluorescence was imaged using a 375 nm to 415 nm bandpass excitation filter, a 425 nm longpass beamsplitter, and a 440 nm to 480 nm bandpass emission filter. Green fluorescence was imaged using a 450 nm to 490 nm bandpass excitation filter, a 495 nm longpass beamsplitter, and a 500 nm to 550 nm bandpass emission filter.

## 5.3 RESULTS

### 5.3.1 *Aequorea* GFP variants with a tyrosine-derived chromophore

avGFP-S65G/S72A/T203F (denoted T203F) is a yellow fluorescing GFP variant that has a strong absorption peak at 510 nm and a weak absorption peak at 405 nm [117]. By analogy with wild type GFP (with absorption peaks at 475 and 396 nm), the species that give rise to the two absorption peaks of T203F is an equilibrating mixture of the lower energy anionic phenolate and higher energy neutral phenol forms of the

chromophore, respectively. If wild type GFP is excited at either absorbance peak, a single fluorescence emission peak, attributable to the excited state of the anionic chromophore, is observed at 508 nm. In contrast, excitation of the T203F variant at the 405 nm peak produces a fluorescence peak at 455 nm while excitation at the 510 nm peak produces a fluorescence peak at 525 nm. The dramatically different fluorescence peaks resulting from excitation of the nominally identical neutral phenol chomophores of wild type and T203F is explained by a fast excited state proton transfer (ESPT) that occurs in wild type but not in T203F. PS-CFP, a photoswitchable variant of a GFP homologue from *Aequorea coerulescens* [141], does not undergo ESPT prior to photoactivation.

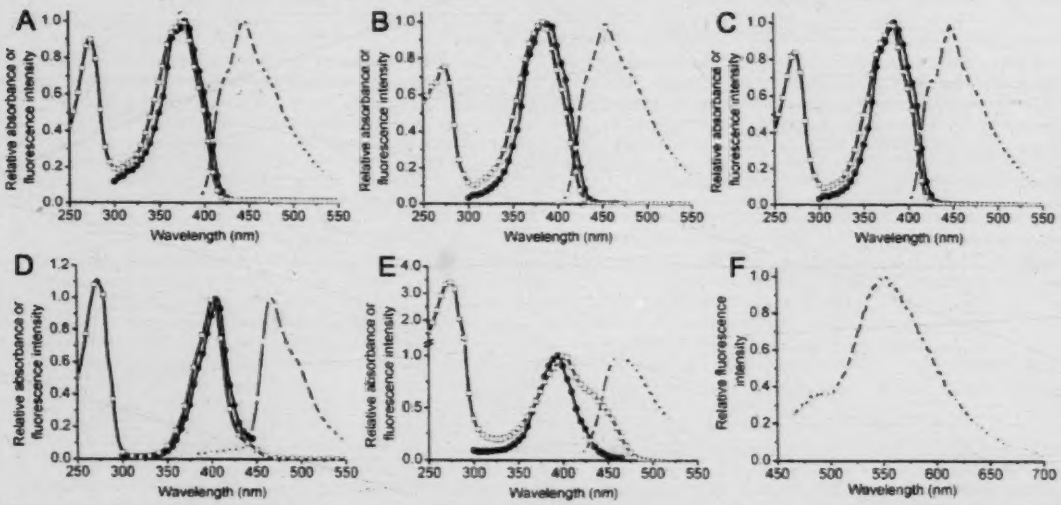


**Figure 5.2** Spectral characterization of new BFP variants. Shown in each panel are the absorbance (green), excitation (black), and emission (red) spectra for the indicated protein. (A) EBFP, (B) mKalama1, (C) EBFP2, (D) mBlueberry2, (E) mCherry2-Tyr67His immediately after purification, (F) fluorescence emission spectrum (excitation at 450 nm) for mCherry2-Tyr67His after 1 day at 4 °C.

It occurred to me that a non-photoswitchable variant of GFP that existed solely in the neutral phenol form in the ground state and that was incapable of ESPT would be a promising alternative to EBFP. With EGFP as the template, I created an initial gene library of ~4000 variants in which Thr65 was mutated to all amino acids and an additional 3 residues in close proximity to the chromophore (His148, Thr203, and Ser205) were simultaneously mutated to a subset of hydrophobic residues. Fluorescence imaging-based screening of this library in bacterial colonies was undertaken to find

variants with strong blue fluorescence (excitation at 400/20 nm and emission 460/40 nm). To screen against variants that existed partially in an anionic phenolate ground state or that were partially capable of ESPT, I performed ratiometric screening for colonies that had high blue fluorescence and low green fluorescence (emission at 525/20 nm when excited with either 400/20 nm or 470/20 nm light). Exhaustive screening of the initial library resulted in the identification of EGFP T65S/H148G/T203V/S205V that exhibited strong blue fluorescence and essentially no green fluorescence (**Figure 5.2B**). Subsequent rounds of both (semi)-saturation (positions 30/39/63/64/105/145/147/153/163/171/175/181) and random mutagenesis were undertaken and halted only when no further improvement had been observed for several rounds of screening. The most brightly fluorescent variant discovered during the directed evolution process had 22 mutations relative to EGFP (**Table 5.1**). In addition, the 'monomerizing' A206K mutation [99] and the Azurite-derived V224R mutation [137] (discussed below) were introduced by site directed mutagenesis. The protein was named mKalama1 after the bright blue waters of Kalamalka lake of southern British Columbia (the preceding 'm' denotes the presence of the A206K mutation). mKalama1 ($\varepsilon$ = 36,000 $M^{-1}cm^{-1}$ and $\phi$ =0.45) is 3.6-fold brighter and 25-fold more photostable than EBFP (**Table 5.2**).

### 5.3.2 Improved versions of *Aequorea*-derived EBFP

I had initially presumed that EBFP was close to the maximum achievable fluorescent brightness for its particular chromophore structure (**Figure 5.1C**). However, the recent report from Waldo and coworkers [129] that introduction of the 'superfolder' mutations into BFP improved the fluorescent brightness in bacterial colonies galvanized us to explore whether these mutations could also benefit EBFP. Mutations S30R/Y39N/S72A/N105T/I171V/N198S/A206V were introduced into EBFP by site-directed mutagenesis to produce EBFP1.2 (EBFP1.2). The fact that EBFP1.2 ($\varepsilon$ = 41,000 $M^{-1}cm^{-1}$ and $\phi$ = 0.45) was 4-fold brighter than EBFP raised the question whether further improvements might be realized by directed evolution. Starting from the EBFP1.2 template, I undertook several rounds of library creation and screening with particular focus on residues in close proximity to the chromophore. This effort resulted in the

identification of EBFP1.2-F145H/H148N/M153A which was designated EBFP1.5 ($\varepsilon$ = 43,000 $M^{-1}cm^{-1}$ and $\phi = 0.53$).

**Table 5.1** Overview of mutations in blue-fluorescing FPs

| Protein | Mutations |
|---|---|
| mKalama1 | EGFP-L18M/H25R/S30R/E32V/Y39H/T50S/T65S/N105S/E124V/ I128T/Y145M/S147V/H148G/M153T/V163A/K166E/I171V/S175G/ P192S/V203T/S205V/A206K/V224R/L213P |
| EBFP | EGFP-Y66H/Y145F |
| EBFP1.2 | EBFP-S30R/Y39N/T65S/S72A/N105T/I171V/N198S/A206V |
| EBFP1.5 | EBFP1.2-F145H/148N/M153A |
| EBFP2 | EBFP1.2-I128V/V150I/ D155V/V224R |
| mBlueberry1 | mCherry2-M66L/Y67F/K70R/Q137R/C138R/Y151C/Q163L/K168R |
| mBlueberry2 | mCherry2-N6aD/M158V/A57T/Y67F/A71V/V73I/L83F/N92R/ E117V/S146F/G159S/Q163T/L202V |
| Azurite | EBFP-T65S/V150I/V224R |

Azurite is a recently described BFP variant with improved brightness and photostability [137]. The two key mutations, V150I and V224R, responsible for the favorable properties of Azurite were introduced into both EBFP1.2 and EBFP1.5. Disappointingly, these substitutions greatly diminished the fluorescence of our most highly optimized EBFP1.5 variant. When introduced into EBFP1.2, these substitutions caused only ~30% decrease in brightness but conferred a remarkable increase in photostability. Additional rounds of random mutagenesis and screening recovered the lost brightness to produce EBFP2, a variant that is 4-fold brighter and 550-fold more photostable than EBFP (**Table 5.1** and **Table 5.2**). Relative to Azurite, EBFP2 is 1.4-fold brighter and 2.9-fold more photostable. Neither Azurite nor EBFP2 contain the A206K

mutation [99] and may retain wild type GFP's tendency to dimerize at high concentrations. However, it has been suggested that the A206V 'superfolder' mutation of EBFP2 could hinder dimerization [129].

**Table 5.2** Properties of new blue-fluorescing FPs

| Parent | Protein | $\lambda_{ab}$ (nm) | $\lambda_{em}$ (nm) | $\varepsilon^a$ | $\phi$ | Bright-ness[b] | pKa | Photo-stability (sec)[c] |
|---|---|---|---|---|---|---|---|---|
| EGFP | mKalama1 | 385 | 456 | 36 | 0.45 | 16 | 5.5 | 2.5 |
| EBFP | EBFP2 | 383 | 448 | 32 | 0.56 | 18 | 5.3 | 55 |
| | EBFP1.5 | 381 | 449 | 43 | 0.53 | 23 | 4.8 | 2.4 |
| | EBFP1.2 | 379 | 446 | 41 | 0.45 | 18 | 6.6 | 0.95 |
| mCherry | mBlueberry2 | 402 | 467 | 51 | 0.48 | 25 | <2.5 | <0.05 |
| | mBlueberry1 | 398 | 452 | 11 | 0.48 | 5 | ND[d] | <0.02 |
| | mCherry2-Y67H[e] | 402 | 464 | 6 | 0.06 | 0.3 | ND | ND |
| Previous work[f] | Azurite | 384 | 450 | 22 | 0.59 | 13 | 5.0 | 19 |
| | EBFP | 377 | 446 | 30 | 0.15 | 4.5 | 6.3 | 0.10 |

[a] Units of $mM^{-1}cm^{-1}$. [b] Product of $\varepsilon$ and $\phi$ in $mM^{-1}cm^{-1}$. For comparison, the brightness of EGFP is 34 $mM^{-1}cm^{-1}$ [68]. [c] Time to photobleach from 1000 to 500 photons/sec/molecule. [d] ND, not determined. [e] Wavelength values are given for the initially purified protein. [f] All values measured in this laboratory.

### 5.3.3 *Discosoma* RFP variants

*Discosoma* RFP (a.k.a DsRed or dsFP583) is a GFP homologue [46] that harbors a chromophore in which the conjugation has been extended through an additional acylimine moiety derived from main chain atoms (**Figure 5.1E**) [134]. The additional conjugation results in a substantial red-shift in the absorbance (558 nm) and fluorescence peaks (583 nm) relative to GFP. Extensive engineering and directed evolution of *Discosoma* RFP has resulted in a series of monomeric variants known as the 'mFruits', where each variant is named for a fruit of similar color [50]. For GFP variants it is known

that the series of variants in which Tyr66 is replaced with Trp (**Figure 5.1B**), His (**Figure 5.1C**), or Phe (**Figure 5.1D**) results in new chromophore structures with increasingly blue-shifted absorbance and fluorescence [37]. A monomeric Tyr67Trp variant known as mHoneydew (**Figure 5.1F**) has previously been investigated and shown to have broad yellow fluorescence [50].

With the expectation of obtaining further blue-shifted variants, the Tyr67His and Tyr67Phe mutations were introduced into the *Discosoma* RFP variant known as mCherry2 (N.C.S. and R.Y.T., unpublished results). The mCherry2-Tyr67Phe variant had absorption (405 nm) and emission peaks (467 nm) (**Figure 5.2D**) significantly red-shifted from the GFP-Tyr66Phe (absorption at 360 nm and emission at 442 nm), indicating that this variant was still capable of all post-translational steps necessary for chromophore formation (**Figure 5.1H**). Started from mCherry2-Tyr67Phe, directed evolution was initiated as described above. The resulting protein, which has been named mBlueberry1 (**Table 5.1**), as it is a new member of the mFruit series, has a very good quantum yield ($\phi$ = 0.48) but a disappointingly low extinction coefficient ($\varepsilon$ = 11,000 $M^{-1}cm^{-1}$) (**0**). In the hopes that an alternative template would be more amenable to improvement, the Tyr67Phe mutation was introduced into mApple, a recent addition to the mFruit series that was derived from mCherry2 (N.C.S. and R.Y.T., unpublished results). Directed evolution of this variant resulted in the creation of mBlueberry2 (**Table 5.1**) which is 4.6-fold brighter than mBlueberry1 (**Table 5.2**). For the sake of consistency, mutations in both mBlueberry1 and mBlueberry2 are listed in **Table 5.1** relative to their common ancestor, mCherry2. The higher brightness of mBlueberry2 relative to mBlueberry1 is attributed to improvements in extinction coefficient ($\varepsilon$ = 51,000 $M^{-1}cm^{-1}$). A particularly interesting feature of mBlueberry2 is that its fluorescent intensity is unchanged over pH values ranging from less than 2.5 to greater than 10 (**Table 5.2**).

By analogy with GFP variants, the mCherry2-Tyr67His mutant had been expected to have a fluorescent hue intermediate between mHoneydew and mBlueberry. The freshly purified protein has a fluorescence peak at 464 nm when excited at 400 nm. However, within 24 h of being purified, a new minor absorbance peak at 450 nm becomes apparent. Excitation of this peak produces an unexpectedly long wavelength fluorescence emission peak at 550 nm (**Figure 5.2F**). Unfortunately this intriguing protein stubbornly resisted

improvement by directed evolution with selection for mutants with improved brightness at either the 464 nm or 550 nm emission peaks. It has previously been shown that the isolated BFP chromophore has a pKa of 12.0 for formation of its red-shifted anionic form [142]. The acylimine extension off the mCherry2-Tyr67His chromophore should enable greater delocalization of the negative charge and may thereby cause a significant decrease in the pKa. It is tentatively speculated that the 550 nm peak may arise from the anionic form of the histidine-derived chromophore. Alternatively, the chromophore may be undergoing an additional post-translational modification that extends the conjugation.

## 5.4 DISCUSSION

Intrinsic fluorescent brightness is, ostensibly, the most obvious characteristic by which to compare FPs. By this criterion, four of the new FPs (EBFP1.5, EBFP2, mKalama1 and mBlueberry2) and the recently reported Azurite variant [137] are all significantly improved relative to EBFP. The brightest of the new variants is mBlueberry2, followed closely by EBFP1.5. However, it is important to note that the primary limitation of EBFP was not its brightness, but rather its susceptibility to photobleaching. I determined the rates of photobleaching [68] for each of the new variants in microdrops of purified protein (**Figure 5.3**). Unfortunately, the brightest variant, mBlueberry2, was notable for a remarkably fast rate of photobleaching that was comparable with EBFP. At light intensities that would typically be used for widefield fluorescence imaging, the fluorescence of mBlueberry2 (and mBlueberry1) decreased to less than 20% in less than 100 ms of total exposure time. This characteristic renders mBlueberry2 impractical for use in routine imaging experiments but is intriguing with regard to future studies of the mechanism of chromophore bleaching. In contrast, the other 3 new variants exhibited rates of photobleaching that were significantly improved relative to EBFP. The most spectacular improvements were observed with EBFP2, which exhibits a 550-fold improvement in photostability relative to EBFP. These benefits stem from the presence of the V150I and V224R mutations to which the similarly impressive photostability of the Azurite variant has been attributed (**Figure 5.3**) [137]. Azurite, EBFP1.5, and EBFP2 each display a biphasic rate of photobleaching in which the magnitude of the fast component increases with increasing intensity of illumination (data

not shown). In contrast, mKalama1 displays a single exponential decrease in fluorescence intensity.

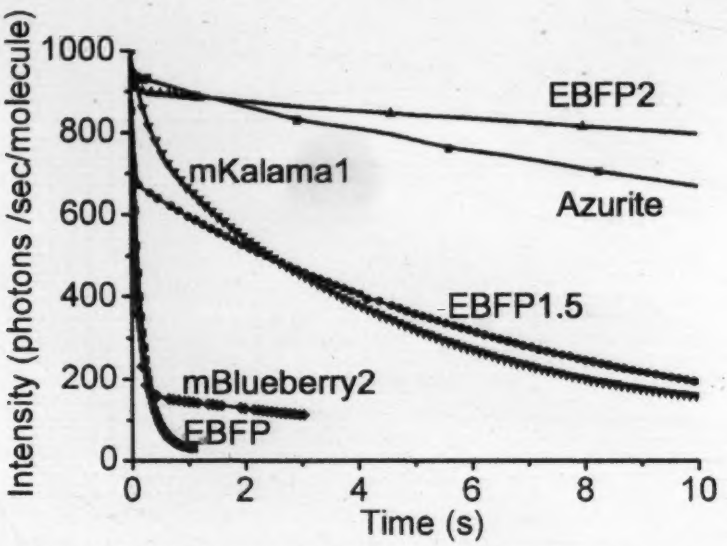


**Figure 5.3** Photobleaching curves for the new blue-fluorescing FPs.

To determine whether the most promising of the new blue FPs were suitable for use in live cell fluorescence imaging, the genes encoding mKalama1, mBlueberry2, EBFP1.5, and EBFP2 were expressed in HeLa cells as a fusion with a nuclear localization sequence. A 6-fold longer exposure time was typically necessary to obtain satisfactory images of the bright but fast-bleaching mBlueberry2 variant. All of the new FPs correctly localized to the nucleus and did not exhibit significant fluorescence in the EGFP emission channel that was used for imaging of a cotransfected EGFP-actin fusion (**Figure 5.4A-D**). Further expression of EBFP2 fusion proteins by Michael W. Davidson confirmed its versatility for live cell imaging (**Figure 5.5**).

Blue FPs, such as the improved versions described in this chapter, have excitation and emission maxima at wavelengths distinct from those of EGFP (excitation maxima at 488 nm and emission maximum at 507 nm) [68]. However, because the absorbance profile of EGFP tails well below 400 nm, EGFP will fluoresce green with 10-20% of its maximum brightness when illuminated at wavelengths used for excitation of blue FPs (approximately 400 nm). This UV-excited fluorescence limits the utility of EGFP for multicolor imaging with the UV-excitable green variant T-Sapphire (excitation maxima

at 399 nm and emission maximum at 511 nm) [140] but does not adversely affect multicolor imaging with blue FPs due to the distinctly different emission wavelengths.

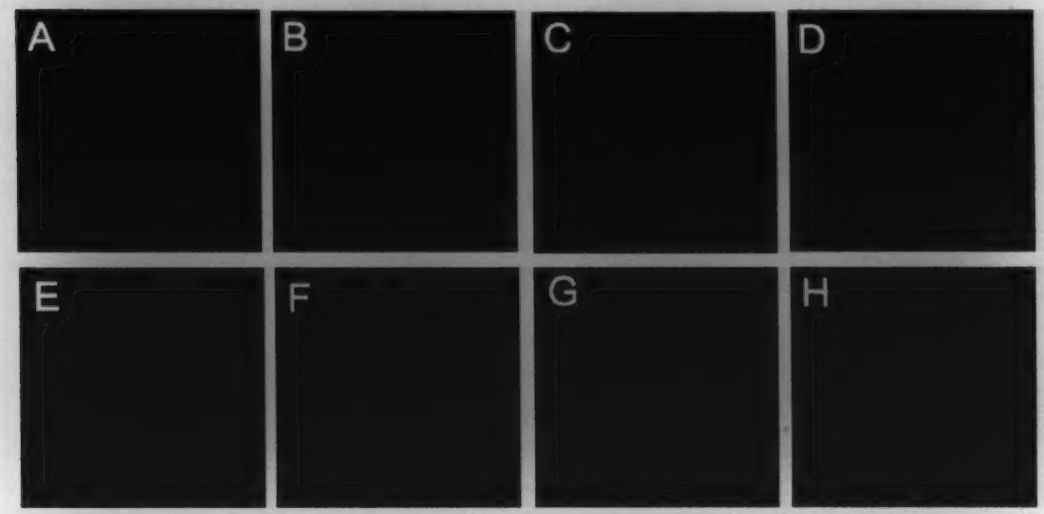


**Figure 5.4** New blue-fluorescing FPs expressed in live cells. (A) mKalama1-NLS, (B) EBFP2-NLS, (C) EBFP1.5-NLS, or (D) mBlueberry2-NLS coexpressed with EGFP-actin in HeLa cells. Colonies of E. coli expressing either (E) mKalama1, (F) EBFP2, (G) Azurite, or (H) EBFP imaged 14 hours after transformation and plating. Relative fluorescent intensities are 8, 5, 2, and 1, respectively. All plates were handled and imaged in parallel under identical conditions.

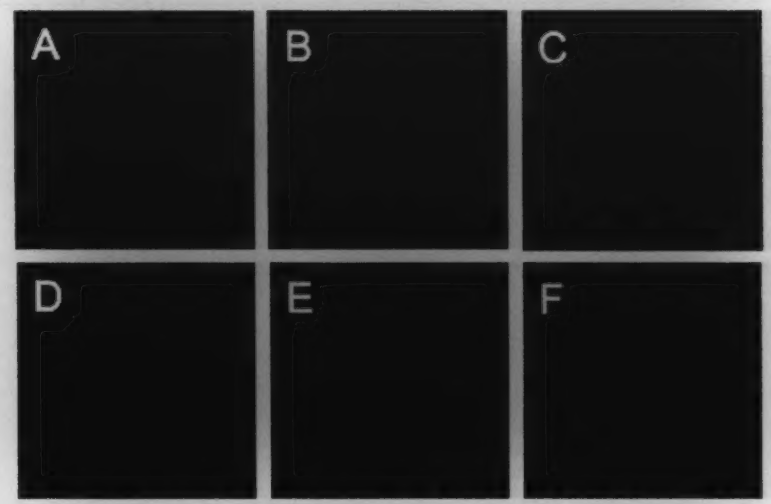


**Figure 5.5** Live cell imaging of EBFP2 fusion vectors. (A) EBFP2-actin (human α-actin); (B) EBFP2-Cx26 (rat b-2 connexin-26); (C) EBFP2-mitochondria (human

cytochrome C oxidase subunit VIII); (D) EBFP2-EB3 (human microtubule-associated protein; RP/EB family); (E) EBFP2-NLS (human); (F) EBFP2-H2B (human). (Image courtesy of Michael W. Davidson)

Despite the fact that it has neither the highest intrinsic brightness nor the best photostability of the new variants (including Azurite), mKalama1 is the brightest blue FP when expressed in bacteria (**Figure 5.4E-H**). This result suggests that the intensive directed evolution effort that produced mKalama1 selected for efficient protein folding and chromophore maturation in bacteria in addition to high intrinsic brightness.

In conclusion, by exploring the potential of a variety of distinct FP chromophore structures, I have arrived at new blue FPs (mKalama1, EBFP1.5, and EBFP2) that are superior alternatives to EBFP. All new FPs are also brighter than Azurite, but only EBFP2 has better photostability and is thus the blue FP of choice for use in live cell fluorescence imaging. For applications in which photostability is not particularly important, such as use as a reporter of gene expression in mammalian cells or bacterial colonies, mKalama1 may provide higher fluorescent signal than EBFP2 due to its high folding and chromophore maturation efficiency.

# CHAPTER 6:

# FLUORESCENT PROTEIN FRET PAIRS FOR RATIOMETRIC IMAGING OF DUAL CASPASE BIOSENSORS

The paper describing the research in this chapter has been published in *Nature Methods* [77]. It should be clearly pointed out that Michael W. Davison and Kristin L. Hazelwood at the National High Magnetic Field Laboratory and the Florida State University should be credited for the work of spectral imaging, photostability measurement and fusion protein localization imaging.

## 6.1 INTRODUCTION

Despite the popularity and versatility of FP technology, there are still some areas in which FPs might be said to be lacking relative to synthetic dye or nanoparticle-based labeling. For example, fluorescence hues of FPs are confined to a relatively narrow region of the electromagnetic spectrum (essentially the visible wavelengths) due to protein-imposed restrictions on the possible manipulations of the chromophore structure and environment. This limitation is exacerbated by the relatively broad excitation and emission peaks of FPs, which further restricts the number of colors that can be distinguished with bandpass filters on a widefield microscope. So consideration of fluorescence emission maxima alone disguises an inconvenient characteristic of the various hues of FPs: their excitation and emission profiles typically approach or exceed 100 nm in spectral width (considering > 10% of maximum intensity). It is for this reason that, in spite of the plethora of various colors of FP variants reported in recent years, imaging of 4 or more FPs with filter-based widefield fluorescence microscopy is generally complicated by the issue of spectral 'bleed-through' [68].

The limitations imposed by the broad spectral profiles of available FPs have also hampered the development of spectrally compatible FRET pairs for ratiometric imaging of two distinct FRET-based biosensors in a shared intracellular compartment of a single cell. Having at least 4 distinct colors is a prerequisite for simultaneous ratiometric imaging of two spectrally orthogonal FRET sensors, and that the current lack of such FRET pairs is a serious limitation of FP technology. For example, BFP coupled with GFP as well as CFP coupled with YFP are FRET pairs that each have good overlap between the donor emission and acceptor absorbance, acceptable levels of excitation crosstalk, and strong sensitized emission due to the high quantum yield of the acceptor [37]. However, due to the substantial excitation and emission profile overlaps between these

FP variants, it is not feasible to image the FRET intensity ratios of both FRET pairs when they are present at the same intracellular locale.

Previously reported strategies for imaging of two FP FRET pairs have involved the 'sharing' of one FP between the two FRET pairs. In one example that involved a triple FP fusion, a single FP was used as both the acceptor in one FRET pair and a donor in another [143]. In other examples the same FP has been used as the acceptor in two separate FRET pairs and the lifetime [144] or intensity [145] of the donor FPs were imaged. These prior studies demonstrate that sharing of one FP between two FRET pairs can be useful in certain applications but is generally impractical for quantitative ratiometric imaging of two FRET pairs in a single cell. In an effort to broaden the scope and versatility of dual FRET pair imaging, I have engineered two spectrally distinct FRET pairs that can each be ratiometrically imaged in the presence of the other.

## 6.2 EXPERIMENTAL

### 6.2.1 General methods and materials

Synthetic DNA oligonucleotides for cloning and library construction were purchased from Integrated DNA Technologies (Coralville, IA). PCR products and products of restriction digests were purified by gel electrophoresis and extraction using either the GenCatch™ gel extraction kit (Epoch Biolabs, TX) or the QIAquick™ gel extraction kit (QIAGEN, Valencia, CA). Plasmid DNA was purified from overnight cultures by using the GeneJET™ Plasmid Miniprep Kit (Fermentas, ON) or the QIAprep Spin Miniprep kit (QIAGEN). Restriction endonucleases were purchased from Invitrogen, Fermentas, or New England Biolabs. Dye terminator cycle sequencing using the DYEnamic ET kit (Amersham Biosciences) was used to confirm the complete cDNA sequences for all FP variants and fusion constructs. Sequencing reactions were analyzed at the University of Alberta Molecular Biology Service Unit or the Florida State University Bioanalytical and Molecular Cloning DNA Sequencing Laboratory. All filters for fluorescence screening and imaging were purchased from Chroma Technology (Rockingham, VT), Omega Filters (Brattleboro, VT) and Semrock (Rochester, NY).

### 6.2.2 Mutagenesis and screening

Gene libraries with saturation or semi-saturation mutagenesis at a particular residue and libraries of randomly mutated genes were constructed as previously described in **Section 2.2**. PCR products were digested with Xho1 and EcoR1 and ligated into similarly digested pBAD/His B vector (Invitrogen). Electrocompetent *E coli* strain DH10B (Invitrogen) was transformed and plated on LB/agar plates supplemented with ampicillin (0.1 mg/ml) and L-arabinose (0.02%). Plates were incubated for 14 h at 37 °C prior to screening.

The screening system has been described previously in **Section 2.2** and **Section 5.2**. Colonies were illuminated with light from a 175 W xenon-arc lamp (Sutter) that had been passed through a 375 to 415 nm or a 490 nm to 510 nm bandpass filter. Colony fluorescence was imaged with a Retiga 1300i 12-bit CCD camera (QImaging) fitted with either a 440 to 480 nm or a 520 to 550 nm emission filter. For each plate of colonies, 3 images were acquired: excite 375-415 nm, emit 440-480 nm; excite 490-510 nm, emit 520-550 nm; and excite 375-415 nm, emit 520-550 nm. Colonies with the highest ratio of fluorescence intensity in the latter image to fluorescence intensity in the other 2 images were picked. These clones were cultured overnight in 4 ml of LB medium containing ampicillin and L-arabinose. The following day 0.1 ml of each culture was dispensed into a 96-well plate (Nunc) and the full emission spectra of each variant measured with a Safire2 plate reader (Tecan). Variants with the most intense emission peak were used as templates in the subsequent round of library construction.

### 6.2.3 Protein characterization

The protein was purified as described in **Section 2.2**. Absorption spectra were recorded on a DU-800 UV-visible spectrophotometer (Beckman). A monochromator-based Tecan Safire2 plate reader was used to acquire the fluorescence excitation and emission spectra. The quantum yield was measured using quinine sulfate in 0.1 M $H_2SO_4$ as the reference standard [139]. The extinction coefficient was measured by the base-denaturation method [50, 103].

To measure the pH-dependence of mAmetrine fluorescence, purified protein was dialyzed into 5 mM Tris-HCl buffer (pH 7.5). This solution was diluted 100-fold into a

series of buffers (200 mM sodium phosphate and 200 mM imidazole) that had been adjusted to pH values ranging from 2.5 to 9.0. The fluorescence of each solution was measured with a fluorescence plate reader.

To determine the relative rates of in vitro protein maturation, a modified version of a previously reported method was used [146]. Samples of mAmetrine, mT-Sapphire, and mCitrine were heated to 95 °C in a denaturing and reducing buffer (8 M urea, 10 mM sodium hydrosulfite in PBS) for 5 min. The samples were cooled to room temperature, another 5 mM freshly dissolved hydrosulfite was added, and the samples were heated to 95 °C for another 5 min. Protein maturation was initiated by 300-fold dilution into 3 ml renaturation buffer (5 mM $MgCl_2$ in PBS, pH 7.4). The recovery of fluorescence at 37 °C was followed using a QuantaMaster spectrofluorometer (Photon Technology International) equipped a temperature controlled cuvette holder. During the recovery time, protein solutions were stirred with a magnetic bar at ~ 500 rpm and cuvettes were not capped.

To elucidate the oligomeric structure of mAmetrine, gel filtration chromatography was performed using an Amersham HiLoad 16/60 Superdex 75 pg size exclusion column with 100 mM phosphate running buffer (pH 7.5). The UV-vis detector on the AKTAbasic HPLC system can monitor multiple wavelengths and was used to detect absorbance at 400 nm, 510 nm and 560 nm for mAmetrine, mCitrine, and tdTomato, respectively.

### 6.2.4 Construction of 10-AA linker FRET constructs for spectral imaging

To construct mAmetrine and mT-Sapphire fusions to tdTomato, mCherry, TurboRFP, TagRFP, and mStrawberry for FRET spectral imaging, the donor FP genes (mAmetrine and mT-Sapphire) were amplified with a 16-nucleotide 5' primer that adds an EcoRI site immediately before three nucleotides comprising the Kozak sequence (ACC; threonine) preceding the start codon, and a 3' primer containing the C-terminal 25 nucleotides of the appropriate FP followed by the sequence: TCCGGACTCAGATCCCCACCGGTCGCCACC, containing an AgeI site. The PCR products were sequentially digested with AgeI and EcoRI and ligated into a similarly digested Clontech-style N1 cloning vector containing the appropriate acceptor to yield the amino acid sequence 'SGLRSPPVAT' flanked by mAmetrine or mT-Sapphire on the

5' terminus and by an orange or red FP (i.e. tdTomato, mCherry, TurboRFP, TagRFP, mKO, or mStrawberry) on the 3' terminus.

### 6.2.5 Construction of fusion proteins for imaging and photostability measurements

To create the mAmetrine fusion protein vectors, the gene encoding mAmetrine was PCR amplified with a 5' primer encoding an AgeI site and a 3' primer encoding either a BspEI (C1 cloning vector) or NotI (N1 cloning vector) site. The purified and digested PCR products were ligated into similarly digested EGFP-C1 and EGFP-N1 (Clontech) cloning vector backbones, to create mAmetrine-C1 and mAmetrine-N1, respectively. To generate fusion vectors, the appropriate cloning vector and a previously constructed EGFP fusion vector were digested, either sequentially or doubly, with the appropriate enzymes and ligated together after gel purification. Thus, to prepare mAmetrine N-terminal fusions, the following digests were performed: human H2B, BamHI and NotI (George Patterson, NIH); rat α-1 connexin-43, EcoRI and BamHI (Matthias Falk, Lehigh University); chicken paxillin, EcoRI and NotI (Alan Horwitz, University of Virginia); human vimentin, BamHI and NotI (Robert Goldman, Northwestern University). To prepare mAmetrine C-terminal fusions, the following digests were performed: human α-tubulin, NheI and BglII (Clontech); human light chain clathrin, NheI and BglII (George Patterson, NIH); human lamin B1, NheI and BglII (George Patterson, NIH).

### 6.2.6 Construction of fusion proteins for 4-color widefield imaging

The pEYFP-Nuc vector was from Clontech and mTFP-actin has been described in **Section 2.2**. The tdTomato-Mito vector was constructed by fusing the mitochondrial targeting sequence derived from the precursor of subunit VIII of human cytochrome C oxidase to the N-terminus of tdTomato. To construct the mAmetrine-Mem vector, the sequence of the N-terminal 20 amino acids of neuromodulin (targeting to plasma membrane and intracellular membranes) was first assembled by PCR with Nhe1 and Xho1 restriction sites on 5' or 3' ends, and mAmetrine was amplified with suitable primers to produce Xho1 and BamH1 restriction sites at the 5' and 3' ends, respectively. The digested PCR products were ligated into pEYFP-Nuc vector digested with Xho1 and

BamH1 in a three-part ligation. To prepare cDNA for transfection, all plasmids were purified by Plasmid Midi kit (Qiagen).

### 6.2.7 Construction of caspase-3 sensors

To construct the genes encoding the caspase-3 sensors, mAmetrine and mCitrine were PCR amplified with a 5' primer containing an Xho1 site and a 3' primer that appended the DNA sequence encoding 'LGGT' followed by a Kpn1 site. The genes encoding tdTomato and mTFP1 were PCR amplified with a 5' primer that appended a Kpn1 site followed by DNA encoding 'GSGSGDEVDG', and a 3' primer with an EcoR1 site. PCR products were digested with the appropriate restriction enzymes and plasmid pBAD/His B was digested with Xho1 and EcoR1. Three-part ligations were performed with the digested mAmetrine PCR product, the digested tdTomato PCR product and the digested plasmid or the digested mCitrine PCR product, the digested mTFP1 PCR product and the digested plasmid. DNA was purified from transformed bacteria and the sequence confirmed by DNA sequencing. The gene products for these sensors consist of the amino acid sequences 'LGGTGSGSGDEVDG' flanked by either mCitrine (1-230) and mTFP1 (1-231) or mAmetrine (1-230) and tdTomato (1-476).

A similar three-part ligation method was used to create the nucleus targeted caspase-3 sensor mammalian expression vectors. The procedure described above was modified such that the outside primers encoded 5' Nhe1 and 3' Xho1 sites rather than 5' Xho and 3' EcoR1 sites. Furthermore, the target plasmid was pEYFP-Nuc (Clontech) rather than pBAD/His B. To construct the expression vector with no targeting, a 3' BamH1 site was used in place of the 3' Xho1 site and the pEYFP-Nuc plasmid was digested with Nhe1/BamH1 rather than Nhe1/Xho1. Digestion of pEYFP-Nuc with Nhe1/BamH1 removes the nuclear localization sequence normally present in this plasmid. To append a C-terminal nuclear export sequence, a 3' primer encoding the amino acid sequence 'LPPLERLTL' peptide followed by a BamH1 site was used.

Control FRET constructs that could not be cleaved by caspase-3 (DEVD sequence replaced with SASG) were constructed by replacing the 5' primer used to amplify tdTomato and mTFP1 with a new primer appended a Kpn1 site followed by DNA encoding 'GSGSGSASGG'. All other primers and ligations for plasmid construction

were identical to those described above. This procedure produced the FRET constructs mAmetrine-SASG-tdTomato-NES and mCitrine-SASG-mTFP1-NES.

### 6.2.8 Spectral imaging of FRET constructs

mAmetrine and mT-Sapphire FRET constructs were imaged and the spectra recorded using an Olympus FV1000 laser scanning confocal microscope equipped with 405 nm and 543 nm lasers and a diffraction grating-based spectral imaging detector system. Log phase HeLa (CCL-2) cells were plated directly into Delta-T imaging chambers and were transfected at 60% confluency as described above. Between 36 and 48 hours after transfection, the chambers were bathed in fresh media, transferred to a stage adapter on the confocal microscope, and maintained at 37 °C under a 5% $CO_2$ for the duration of the experiments. After examination of general cell viability and FP expression at low (10× - 20×) magnification, selected candidates were chosen for further analysis at higher magnification (40× Plan Apo). Spectra of all FRET constructs were recorded with a 405 nm diode laser over the range of 450-720 nm (2 nm bandwidth) at 3% of total laser output power (15 μW), a 4x zoom setting, 100 μs dwell time, and a fixed pinhole size of 550 μm.

### 6.2.9 4-color widefield imaging

HeLa cells in 35 mm imaging dishes were transfected by the method described in the **Section 2.2** with a total of 4 μg of plasmid DNA encoding, EYFP-Nuc, mTFP-actin, tdTomato-Mito, and mAmetrine-Mem (1 μg × 4). The next day the culture medium was exchanged with Hank's buffered salt solution (HBSS) and then the cells were imaged on an Axiovert 200M (Zeiss) microscope equipped with a 75 W xenon-arc lamp, 40× objective lens (NA = 1.3, oil) and a 25% neutral density filter in the light path. Exposure times were adjusted between 200 ms to 3 s to obtain suitable intensities in each channel. The filters used for imaging are listed in the **Table 6.3**.

### 6.2.10 Imaging of mAmetrine fusion proteins

mAmetrine fusion vectors were transfected using Effectene (1 μg DNA/ml) into HeLa cells (ATCC CCL-2 and CCL-2.2) for routine visual examination of morphology

and live cell imaging using widefield fluorescence illumination. 24 hours post-transfection, the cells were trypsinized and seeded into either Delta-T imaging chambers or 35-mm Petri dishes containing an 18 × 18 mm #1.5 coverslip and allowed to grow for another 24-36 hour period. Cultures in the Petri dishes were then washed with PBS, fixed with 2% paraformaldehyde (EMS; Hatfield, PA) in PBS and washed again with 4 exchanges of PBS to completely remove fixer. The adherent cells on coverslips were then treated with 0.1M glycine in PBS to reduce autofluorescence and mounted using gelvatol (25% w/v polyvinyl alcohol in 40% v/v glycerol/PBS). The mounted coverslips were examined at high magnification (100× Plan Apo) to verify correct localization of the fusion protein.

For live cell imaging, the adherent cultures in Delta-T chambers were placed in a stage adapter (Bioptechs) on a Nikon TE2000 inverted microscope with a heated lid (Bioptechs) and equilibrated at 37 °C under a 5% CO2 for 30 minutes to 1 hour. Cells expressing the fusion construct were imaged with a Cascade II or Retiga EXi (QImaging; Vancouver, CA) camera system using Nikon NIS-Elements software.

### 6.2.11 Photostability measurements in live cells

For determination of photostability of FPs in live HeLa cells, N-terminal fusions of each FP were constructed to human histone H2B with a 6 amino acid linker in order to restrict fluorescence to the nucleus. This system closely approximates the dimensions of the aqueous droplets of purified FPs commonly used for *in vitro* widefield measurements [68]. Log phase HeLa (S3; ATCC 2.2) were transfected with the appropriate H2B construct using Effectene (1 μg DNA/ml; QIAGEN) and maintained in a 5% $CO_2$ incubator for 24-36 hours in Delta-T (Bioptechs) imaging chambers prior to conducting photobleaching measurements. The chambers were then transferred to a specialized stage adapter (Bioptechs) on a Nikon TE2000 widefield inverted microscope equipped with an X-Cite 120 metal-halide lamp (EXFO; Mississauga, Ontario, CA), and imaged at low magnification (20×) to ensure cell viability. Selected regions containing 3-10 nuclei were photobleached without neutral density filters using a 40× Plan Fluor (numerical aperture, NA = 0.75) objective, recording images in 1-second intervals using a Cascade II or QuantEM camera system (Photometrics; Tucson, AZ) in direct readout mode (bypassing

the electron multiplier circuitry). Filter sets used for widefield photobleaching were provided by Omega: mAmetrine and mT-Sapphire, XF76; mTFP1, XF114-2; EYFP, mCitrine, XF104-2; EGFP, XF100-2; tdTomato, XF108-2. Light power at the objective output was measured with a FieldMaxII-TO power meter (Coherent; Santa Clara, CA) equipped with a high-sensitivity silicon/germanium optical sensor (Coherent, OP-2 Vis). Widefield photobleaching raw data was collected with NIS-Elements software (Nikon) and analyzed with Simple PCI software (Hamamatsu).

For laser scanning confocal microscopy photobleaching measurements, cells in Delta-T chambers were transferred to a Bioptechs stage adapter on an Olympus FluoView 1000 microscope. Photobleaching was conducted using a 40× oil immersion objective (Olympus UPlan Apo, NA = 1.0) using laser lines (405 nm, diode; 458, 488, 514, argon-ion; 543, HeNe) adjusted to an output power of 50 μW. The instrument was set to a zoom of 4×, a region of interest of 341.2 $\mu m^2$ (108 × 108 pixels), a photomultiplier voltage of 650 V, and an offset of 9% with a scan time of 0.181 seconds per frame. Nuclei having approximately the same dimensions and intensity under the fixed instrument settings were chosen for photobleaching assays. Photobleaching curves were adjusted for the time to bleach the proteins from an emission rate of 1000 photons/second/molecule to 500 photons/second/molecule as previously described [68].

### 6.2.12 Widefield imaging of staurospaurine-induced apoptosis

The plasmids encoding caspase-3 sensors and control FRET constructs were purified using the Plasmid Midi kit (Qiagen). HeLa cells in 35 mm imaging dishes were transfected with 0.5 μg mCitrine-mTFP1 cDNA and 3.0 μg mAmetrine-tdTomato cDNA by the method described previously in **Section 2.2**. Between 36 to 60 hours post-transfection, staurospaurine was added into culture medium to the final concentration of 2 μM. After incubated for another 100 mins, cells were taken out from the incubator and washed 3× with HBSS. Cells were then maintained in HBSS and subjected to imaging on an Axiovert 200M microscope (Zeiss) equipped with a 75 W xenon-arc lamp and 20× objective lens (NA = 0.75, air). For a typical experiment, 1 second exposure time for each channels, 1 minute intervals between every measurements of all 4 channels, and a 25% neutral density filter were used. The excitation, dichroic and emission filters used for

imaging are detailed in **Table 6.3**. Cells were maintained at 37 °C during all imaging experiments.

Control experiments were performed by coexpressing either mCitrine-DEVD-mTFP1-NES and mAmetrine-SASG-tdTomato-NES or mCitrine-SASG-mTFP1-NES and mAmetrine-SASG-tdTomato-NES. Live cell imaging and induction of apoptosis by staurosporine was performed exactly as described above.

### 6.2.13 Image processing

QEDImaging Invivo (Media Cybernetics), NIS-Elements (Nikon), FluoView (Olympus), and Simple PCI (Hamamatsu) software was used for all data collection and camera and microscope control. ImagePro Plus 6.0 (Media Cybernetics) was used to prepare the composite image shown in **Figure 6.6**. ImageJ [147] was used for processing of dual FRET caspase-3 imaging. A custom macro was used to create the ratiometric and intensity scaled timelapse sequences represented in **Figure 6.8**, **Figure 6.9** and **Figure 6.10**.

## 6.3 RESULTS AND DISCUSSION

### 6.3.1 Directed evolution of mAmetrine

I recently engineered mTFP1 (refer to **Chapter 2**) and demonstrated that mTFP1 compares favorably to CFPs, such as ECFP or Cerulean, when used as a FRET donor to a YFP such as mCitrine. Due to the narrower and red-shifted absorbance peak of mTFP1, the mTFP1-mCitrine FRET pair predominates over less of the visible spectrum than the ECFP-mCitrine FRET pair. I recognized that the weak excitation of mTFP1 at wavelengths below 400 nm presented an opportunity to combine its use with a violet-excitable FP such as BFP or a long Stokes shift Sapphire-type variant [140].

During the development of the violet-excitable blue-fluorescing avGFP variant known as mKalama1 (**Section 5.3.1**) I made the fortuitous discovery of a long Stokes shift violet-excitable yellow-fluorescing FP. As I was not aware of any existing FP variant of this particular color, I subjected this new FP to aggressive directed protein evolution and eventually produced a brightly fluorescent variant ($\varepsilon$ = 44,800 $M^{-1}cm^{-1}$, $\Phi$ = 0.58) with 20 mutations relative to GFP (**Table 6.1** and **Figure 6.1**).

My initial library had been designed with the goal of identifying avGFP variants with a violet-excitable blue-fluorescing chromophore that was protonated in both the ground and excited states [76]. Starting from *Aequorea* EGFP, I created a gene library in which positions Thr65, Thr203, and Ser205 were randomized. During exhaustive screening of this initial library I made the unexpected identification of EGFP Thr65Ser/Thr203Phe that exhibited strong violet absorption and strong yellow fluorescence at 520 nm. A subsequent library with randomization of Ser147 and His148 resulted in the identification of the additional Ser147Val/His148Trp mutations that contributed a further red-shift to 526 nm. To further improve the brightness of this protein I undertook many rounds of library creation and screening. Libraries were created by randomly substituting all 20 amino acids at a single position, or by randomly substituting a subset of all amino acids at a single position, or by employing random mutagenesis of the whole gene. Positions targeted for randomization included 30, 39, 63, 64, 72, 105, 145, 153, 163, 171, 175, and 181. In each round of this process, libraries were created as described above and screened as described in **Section 6.2.2**. This process was halted only when no further improvement had been observed for several rounds of screening. The final variant resulting from this process was designated mAmetrine (**Table 6.1** and **Figure 6.1**). mAmetrine retains violet excitation ($\lambda_{ex}$ = 406 nm) due to a protonated ground state and yellow emission ($\lambda_{em}$ = 526 nm) resulting from excited state proton transfer (ESPT) and a π-stacked chromophore.

**Table 6.1** Properties of FPs of the spectrally compatible FRET pairs.

| Protein | $\lambda_{ex}$ (nm) | $\lambda_{em}$ (nm) | ε ($10^3$ $M^{-1}cm^{-1}$) | ϕ | Brightness[a] ($mM^{-1}cm^{-1}$) | pKa | Photostability[b] (s) |
|---|---|---|---|---|---|---|---|
| mAmetrine | 406 | 526 | 45 | 0.58 | 26 | 6.0 | 2.8/281 |
| mTFP1 | 462 | 492 | 64 | 0.85 | 54 | 4.3 | 82/2721 |
| mCitrine | 516 | 529 | 77 | 0.76 | 59 | 5.7 | 6.6/349 |
| tdTomato | 554 | 581 | 138 | 0.69 | 95 | 4.7 | 159/419 |
| mT-Sapphire | 399 | 511 | 44 | 0.60 | 26 | 4.9 | 12/397 |

[a] Product of EC and QY. [b] Time in sec to photobleach from 1000 to 500 photons/sec/molecule under widefield and confocal (50 mW) illumination, respectively [68].

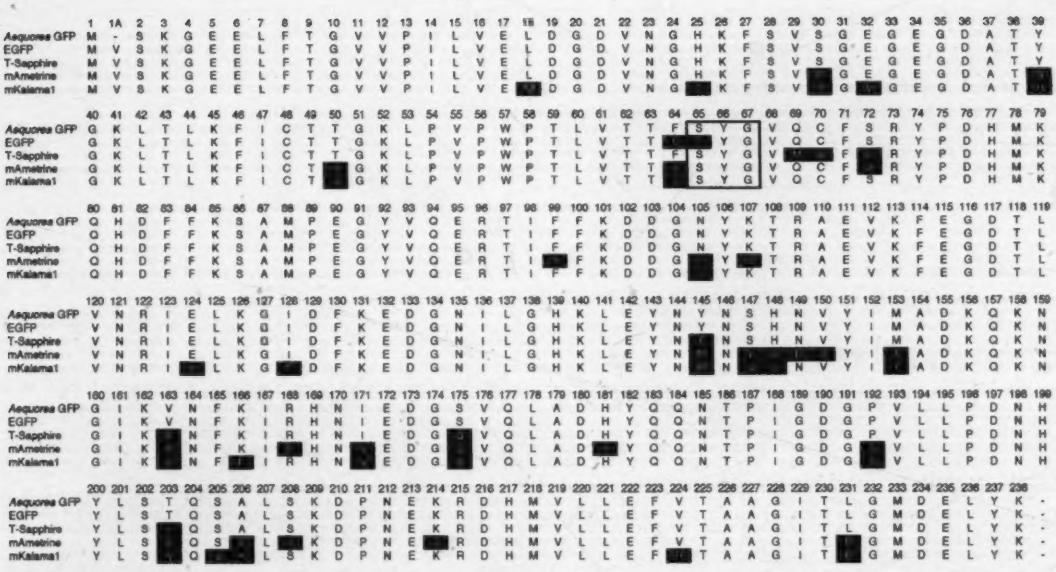

**Figure 6.1** Sequence alignment of wild-type avGFP [113], EGFP [37], T-Sapphire [140], mAmetrine, and mKalama1 (**Section 5.3.1**). Mutations relative to avGFP are indicated as white text on a black background. The chromophore precursor residues are boxed.

### 6.3.2 Further characterization of mAmetrine

The resulting FP mAmetrine showed modest pH stability and has an apparent fluorescence pKa of 6.0 (**Figure 6.2A**). The maturation of mAmetrine, mT-sapphire and mCitrine at 37 °C was also compared and they have maturation half-times of 108 s, 970 s, and 690 s, respectively (**Figure 6.2B**). So it is clear that the directed evolution process of mAmetrine is efficient to search for robust variants for maturartion.

To elucidate the oligomeric structure of mAmetrine, gel filtration chromatography was performed to compare mAmetrine, mCitrine. The upper trace of **Figure 6.2C** shows a co-injection of mAmetrine and mCitrine. The lower trace of **Figure 6.2C** shows a co-injection of mAmetrine and tdTomato. The co-elution of mAmetrine and mCitrine in the upper trace clearly demonstrates that mAmetrine is a monomer as expected for an avGFP variant.

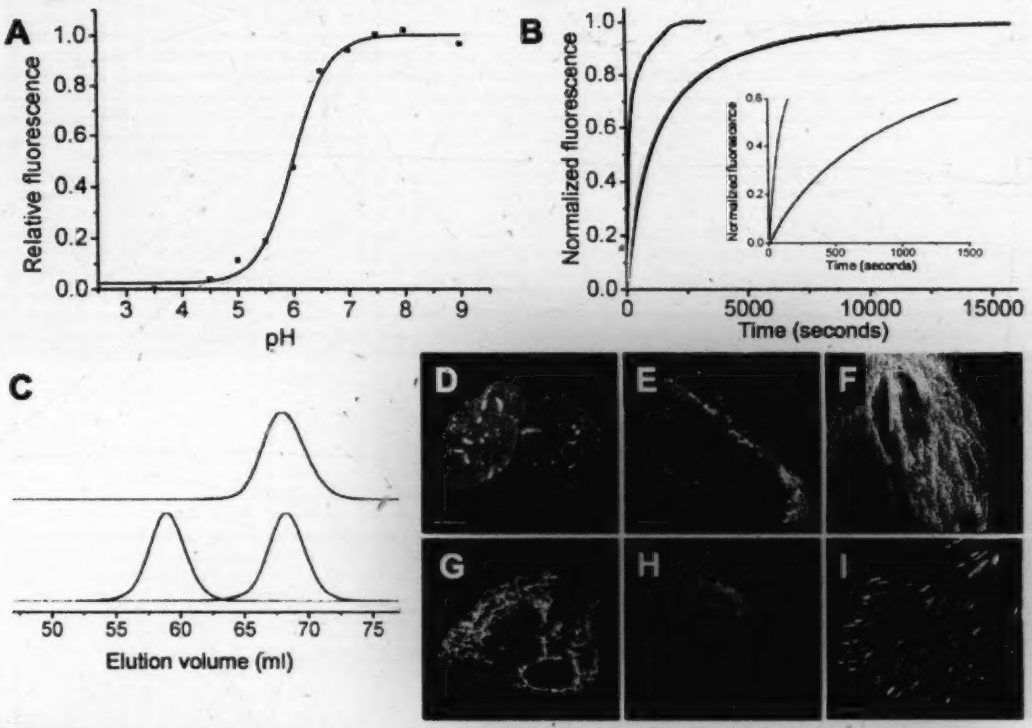


**Figure 6.2** Characterization of mAmetrine. (A) The pH dependence of mAmetrine fluorescence. (B) Maturation rate profiles of mAmetrine (violet), mT-sapphire (green) and mCitrine (yellow) normalized to final fluorescence intensity. Inset shows the first 1500 s of the time course. (C) Gel filtration analysis of mAmetrine (detection at 400nm, violet line) using mCitrine (detection at 510 nm, yellow line) and tdTomato (detection at 560 nm, red line) as mass standards. (D-I) Imaging of mAmetrine as fusions with: (D) lamin B1; (E) connexin43; (F) tubulin; (G) vimentin; (H) clathrin; and (I) paxillin.

To test the adaptability of mAmetrine as a protein fusion partner, several mAmetrine fusion constructs were created and imaged. As shown in **Figure 6.2D-I**, the localization of all fusion constructs was consistent with the pattern expected for avGFP variant. This conclusion was verified by comparison to cells expressing analogous EGFP fusions that were imaged under identical conditions. HeLa S3 (ATCC CCL-2.2) fusions of mAmetrine to human histone H2B were observed to complete all stages of mitosis (data not shown).

The photostability of mAmetrine was also measured by bleaching mAmetrine-H2B fusion expressed in HeLa cells. mAmetrine is only modest relative to popular FP

variants, with a $t_{0.5}$ for photobleaching that is 42% that of mCitrine and 23% that of mT-Sapphire under widefiled illumination, or 81% and 71%, respectively under laser scanning confocal microscopy (**Table 6.1, Table 6.2** and **Figure 6.3**). This is sufficient for certain prolonged widefield and confocal imaging experiments discussed below.

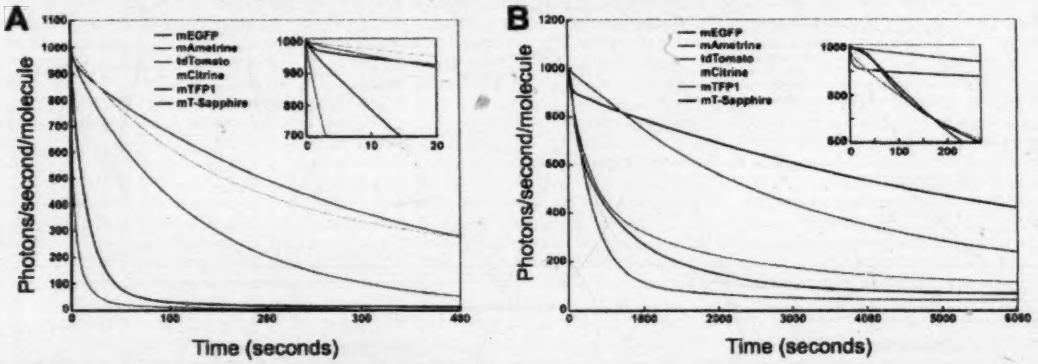


**Figure 6.3** Corrected photobleaching curves for FPs used in this work. (A) Photobleaching curves with widefield (metal-halide lamp) illumination. (B) Photobleaching curves with confocal (laser scanning) illumination. Numerical values are provided in **Table 6.1** and **Table 6.2**.

**Table 6.2** Photobleaching rates for FPs of the spectrally compatible FRET pairs. Curves are shown in **Figure 6.3**.

| Protein | Widefield | | | | Confocal (@ 50 mW) | | |
|---|---|---|---|---|---|---|---|
| | Filter Set | Power (mW) | Uncorrected $t_{0.5}$ (s) | Corrected[a] $t_{0.5}$ (s) | Laser line (nm) | Uncorrected $t_{0.5}$ (s) | Corrected[a] $t_{0.5}$ (s) |
| mAmetrine | Omega XF 76 | 46.6 | 12 | 2.8 | 405 | 95 | 281 |
| mT-Sapphire | Omega XF 76 | 46.6 | 62 | 12 | 405 | 143 | 397 |
| mCitrine | Omega XF 104-2 | 30.6 | 22 | 6.6 | 514 | 42 | 349 |
| tdTomato | Chroma HQ TRITC | 89.5 | 68 | 159 | 543 | 35 | 419 |
| mTFP1 | Omega XF 114-2 | 65.7 | 108 | 82 | 458 | 395 | 2721 |
| EGFP | Omega XF 100-2 | 57.3 | 332 | 198 | 488 | 1087 | 5008 |

[a] Time to bleach from an emission rate of 1000 photons/second/molecule to 500 photons/second/molecule

### 6.3.3 Identification of FRET acceptor for mAmetrine

Although the fluorescence emission profiles of mAmetrine and mCitrine ($\lambda_{ex}$ = 516 nm, $\lambda_{em}$ = 529 nm) are practically identical, the dramatically different excitation profiles allow each FP to be specifically excited in the presence of the other. With mAmetrine in hand I suspected that it was a near ideal donor for pairing with an orange FP (OFP) or red FP (RFP) to produce a new FRET pair that would be spectrally compatible with the mTFP1-mCitrine FRET pair for ratiometric imaging of dual FRET-based biosensors. To find an appropriate acceptor to match with the mAmetrine donor, my collaborators, Michael W. Davison and Kristin L. Hazelwood, and I systematically tested a variety of non-oligomerizing OFPs and RFPs as FRET acceptors to identify the one that would give the strongest sensitized emission and most robust ratiometric signal. We found that regardless of the donor (be it a GFP, a YFP, mT-Sapphire, or mAmetrine) the currently available 'true' monomeric OFPs and RFPs [50] give poor sensitized emission and are thus not suitable for use as FRET acceptors for ratiometric imaging (**Figure 6.4AB**). The non-oligomerizing RFP that gives the strongest sensitized emission is tdTomato ($\varepsilon$ = 138,000 $M^{-1}cm^{-1}$, $\Phi$ = 0.69); an exceptionally bright variant of DsRed that consists of concatenated genes encoding the dimeric dTomato [50].

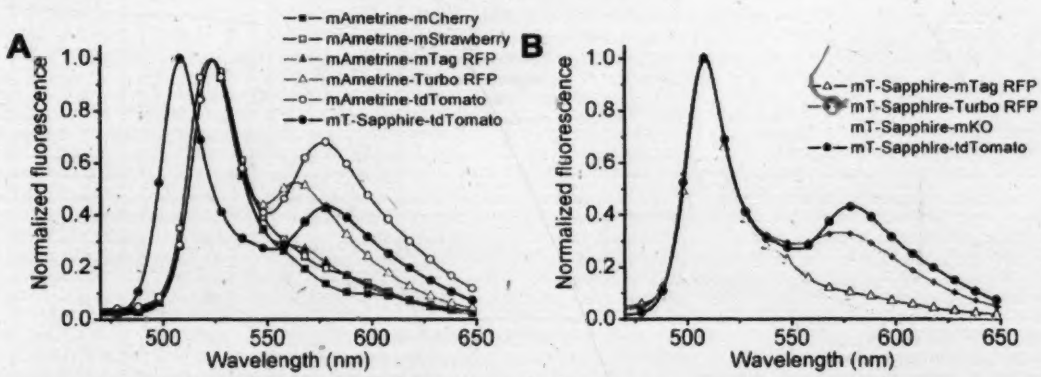


**Figure 6.4** Fluorescence emission spectra for a series of analogous FRET constructs in live cells. (A) mAmetrine as the donor FP. mT-Sapphire-tdTomato is also shown for the sake of reference. (B) mT-Sapphire as the donor FP.

### 6.3.4 4-color live cell imaging

If the combination of mTFP1, mCitrine, mAmetrine, and tdTomato is useful in dual FRET experiments, bleed-through between the four different fluorescence channels must be negligible. I designed fluorescence microscopic bandpass filters for each FPs (**Figure 6.5** and **Table 6.3**). mAmetrine was fused with the N-terminal 20 amino acids of neuromodulin (signal sequence for posttranslational palmitoylation), and coexpressed with EYFP-Nuc, mTFP1-Actin and tdTomato-Mito vectors in HeLa cells. Images of four independent color channels were successfully acquired with small crosstalks (**Figure 6.6**).

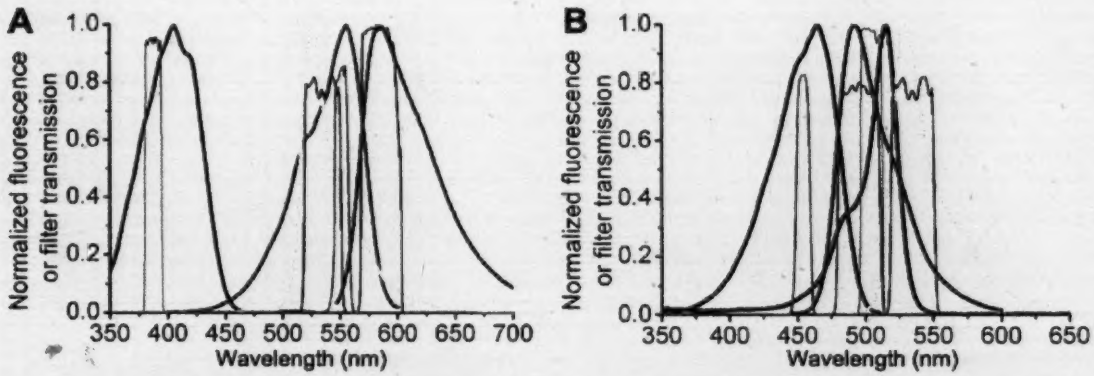


**Figure 6.5** (A) Fluorescence excitation and emission spectra of mAmetrine (violet and yellow) and tdTomato (brown and red). (B) Fluorescence excitation and emission spectra of mTFP1 (blue and cyan) and mCitrine (green and yellow). In both panels, the transmission profiles of the excitation (gray) and emission (black) filters (**Table 6.3**) are shown.

**Table 6.3** Filters used for widefield dual FRET or four-color imaging.

| Protein | Filters | | |
|---|---|---|---|
| | Donor (Ex; Em; dichroic) | Acceptor (Ex; Em; dichroic) | FRET (Ex; Em; dichroic) |
| mTFP1 (donor) mCitrine (acceptor) | 3RD450-460[a]; HQ495/30m[b]; 470dcxr[b] | FF01-504/12[c]; ET535/30m[b]; 515dclp[b] | 3RD450-460[a]; ET535/30m[b]; 470dcxr[b] |
| mAmetrine (donor) tdTomato (acceptor) | FF01-387/11[c]; ET535/30m[b] 470dcxr[b] | 3RD550-560[a]; FF01-585/29[c]; 565dclp[b] | FF01-387/11[c]; FF01-585/29[c]; 470dcxr[b] |

[a] Omega Optical Inc. part number. [b] Chroma Tech. Corp. part number. [c] Semrock part number.

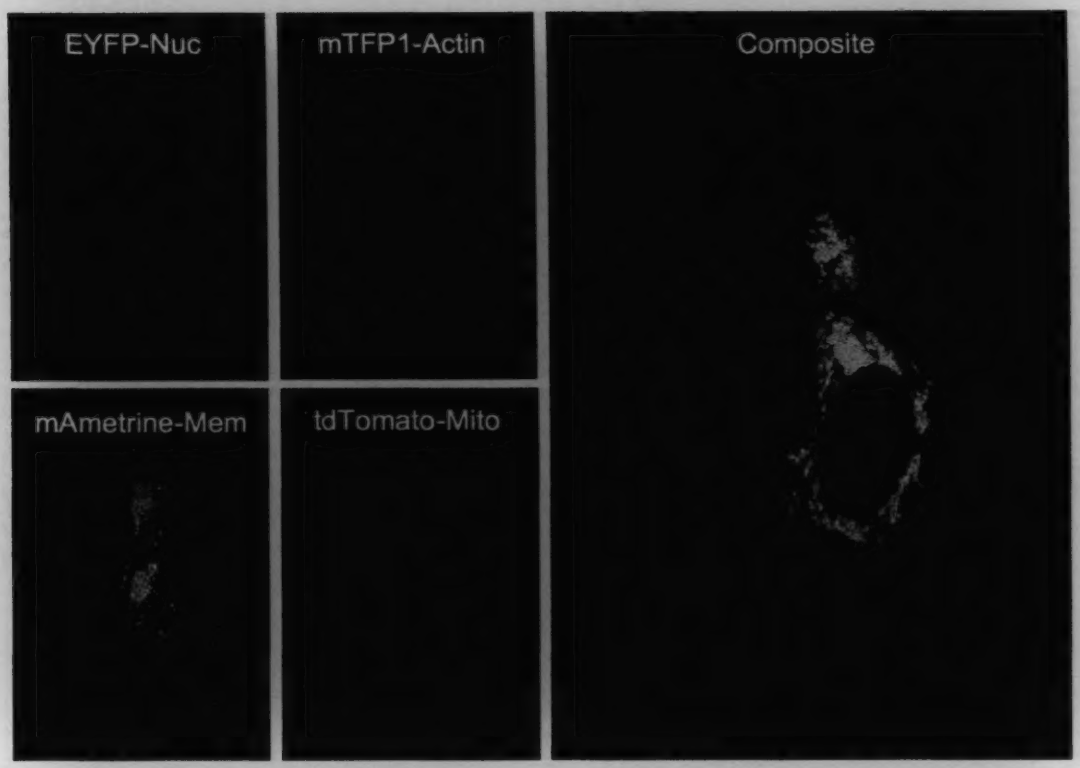


**Figure 6.6** Four-color widefield imaging of an adherent HeLa cell expressing mAmetrine, mTFP1, EYFP, and tdTomato in targeted fusion constructs.

### 6.3.5 Compatible dual FRET imaging of single cells

To test the ability of mTFP1-mCitrine and mAmetrine-tdTomato to function as spectrally compatible FRET-pairs for ratiometric imaging of dual biosensors, I constructed caspase-3 activity biosensors [148] by fusing the effector caspase substrate sequence DEVD between the two FPs of the respective FRET constructs (**Figure 6.7AB**). *In vitro* characterization of the resulting biosensors, mCitrine-DEVD-mTFP1 and mAmetrine-DEVD-tdTomato, revealed FRET efficiencies of 42% and 45%, respectively. Proteolysis of these constructs resulted in a change in acceptor over donor emission peak intensity ratio from 1.35 to 0.55 and 0.67 to 0.22, respectively (**Figure 6.7CD**). HeLa cells were co-transfected with plasmids encoding nucleus-targeted mCitrine-DEVD-mTFP1 and nucleus-excluded mAmetrine-DEVD-tdTomato. At 36 h to 60 h post-transfection, 2 μM staurosporine was added to the culture media for 100 min to induce apoptosis. Cells were then imaged with appropriate filter sets at 37 °C. Approximately

equal exposure times provided similar fluorescence intensities for the both the donor and sensitized acceptor emission channels in those cells that showed no morphological signs of apoptosis. Within 60 min of the start of imaging, the ratio of sensitized tdTomato (acceptor) to mAmetrine (donor) fluorescence intensity in the cytoplasm of individual cells was observed to undergo a stochastic and robust decrease (**Figure 6.8**). Following a delay of 2.6 +/- 1.6 min (17 cells, Δt for 50% FRET change), the ratio of sensitized mCitrine (acceptor) to mTFP1 (donor) fluorescence intensity in the nucleus underwent a similar decrease. When non-targeted mAmetrine-DEVD-tdTomato (i.e. freely diffusing between cytoplasm and nucleus) and nucleus-targeted mCitrine-DEVD-mTFP1 were co-expressed, the delay between the onset of caspase-3 activity in the cytoplasm and nucleus was unchanged (Δt for 50% FRET change = 2.2 +/- 1.1 min for 11 cells; **Figure 6.9**). When both biosensors were nucleus-excluded, apoptosis-associated ratio changes occurred simultaneously demonstrating that there is no bias as caspase-3 substrates (**Figure 6.10**). Additional control experiments were performed using cells expressing both a caspase-3 FRET biosensor (DEVD linker) and a control FRET construct (SASG linker) that is not cleaved by caspase-3 (**Figure 6.11AB**). Consistent with the results when using two caspase-3 biosensors, I observed that large changes in the emission ratio of one FRET pair do not significantly influence the emission ratio of the second.

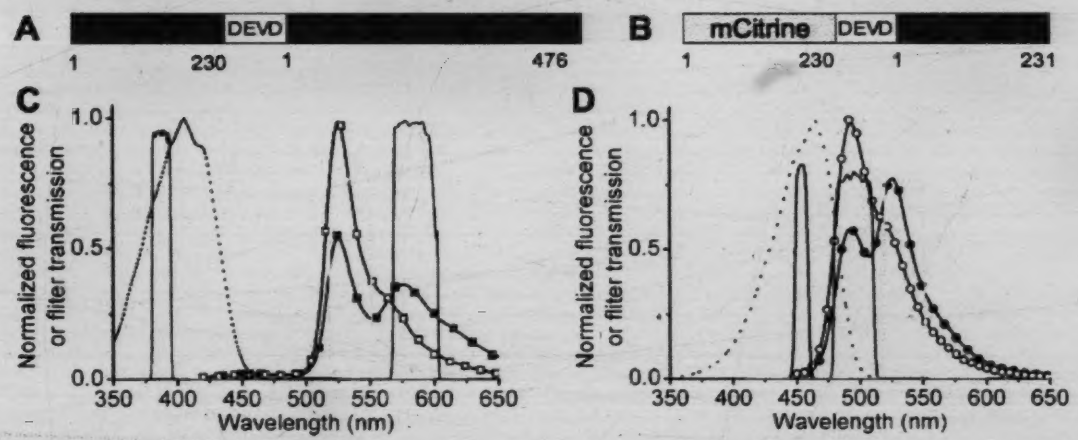


**Figure 6.7** Caspase-3 biosensors based on dual FRET pairs. (A, B) Primary structures of caspase-3 biosensors. 'DEVD' in the figures represents the sequence 'LGGTGSGSGDEVDG'. (C) The emission spectrum of mAmetrine-DEVD-tdTomato before (filled squares) and after (open squares) proteolysis, the excitation spectrum of

mAmetrine (dashed line), and the transmission profiles of excitation (violet line) and emission (yellow and red lines) bandpass filters used for FRET imaging. (D) The emission spectrum of mCitrine-DEVD-mTFP1 before (filled circles) and after (open circles) proteolysis, the excitation spectrum of mTFP1 (dashed line), and the profiles of the excitation (blue line) and emission (cyan and yellow lines) filters.

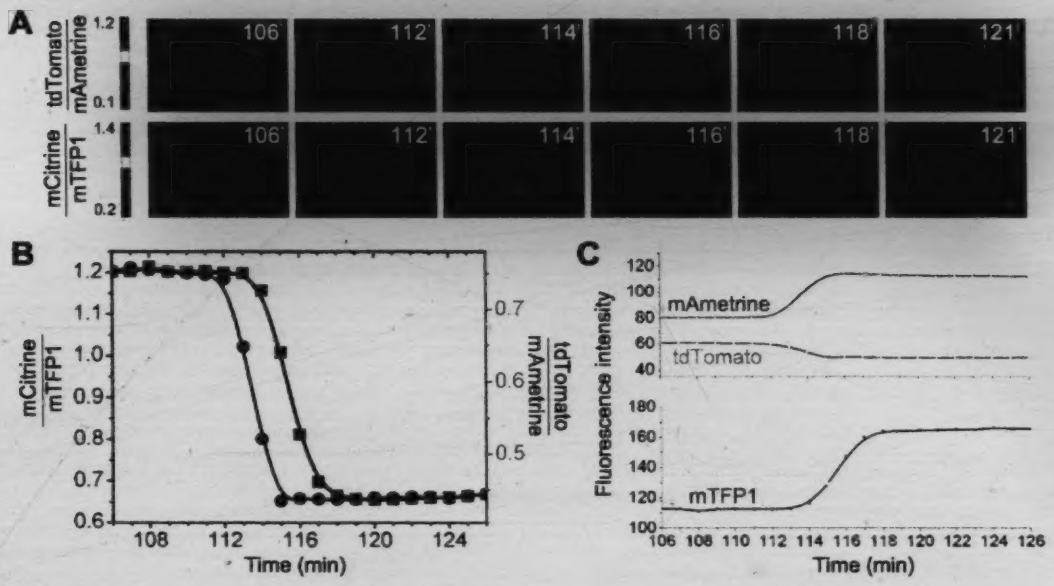


**Figure 6.8** Live cell imaging with dual FRET pairs. (A) Pseudocolored ratio images of a representative staurosporine-treated HeLa cell expressing dual caspase biosensors. In this experiment, mCitrine-DEVD-mTFP1 is localized to the nucleus and mAmetrine-DEVD-tdTomato is nucleus-excluded. (B) Ratio versus time for tdTomato/mAmetrine (red line) and mCitrine/mTFP1 (blue line) for the cell shown in panel A. (C) Intensities in the 4 fluorescence channels for the cell shown in panel A.

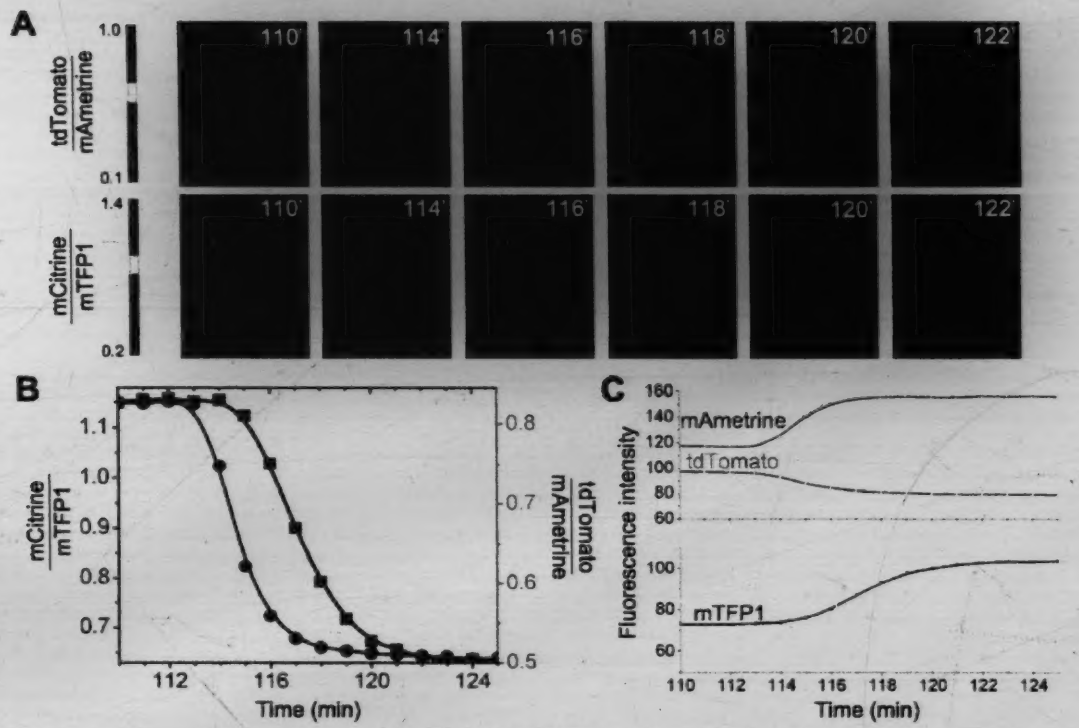


**Figure 6.9** Live cell imaging with dual FRET pairs. (A) Pseudocolored ratio images of a representative staurosporine-treated HeLa cell expressing dual caspase biosensors. In this particular experiment, mCitrine-DEVD-mTFP1 is localized to the nucleus and mAmetrine-DEVD-tdTomato is expressed with no targeting and is rapidly exchanging between nucleus and cytoplasm. (B) Ratio versus time for whole-cell tdTomato/mAmetrine (red line) and nuclear mCitrine/mTFP1 (blue line) for the cell shown in panel A. (C) Intensities in the 4 fluorescence channels for the cell shown in panel A.

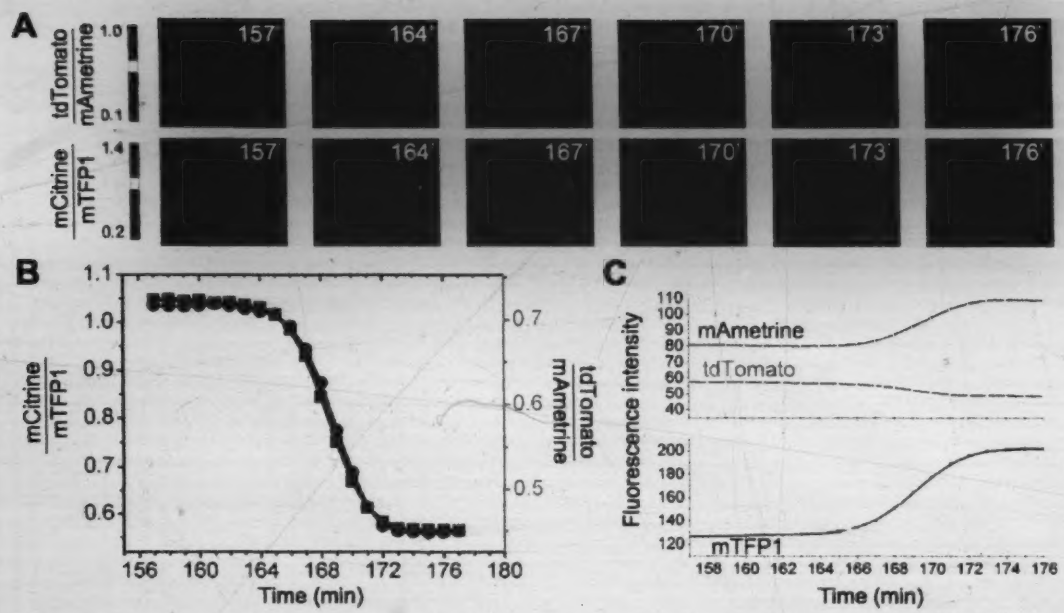


**Figure 6.10** Live cell imaging with dual FRET pairs. (A) Pseudocolored ratio images of a representative staurosporine-treated HeLa cell expressing dual caspase biosensors. In this particular experiment both mCitrine-DEVD-mTFP1 and mAmetrine-DEVD-tdTomato are expressed with a single copy of a C-terminal nuclear export sequence. Proteolysis releases mAmetrine and mCitrine that rapidly diffuse into the nucleus. This explains the decreased tdTomato/Ametrine ratio and increased mCitrine/mTFP1 ratio observed in the nucleus at the 170-minute time point. (B) Ratio versus time for cytoplasmic tdTomato/mAmetrine (red line) and cytoplasmic mCitrine/mTFP1 (blue line) for the cell shown in panel A. (C) Cytoplasmic intensities in the 4 fluorescence channels for the cell shown in panel A.

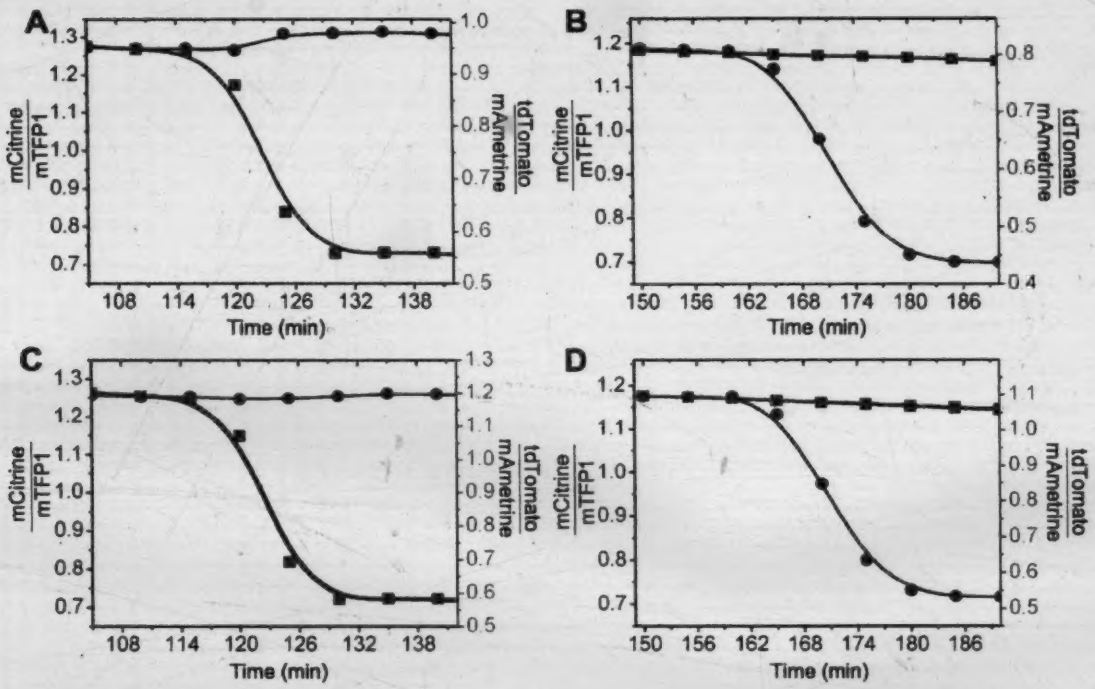


**Figure 6.11** Cytoplasmic ratios versus time for single staurosporine-treated HeLa cells expressing both a caspase-3 FRET biosensor (DEVD linker) and a control FRET construct (SASG linker) that is not a substrate for caspase-3. Data presentation is identical to that in **Figure 6.8**. A) Ratios versus time for a cell expressing mCitrine-DEVD-mTFP1 (blue line) and mAmetrine-SASG-tdTomato (red line). (B) Ratios versus time for a cell expressing mCitrine-SASG-mTFP1 (blue line) and mAmetrine-DEVD-tdTomato (red line). (C) The data of panel A corrected for inter-FRET pair bleed-through using the equations described in **Section 6.3.6**. (D) The data of panel B corrected for inter-FRET pair bleed-through as in C.

### 6.3.6 Spectral bleed-through and correction

An important caveat to this dual FRET approach is that the intensities in all four emission channels should be similar (i.e. within a factor of two) in order to minimize spectral bleed-through. The most likely source of potentially confounding bleed-through is sensitized mCitrine emission contributing to the mAmetrine fluorescence channel in the case where mTFP1-mCitrine is expressed at a significantly higher concentration than mAmetrine-tdTomato. As mAmetrine and mCitrine use the same emission filter, the

extent of the bleed-through depends only on the relative intensities of the two emission signals and the amount of cross-excitation between the donor FPs of the two FRET pairs. By convolving and integrating the excitation spectra of mTFP1 and mAmetrine with each excitation filter, I have determined the amount of cross-excitation and derived a simple equation that corrects for inter-FRET pair bleed-through.

The dual FRET imaging experiments described in this chapter require the use of two excitation filters (**Table 6.3**): one that primarily excites mAmetrine and one that primarily excites mTFP1. As shown in **Table 6.4** below, there is some degree of cross-excitation between the dual FRET pairs. That is, the filter set used to excite mAmetrine gives some excitation of mTFP1 (14% of the mTFP1 excitation as measured by convolving and integrating the excitation spectrum of mTFP1 for each filter), and the filter set used to excite mTFP1 gives some excitation of mAmetrine (2% of the mAmetrine excitation as measured by convolving and integrating the excitation spectrum of mAmetrine for each filter).

**Table 6.4** Relative emission intensities for each protein of the spectrally compatible FRET pairs when imaged with each of the filter sets listed in **Table 6.3**. For each protein the intensity provided by each filter set has been divided by the intensity provided by the recommended filter set.

| **Protein** | **Filter Set**[a] | | | | | |
|---|---|---|---|---|---|---|
| | **ex TFP em TFP** | **ex TFP em Cit** | **ex Cit em Cit** | **ex Ame em Ame** | **ex Ame em Tom** | **ex Tom em Tom** |
| mTFP1 | **1.0** | 0.390 | 0.054 | 0.055 | 0.008 | < 0.001 |
| mCitrine | 0.002 | 0.057 | **1.0** | 0.010 | 0.002 | < 0.001 |
| mAmetrine | 0.001 | 0.020 | < 0.001 | **1.0** | 0.264 | < 0.001 |
| tdTomato | < 0.001 | < 0.001 | 0.001 | < 0.001 | 0.001 | **1.0** |

[a] Abbreviations: ex = excitation, em = emission, TFP = mTFP1, Cit = mCitrine, Ame = mAmetrine, and Tom = tdTomato.

Fortunately, due to differences in FP emission profiles, this cross-excitation is much less of a problem than it might first appear and it can be accounted for with a straightforward mathematical correction factor. Since the emission filter for both mAmetrine and mCitrine are the same, the experimental fluorescence intensities can be calculated using the following equations:

$$I_{Cit}^{raw} = I_{Cit}^{cor} + 0.02 * I_{Ame}^{cor}$$

and

$$I_{Ame}^{raw} = I_{Ame}^{cor} + 0.14 * I_{Cit}^{cor}$$

where $I_{Ame}^{raw}$ and $I_{Ame}^{cor}$ are the experimental and corrected intensities for mAmetrine and $I_{Cit}^{raw}$ and $I_{Cit}^{cor}$ are the respective intensities for mCitrine. Rearranging these equations gives the following relationships between the corrected intensities and the raw intensities:

$$I_{Cit}^{cor} = 1.003 * I_{Cit}^{raw} - 0.020 * I_{Ame}^{raw}$$

and

$$I_{Ame}^{cor} = 1.003 * I_{Ame}^{raw} - 0.14 * I_{Cit}^{raw}$$

These correction factors can be used to scale each image in a time-lapse series on a time-point by time-point basis. It is important to note that these simple correction factors are specific for the FPs and filters used in this work but are general with respect to the FRET construct and FRET efficiency. Furthermore, the simplicity of these correction factors stems from the fact that mAmetrine and mCitrine use the same emission filter. If this were not the case (e.g. if mAmetrine was substituted with T-Sapphire and a green emission filter was used), these correction factors would be significantly more complex. As shown in **Table 6.4** above, both the mTFP1 channel and the tdTomato channel are free from bleed-through from other FPs.

Application of this correction factor had no significant impact on the quantitative analysis of images acquired in this work; a result attributed to matched expression levels and large ratio changes for both FRET constructs. However, in cases where expression levels can not be matched by adjustment of transfection conditions, or ratio changes are small in magnitude, application of this correction factor may be required. It has also been noted that control experiments using individual biosensors are essential for establishing the expected magnitude of ratio changes in the dual FRET scenario.

### 6.3.7 Comparison of mAmetrine to mT-sapphire

mT-Sapphire could, in principle, be used in place of mAmetrine for this dual FRET application. However, its use would be encumbered by both increased emission bleed-through with the mTFP1 channel, and decreased sensitized emission of tdTomato due to decreased spectral overlap. The first of these issues could be addressed with appropriate intensity corrections, though the correction factors would be larger in magnitude.

Assuming use of an appropriate emission bandpass filter for mT-Sapphire (i.e. 500-530 nm) the intensity corrections would also be more complex, with both the mTFP1 and mCitrine intensities appearing as terms in the equation for correction of the mT-Sapphire intensity. Likewise, both the mTFP1 and mCitrine intensities would require correction based on the mT-Sapphire intensity. With respect to the second issue I see no obvious recourse, since no other potential acceptor from the current palette of OFPs and RFPs provides sensitized emission with intensity greater than tdTomato when paired with a green- or yellow-fluorescing donor (**Figure 6.4AB**). The advantages of mT-Sapphire include greater photostability and less pH sensitivity than mAmetrine (**Table 6.1**). Evolution of mAmetrine for improved photostability should be carried out as the future work.

## 6.4 CONCLUSIONS

FRET with fluorescent proteins (FP) is a powerful method for detection of protein-protein interactions, enzyme activities, and changes in local concentrations in the intracellular milieu. I have described the application of dual FRET pairs for accurate measurement of the delay between the onset of caspase-3 activity in the cytoplasm and in the nucleus during apoptosis [149]. Due to distinct excitation profiles, each FRET biosensor can be ratiometrically imaged in the presence of the other. This technology should enable a broad community of researchers to interrogate the interplay and relative kinetics of multiple biological processes with a spatiotemporal precision that was previously inaccessible.

# CHAPTER 7:

# SPECTRALLY COMPATIBLE FP-BASED FRET SENSORS FOR SIMULTANEOUS CALCIUM IMAGING

## 7.1 INTRODUCTION

The calcium ion ($Ca^{2+}$) is one of the most important and versatile second messengers and is involved in many important cellular processes [150]. $Ca^{2+}$ ions form concentration gradients across membranes, and help to establish different microenvironments in cell compartments and intracellular spaces. External signals can often lead to transit $Ca^{2+}$ concentration increases in the cytoplasm. At this elevated concentration, $Ca^{2+}$ can bind to lower affinity sites on regulatory proteins causing them to undergo conformational changes and/or new interactions. In this way, the external signal is turned into a specific biochemical response. A classic example of such a process is the regulation of certain kinases by the protein calmodulin (CaM) [151]. At elevated concentrations, $Ca^{2+}$ binds CaM and the protein is induced to undergo a conformational change. This change enables CaM to bind to and regulate the activity of other proteins (e.g. CaM-dependent protein kinases), and thus results in a specific response. What's more, cells have an intracellular $Ca^{2+}$ storehouse: the endoplasmic reticulum (ER). The release of $Ca^{2+}$ from the ER has crucial roles in the regulation of many biological pathways from the beginning of life until death [152].

The dynamics of intercellular $Ca^{2+}$ has been a major research focus in life sciences in the past years [150]. The concentration of $Ca^{2+}$ is highly heterogeneous within cells and defined in local compartments, and also it changes very abruptly, so monitoring $Ca^{2+}$ with spatial and temporal resolution presents a significant challenge. Fortunately many fluorescent probes of intracellular $Ca^{2+}$ concentration have been developed. Much of the pioneering work in this area was done by Roger Tsien of the University of California San Diego, who synthesized the first rationally designed fluorescent $Ca^{2+}$ probes for intracellular use in the late 1970s [153].

Fluorescent $Ca^{2+}$ probes could be broadly classified into either synthetic or protein-based indicators. The former are synthetic organic molecules, usually polycarboxylate dyes. Those dyes often have high dynamic range and are invaluable tools for many research applications [150]. The major advantage of protein-based indicators is that they are genetically encoded and can be specifically targeted to subcellular compartments or microenvironments by inserting small signal sequences or fusing to another protein of interest.

A landmark event in the history of protein-based $Ca^{2+}$ sensors is Shimomura's isolation of bioluminescent and fluorescent proteins from the jellyfish *Aequorea victoria* in the 1960s [36] [154]. Aequorin is a chemiluminescent (or bioluminescent) protein that emits photons upon calcium binding and oxidation of the substrate coelenterazine [36]. Aequorin can be used to detect changes in $Ca^{2+}$ concentration in live cells, provided that coelenterazine is present. Fortunately, coelenterazine is cell membrane permeable so aequorin is suitable for luminescent imaging in cell culture if coelenterazine is added to the growth media. However, the amount of chemiluminescence from a single cell is usually low, so signal integration is required during measurement, at the expense of both temporal and spatial resolution [155].

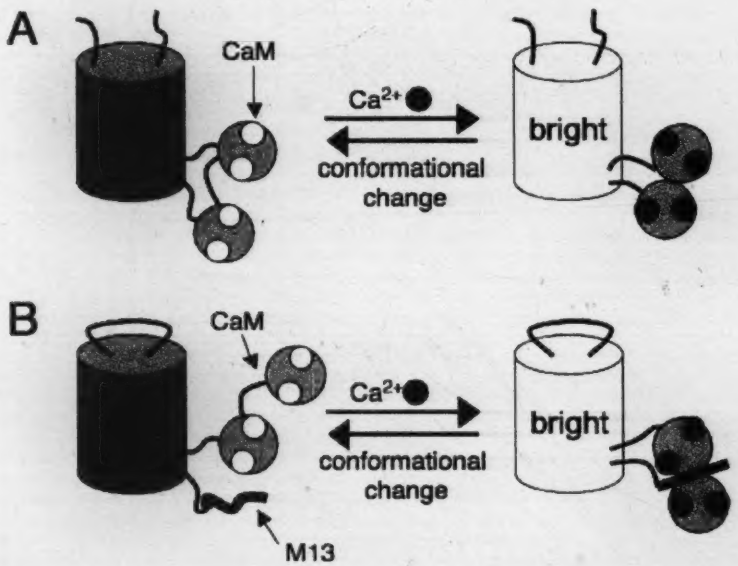


**Figure 7.1** The schematic representaion of single FP-based $Ca^{2+}$ sensors created by (A) inserting the CaM domain into the middle of a FP [64]; (B) fusing CaM and another CaM-binding peptide on the termini of a circularly permutated FP [65, 66].

Recombinant $Ca^{2+}$ probes based on engineered FPs have been under a continual state of development since the mid-1990s [37]. There are several different strategies to create FP-based $Ca^{2+}$ probes, and all strategies require a $Ca^{2+}$-binding domain, typically CaM. The single-FP-based sensors were designed by inserting the CaM domain into the middle of a FP (**Figure 7.1A**) [64], or fusing CaM and another CaM-binding peptide on the termini of a circularly permutated FP (**Figure 7.1B**) [65, 66]. Upon the binding of

$Ca^{2+}$, the conformational change in the CaM is 'communicated' to the chromophore of the FP and alters the fluorescence properties of the FP moieties. This 'communication' between CaM and the chromophore likely involves subtle conformational changes that result in increase of the fluorescence due to reduced solvent accessibility or reduced chromophore conformational freedom.

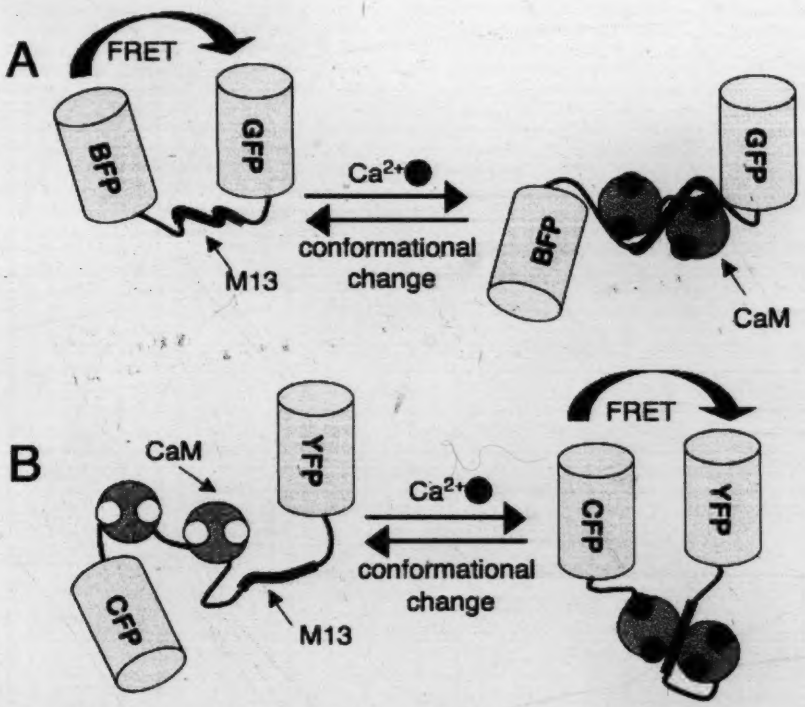


**Figure 7.2** The schematic representaion of FRET-based $Ca^{2+}$ sensors created by (A) linking a BFP and a GFP through an M13 peptide [156]; (B) inserting both CaM and M13 between the FPs (e.g. CFP and YFP) [70].

Another important design for FP-based $Ca^{2+}$ sensors is to sandwich binding motifs between two FPs of a FRET pair. The FRET efficiency is used as the parameter indicating $Ca^{2+}$ concentration. Persechini and his colleagues approached one of the earliest designs by linking a BFP and a GFP through an M13 peptide (**Figure 7.2A**) [156]. If the $Ca^{2+}$ concentration increases, the endogenous or transfected CaM binds M13, leading to a FRET decrease. Simultaneously, Tsien and co-workers reported the now well-known Cameleons (**Figure 7.2B**). Cameleons were created by inserting both CaM and M13 between the FPs (e.g. CFP and YFP) [70]. In this design, binding of $Ca^{2+}$ to CaM leads to intramolecular binding of CaM and M13 that dramatically changes the

orientation and/or distance between the two FPs at the ends of the sensor. Accordingly, the increase of $Ca^{2+}$ concentration causes a FRET increase.

Since the first generation of Cameleons appeared in 1997, much work has been done to improve their performance, including mutation of the calmodulin domain, systematic modification of the linker regions, and replacing M13 with different calmodulin-binding peptides [111, 157, 158]. In the recent work, Tsien and colleagues have described the development of redesigned Cameleons with broader dynamic range that can monitor $Ca^{2+}$-concentration fluctuations in different cell compartments and have less perturbation due to endogenous CaM [159, 160]. Based on previously obtained structural data, the CaM and CaM-binding peptide interaction surface was computationally and experimentally redesigned. From this work new Cameleons, known as D1, D2, D3 and D4, were derived, characterized and applied to a variety of $Ca^{2+}$ measurements.

In the previous chapter, I described the creation and validation of new spectrally compatible FRET pairs: mTFP1-mCitrine coupled with mAmetrine-tdTomato. These new FRET pairs enable simultaneous ratiometric live cell imaging of two different sensors. In order to expand the use of the new FRET pairs, I have created $Ca^{2+}$ sensors based on the compatible FRET pairs. Two groups of $Ca^{2+}$ sensors were made based on either mTFP1 and a YFP variant (Citrine or cpVenus), or mAmetrine (or its circularly permutated version) and tdTomato. The new $Ca^{2+}$ sensors are designated 'CaYang' and 'CaYin' respectively. Yang and yin in Chinese philosophy describe 'unity in duality' [161]. Accordingly the names for these new sensors combine their function (calcium sensors) and either yang (for the mTFP1-YFP sensor) or yin (for the mAmetrine-tdTomato sensor) to emphasize their spectral orthogonality and compatibility. This chapter describes the efforts to make spectrally compatible $Ca^{2+}$ sensors, and their preliminary application to simultaneous $Ca^{2+}$ imaging.

## 7.2 EXPERIMENTAL

### 7.2.1. General methods

Synthetic DNA oligonucleotides for cloning and library construction were purchased from Integrated DNA Technologies (Coralville, IA). PCR products and

products of restriction digests were purified by gel electrophoresis and extraction using either the GenCatch™ gel extraction kit (Epoch Biolabs, TX) or the QIAquick™ gel extraction kit (QIAGEN, Valencia, CA). Plasmid DNA was purified from overnight cultures by using either the GeneJET™ Plasmid Miniprep Kit (Fermentas, ON) or the QIAprep Spin Miniprep kit (QIAGEN, Valencia, CA). Restriction endonucleases were purchased from either Invitrogen or New England Biolabs. Dye terminator cycle sequencing using the DYEnamic ET kit (Amersham Biosciences) was used to confirm the complete cDNA sequences for all fusion constructs. Sequencing reactions were analyzed at the University of Alberta Molecular Biology Service Unit. All filters for fluorescence screening and imaging were purchased from Chroma Technology (Rockingham, VT), Omega Filters (Brattleboro, VT) and Semrock (Rochester, NY.

### 7.2.2. Evolution of circularly permutated mAmetrine 173 (cpmAmetrine-173)

A gene encoding mAmetrine circularly permutated at the position 173 was created by overlap PCR. The 5' end of the gene was PCR amplified with primers 5'-GTAACTCGAGCNNKGACGGCGGCGTGCAGCTCGCC-3' and 5'-TCCGCCGGATCCGCCCTTGTACAGCTCGTCCAT-3'. The 5' end of the gene was PCR amplified with primers 5'-AAGGGCGGATCCGGCGGAATGGTGAGCAAGGGCGAG-3' and 5'-TGACGAATTCTTAMNNCTCGACGTTGTGCTCGATCTT-3'. The two resulting PCR products were mixed and used as the template in a 3$^{rd}$ PCR reaction with outside primers 5'-GTAACTCGAGCNNKGACGGCGGCGTGCAGCTCGCC-3' and 5'-TGACGAATTCTTAMNNCTCGACGTTGTGCTCGATCTT-3'. This procedure provides a new gene in which a peptide linker (GGSGG) connects the original N- and C-termini of mAmetrine. The new N- and C-termini of the gene product would occur between what were originally residue numbers 173 and 174. An extra-randomized residue is appended to each of the new termini to create a gene library of 400 members.

When randomizing the whole cpmAmetrine gene, EP-PCR were carried out as previously described in **Section 2.2**. Generally, under the same condition of regular PCR with Taq polymerase, $MnCl_2$ was added to a final concentration of 200 μM, and 4 individual reactions were carried out with dNTP mixtures in which the concentration of

one component (dATP, dTTP, dGTP or dCTP individually) was reduced from the typical concentration of 200 μM to a final concentration of 50 μM. The reactions were carried out with 38 cycles.

PCR products were digested with Xho1 and EcoR1 and ligated into similarly digested pBAD/HisB vector (Invitrogen). Electrocompetent *E. coli* strain DH10B (Invitrogen) was transformed and plated on LB/agar plates supplemented with ampicillin (0.1 mg/ml) and L-arabinose (0.02%). Plates were incubated for 14 h at 37 °C prior to screening. The library was screened as the method described in the previous chapter. Colonies were illuminated with light from a 175 W xenon-arc lamp (Sutter) that had been passed through a 375 to 415 nm or a 490 nm to 510 nm bandpass filter. Colony fluorescence was imaged with a Retiga 1300i 12-bit CCD camera (QImaging) fitted with either a 440 to 480 nm or a 520 to 550 nm emission filter. For each plate of colonies, 3 images were acquired: excite 375-415 nm, emit 440-480 nm; excite 490-510 nm, emit 520-550 nm; and excite 375-415 nm, emit 520-550 nm. Colonies with the highest ratio of fluorescence intensity in the latter image relative to fluorescence intensity in the other 2 images were picked.

### 7.2.3. Construction of Cameleons (CaYang and CaYin) for *in vitro* study

To construct new Cameleon variants, the gene encoding mTFP1 Cameleon described in **Chapter 2** was used as the initial cloning template. This plasmid harbours cDNA encoding mTFP1 (1-220), followed by the binding motif of YC3.3 (mutated calmodulin and M13 peptide), followed by Citrine. The mTFP1 sequence is inserted between XhoI and SphI restriction sites, the binding motif is between SphI and SacI, restriction sites, and Citrine is between SacI and EcoRI. The whole fusion gene was cloned in a pBAD/His B vector in frame with a $His_6$ purification tag attached to the N-terminus of the protein.

To construct $Ca^{2+}$ sensors suitable for use in the ER, a variety of different YFPs and binding domains were used to replace the corresponding domains of the mTFP1-mCitrine Cameleon described above. For example, mCitrine was amplified by primers harbouring SacI and EcoRI restriction sites and double digested by SacI and EcoRI restriction enzymes and cpVenus-173 was excised from D3 Cameleon by digestion with SacI and

EcoRI. The binding motif from YC4.3 was excised by digestion with SphI and SacI and the binding motif from D1 Cameleon was excised by digestion with SphI and SacI. Sequential ligations were used to make respective constructs by pasting the digested gene fragments together with the digested initial cloning template to replace the original YC3.3 binding motif or Citrine gene.

To construct cytoplasm $Ca^{2+}$ sensors, a variety of alternative arrangements of mAmetrine, binding domain, and tdTomato were attempted. To generate appropriate gene fragments encoding the N-terminal FP of the FRET pair, mAmetrine (1-227), cpmAmetrine-173, tdTomato (1-437) or tdTomato (1-452) were each amplified by primers harbouring XhoI and SphI restriction sites and double digested by XhoI and SphI restriction enzymes. To generate appropriate gene fragments encoding the C-terminal FP of the FRET pair, mAmetrine (6-238), cpmAmetrine-173 or tdTomato were amplified by primers harbouring SacI and EcoRI restriction sites and double digested by SacI and EcoRI restriction enzyme. To generate gene fragments encoding the binding motif, the cDNA encoding the binding motif of YC2.1 was excised by SphI and SacI and the binding motif from D3 Cameleon was excised by SphI and SacI. Sequential ligations were used to make respective constructs by pasting the digested gene fragments together with the digested initial cloning template to replace the original mTFP1 (1-227), YC3.3 binding motif, or Citrine gene.

A modified procedure was used to construct the genes encoding the two cytoplasm calcium sensors with modified CaM from D3 Cameleon sitting at the C- terminal end (CaYin0.6 and CaYin0.7). Overlap PCR with primers harbouring SphI and EcoRI sites was first used to join the modified CaM-binding peptide from D3, tdTomato, and the modified CaM together, followed by digestion with Sph1 and EcoR1. The digested product was ligated into pBAD/His B plasmid of CaYin0.2 or CaYin0.3 pre-digested by Sph1 and EcoR1.

### 7.2.4. Protein purification and characterization

For production of protein, *E. coli* strain LMG194 was transformed with the pBAD/His B expression vector containing the each of the various Cameleon constructs. A single colony was used to inoculate a 4 mL culture that was allowed to grow overnight

(37 °C, 225 rpm) before being diluted into 1 L of LB medium supplemented with ampicillin and L-arabinose. The culture was grown for 48 h at 25 °C before cells were harvested by centrifugation and lysed by French Press. Proteins were initially purified by Ni-NTA chromatography (Amersham) from the supernatant of the lysate, followed by size exclusion column chromatography (Amersham Superdex 75 prep) in Tris-buffered saline (pH 7.5).

To measure fluorescence quantum yield and extinction coefficient of cpmAmetrine, mAmetrine was used as a reference standard. Base-denaturation method was used to match the protein concentration.

To determine the fluorescence response upon $Ca^{2+}$ binding, Cameleons (500 nM) were mixed with equal volume of 200 mM $CaCl_2$ or 200 μM EGTA in Tris-buffered saline (pH 7.5). The fluorescence of both mixtures of the same protein was recorded by a Tecan Safire2 fluorescence plate reader.

### 7.2.5. Construction of Cameleon mammalian expression vectors

To construct the expression vector of endoplasmic reticulum $Ca^{2+}$ sensor, the corresponding construct in pBAD/His B vector was amplified with primers 5'-CGTTAGAAGCTTGCCACCGCCATGCTGCTATCCGTGCCCCTGCTGCTCGGCCT GCTGGGCCTGGCCGCCGCCGACCAGGGCTCGAGCACGGTGAGCAAG-3' and 5'-TCGGAATTCTTACAGCTCGTCCTTCTTGTACAGCTCGTCCATGCC-3'. This reaction appended a HindIII restriction site followed by a Kozak sequence and a calreticulin signal peptide (MLLSVPLLLGLLGLAAA) at the 5'- end, and an ER retention sequence (KDEL) followed by an EcoRI restriction site at the 3'- end. The PCR product was digested with HindIII and EcoRIII and inserted into pre-digested pcDNA3 vector (Invitrogen).

To construct the expression vector for the cytoplasmic $Ca^{2+}$ sensor, the corresponding construct in pBAD/His B vector was amplified with primers 5'-GATAAGCTAGCGCTACCGGTCGCCACCATGGTGAGCAAGGGCGAGGAG-3' and 5'-ATTACCTCGAGATCTGAGTCCGGACTTGTACAGCTCGTCCATGCC-3'. This reaction appended an NheI restriction site followed by a Kozak sequence at the 5'-end, and an XhoI restriction site at the 3'- end. The PCR product was digested with NheI

and XhoI and inserted in to pre-digested pEYFP-Nuc vector (Clontech). The sequence of EYFP and nuclear localization sequence were removed when the vector was digested with NheI and XhoI.

### 7.2.6. Live cell imaging

All DNA for mammalian cell transfection was purified by Plasmid Midi kit (Qiagen). HeLa cells were cultured in DMEM (Invitrogen) supplemented with 10% FBS (Sigma) at 37 °C. Cells in 35 mm imaging dishes were transfected with 4 μg plasmid DNA (3 μg DNA of CaYin0.9 and 1 μg DNA of CaYang1) mixed with 10 μg polyethylenimine (linear, molecular weight ~25,000, Polysciences Inc.) in 0.5 ml OptiMEM (Invitrogen). The buffer was changed back to DMEM with 10% FBS after 1 h. Approximately 24 to 48 h later the medium was exchanged for Hanks' Balanced Salt Solution (HBSS) containing no phenol red (Invitrogen) and the cells were imaged. HeLa cells expressing both sensors were imaged with a Zeiss Axiovert 200M epi-fluorescence inverted microscope equipped with a xenon arc lamp and a monochrome Retiga 2000R 12-bit cooled CCD camera (QImaging). The external excitation filter wheel, excitation shutter, and emission filter wheel are controlled through a Lambda 10-3 controller (Sutter). Only dichroic mirrors are housed in the motorized reflector turret. The same filter combinations for dual FRET described in the previous chapter were used. The QED InVivo software package (Media Cybernetics) is used for automated computer control of all microscope hardware and for quantitative image analysis.

## 7.3 RESULTS AND DISCUSSION

### 7.3.1. Circularly permutated mAmetrine 173

It has previously been shown that incorporation of cpFPs into FRET-based biosensors can dramatically increase the dynamic range of the FRET response [160]. The dynamic range of Cameleons, FRET-based $Ca^{2+}$ sensors, is the difference of FRET efficiency between a low FRET state (typically the $Ca^{2+}$ free state) and a high FRET state (typically the $Ca^{2+}$ bound state). The FRET efficiency change between the two states is determined by the distance change of the donor and acceptor, and probably more importantly, by the dipole orientation change of the donor and acceptor. Incorporation of

cpFPs provides different dipole-dipole interaction in both states, and possibly enhances the dynamic range. Therefore creating new cpFP variants of mAmetrine is an avenue for improving the dynamic range of FRET sensors based on mAmetrine.

Previously circularly permutated mutant of Venus at the position 173 (cpVenus-173) were demonstrated to greatly increase the dynamic range when swapped with Citrine in Cameleons [160]. For this reason, I first decided to create its mAmetrine analogue by creating new termini at the position 173 of mAmetrine. The new termini of cpmAmetrine are located at the opposite end of the β-barrel from the original N- and C-termini (**Figure 7.3**). Therefore, it should also theoretically provide remarkably different dipole-dipole interactions.

Overlap PCR was used to connect the original N- and C- termini of mAmetrine. The new N- and C-termini were created from the site between the original 173 and 174 residues and an extra randomizing residue was appended on each new terminus. Therefore this modest library has $20^2$ possibilities of protein sequence. The library was screened in colonies of *E. coli* to find the brightest yellow fluorescent variant when excited with violet light. Sequencing the 'best' variant identified revealed that it had a lysine at the 5' end and a proline at the 3'end. Although it was the brightest of the circularly permuted variants, it only retained about 10% of the brightness of original mAmetrine, when expressed in *E. coli* grown overnight in a 37 °C incubator. In order to improve the fluorescent brightness, a process of directed evolution was carried out by performing 5 sequential rounds of error-prone PCR and screening for brightness. The plasmid DNA of brightest colony of the $5^{th}$ round was purified, and this variant was designated as circularly permuted mAmetrine 173 (cpmAmetrine-173). This variant retains about 80% of the brightness of original mAmetrine, as determined in *E. coli* grown overnight in a 37 °C incubator. Gene sequencing showed that cpmAmetrine-173 is a mutant of mAmetrine with E32G/I123V/K131R/E142G/N144S/A181V/Q204R mutations, the original termini of mAmetrine is linked by GGSGG pentapeptide, and the new termini is between the position 173 and 174 with a lysine and a proline appended on the N- and C-terminal ends, respectively (**Figure 7.3B**).

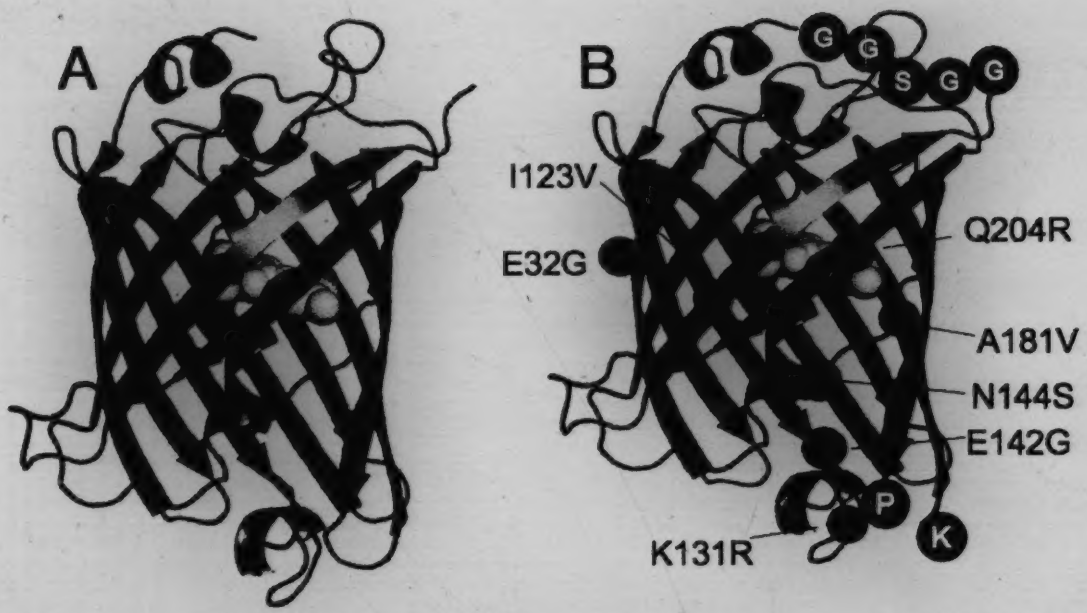


**Figure 7.3** Modeled structures of (A) mAmetrine and (B) cpmAmetrine-173. The linker sequence and the appended residues of cpmAmetrine-173 are shown in gray circles. The black balls illustrate the mutations generated by random mutagenesis.

The cpmAmetrine-173 protein was purified for further characterization. The measured intrinsic brightness (product of quantum yield and extinction coefficient) of the purified protein is almost identical to the original mAmetrine (**Table 7.1**). So the reduced brightness in colonies should be the result of reduced protein expression or, very likely, reduced protein folding and maturation efficiency. Unfolded protein often enters the inclusion bodies, so wasn't purified from the supernatant of the cell lysate. Only the folded and mature protein was purified and shown to have effectively the same brightness of mature mAmetrine.

**Table 7.1** Fluorescence properties of mAmetrine and cpmAmetrine-173.

| | $\lambda_{ex}$ (nm) | $\lambda_{em}$ (nm) | $\varepsilon$ ($10^3$ $M^{-1}cm^{-1}$) | $\phi$ | Brightness[a] |
|---|---|---|---|---|---|
| mAmetrine | 406 | 526 | 45 | 0.58 | 26 |
| cpmAmetrine-173 | 402 | 522 | 45 | 0.60 | 27 |

[a] Product of EC and QY.

### 7.3.2. Endoplasmic reticulum calcium sensors (CaYangs)

The concentration of $Ca^{2+}$ in the ER is usually about 100-1000 times higher than in cytoplasm and in micromolar range. The $Ca^{2+}$ sensor in the ER should thus have a relatively low affinity to calcium. The previously desribed mTFP1-based biosensor (refer to **Chapter 2**) was created by replacing ECFP of $Ca^{2+}$ sensor YC3.3 with mTFP1. Although this sensor has been used to monitor $Ca^{2+}$ changes in ER, it showed only small dynamic range both *in vitro* and *in vivo*, and therefore broader application of this sensor is limited.

The initial attempt to improve this sensor was to replace the binding domain with other candidates. The binding domain of YC4.3, a $Ca^{2+}$ sensor with higher $Ca^{2+}$ affinity than YC3.3, was used first. The purified protein of the new construct (designated as CaYang0.1), however, showed reduced dynamic range (**Figure 7.4** and **Table 7.2**).. The Tsien group had reported the new designed D1 Cameleon with $Ca^{2+}$ affinity suitable for ER $Ca^{2+}$ imaging [159]. D1 was considered as a big improvement of cyan/yellow FP-based $Ca^{2+}$ sensors, with enhanced dynamic range and less perturbation by endogenous CaM. The binding domain of D1 replaced the original YC3.3-binding domain to create CaYang0.2 (**Figure 7.4**). CaYang0.2 showed improved dynamic range compared to the other two constructs (**Table 7.2**).

The Tsien group also reported that replacing Citrine with cpVenus-173 greatly increased the dynamic range of Cameleons [160]. It was logical for me to test whether or not this improvement is maintained when paired with the different FRET donor mTFP1. Replacing mCitrine of CaYang0.2 with cpVenus-173 produced CaYang1, which showed ~3× enhancement of dynamic range (**Figure 7.4** and **Table 7.2**).

For all four constructs created, CaYang1 showed the biggest dynamic range for purified proteins (**Figure 7.5A** and **Table 7.2**). What's more, it should also inherit the good characters from D1 Cameleon, such as less perturbation by endogenous CaM and affinity suitable for ER $Ca^{2+}$. Therefore, CaYang1 is the best sensors created from teal and yellow FPs for ER $Ca^{2+}$ imaging.

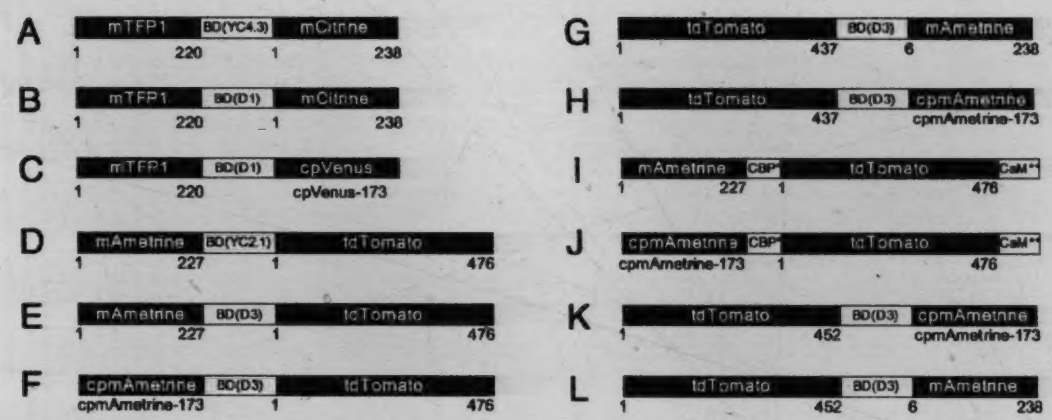


**Figure 7.4** Primary structures of (A) CaYang0.1; (B) CaYang0.2; (C) CaYang1; (D) CaYin0.1; (E) CaYin0.2; (F) CaYin0.3; (G) CaYin0.4; (H) CaYin0.5; (I) CaYin0.6; (J) CaYin0.7; (K) CaYin0.8; (L) CaYin0.9. (*CBP = CaM-binding peptide of D3; **CaM = mutated CaM of D3.)

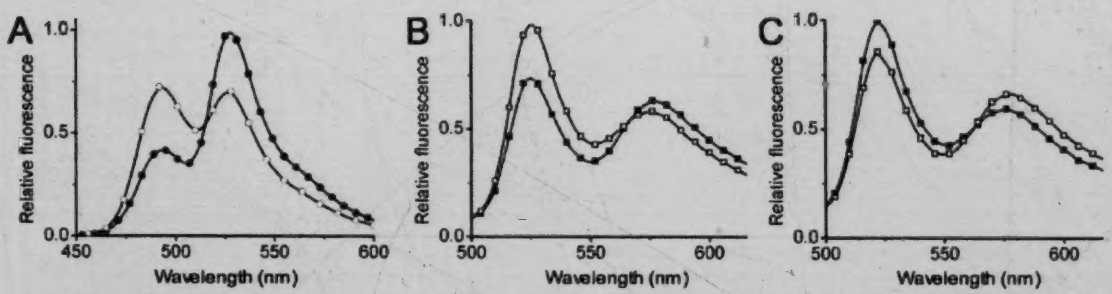


**Figure 7.5** The $Ca^{2+}$ response of (A) CaYang1; (B) CaYin0.9; and (C) CaYin0.7. The solid symbols represent the fluorescence of proteins in Tris-buffered saline with 100 mM calcium; the open symbols represent the fluorescence of proteins in Tris-buffered saline with 100 μM EGTA.

**Table 7.2** Cameleon constructs and their $Ca^{2+}$ response.

| Name | Gene construction[a] | Ratio (sensitized emission/donor emission) | | |
|---|---|---|---|---|
| | | $-Ca^{2+}$ | $+Ca^{2+}$ | % of Change |
| | mTFP1(1-220) – BD[b](YC3.3) – Citrine (**Section 2.3.4**) | 1.37 | 1.84 | **+35** |
| CaYang0.1 | mTFP1(1-220) – BD(YC4.3) - mCitrine | 1.07 | 1.18 | **+10** |
| CaYang0.2 | mTFP1(1-220) – BD(D1) - mCitrine | 0.99 | 1.55 | **+57** |
| CaYang1 | mTFP1(1-220) – BD(D1) – cpVenus-173 | 0.97 | 2.44 | **+151** |
| CaYin0.1 | mAmetrine(1-227) – BD(YC2.1) - tdTomato | 0.46 | 0.59 | **+26** |
| CaYin0.2 | mAmetrine(1-227) – BD(D3) - tdTomato | 0.49 | 0.58 | **+17** |
| CaYin0.3 | cpmAmetrine-173 – BD(D3) - tdTomato | 0.44 | 0.58 | **+33** |
| CaYin0.4 | tdTomato(1-437) – BD(D3) – mAmetrine(6-238) | N/A[c] | N/A | **N/A** |
| CaYin0.5 | tdTomato(1-437) – BD(D3) – cpmAmetrine-173 | N/A | N/A | **N/A** |
| CaYin0.6 | mAmetrine(1-227) – CBP[d](D3) – tdTomato-CaM[e](D3) | 0.78 | 0.66 | **-15** |
| CaYin0.7 | cpmAmetrine-173 – CBP(D3) - tdTomato-CaM(D3) | 0.77 | 0.59 | **-23** |
| CaYin0.8 | tdTomato(1-452) – BD(D3) – cpmAmetrine-173 | 0.81 | 1.0 | **+24** |
| CaYin0.9 | tdTomato(1-452) – BD(D3) – mAmetrine(6-238) | 0.58 | 0.84 | **+45** |

[a] If not indicated, the whole gene of the FP was cloned.
[b] BD = binding domain (including mutated camodulin and camodulin-binding peptide).
[c] N/A = not available.
[d] CBP = mutated camodulin-binding peptide of D3 Cameleon.
[e] CaM = mutated camodulin of D3 Cameleon.

### 7.3.3. Cytoplasm calcium sensors (CaYins)

The concentration of $Ca^{2+}$ in cytoplasm is much lower than in the ER and thus cytoplasmic $Ca^{2+}$ sensors require higher $Ca^{2+}$ affinity. The ER sensors described above were based on teal and yellow FPs, and the goal here was to make two groups of

spectrally compatible $Ca^{2+}$ sensors, so the sensors for cytoplasm $Ca^{2+}$ were created from mAmetrine (or cpmAmetrine) and tdTomato.

The binding domain of YC2.1 was initially tested because YC2.1 has been demonstrated to be a good cytoplasmic $Ca^{2+}$ sensor. Also, it was reasonable to examine the binding domain of D3 Cameleon, a reported cytoplasm $Ca^{2+}$ sensor based on ECFP and cpVenus-173 [160]. CaYin0.1, CaYin0.2 and CaYin0.3 (**Table 7.2**) are the constructs in which the binding motif from YC2.1 or D3 is sandwiched between mAmetrine (or cpmAmetrine) and tdTomato. In CaYin0.4 and CaYin0.5 the positions of mAmetrine (or cpmAmetrine) and tdTomato were swapped (**Table 7.2**). It is important to notice that the residue 227 of mAmetrine and the residue 437 of tdTomato are structurally aligned with the residue 220 of mTFP1.

Other efforts were made to split the CaM-binding peptide and the mutated CaM of D3 Cameleon, and then fuse CaM to the C-terminus of tdTomato (**Figure 7.4IJ**). Inspection of the x-ray structure of DsRed led us to predict that one subunit of tdTomato would be relatively distant from the donor in the fusion protein [49]. The theory of this design is that the calcium binding event will cause a structural change favouring FRET to both subunits of tdTomato. Surprisingly this was not the case, and the purified proteins of CaYin0.6 and CaYin0.7 both showed reduced FRET upon $Ca^{2+}$ increase (**Table 7.2** and **Figure 7.5C**). This result demonstrated that the success of optimizing FRET-based biosensors mainly relies on the tedious work of creating as many variants as possible, then characterizing and comparing them.

CaYin0.4 and CaYin0.5 were less soluble when expressed in *E. coli* and efforts to purify them from supernatants of cell lysates failed. Most likely the truncation of tdTomato from its C-terminus changed its dimerization. The full-length tdTomato works as a monomer because intramolecular interface interaction is favored. However the truncated tdTomato might favor intermolecular dimerization. Therefore the proteins of CaYin0.4 and CaYin0.5 could form a non-covalently lattice of crosslinked proteins. In order to overcome this problem, new versions later designated as CaYin0.8 and CaYin0.9 (**Table 7.2** and **Figure 7.4KL**) were created with tdTomato which is less truncated from the C-terminus. tdTomato(1-452) includes all residues involved in intersubunit interactions as based on inspection of the DsRed crystal structure [49].

Among all nine sensors based on mAmetrine (or cpmAmetrine-173) and tdTomato (**Table 7.2**), two of them (CaYin0.4 and CaYin0.5) are less soluble so not suitable for live cell imaging, and two of them (CaYin0.6 and CaYin0.7) showed reversed $Ca^{2+}$ response, and CaYin0.9 has the largest dynamic range (**Figure 7.5B**). CaYin0.9 is a construct with a tdTomato fused to the N- terminus of D3 binding motif, a mAmetrine fused to the C- terminus of D3 binding motif. Akin to D3 Cameleon, CaYin0.9 should be less perturbed by endogenous CaM, and suitable for cytoplasmic $Ca^{2+}$ imaging.

### 7.3.4. Compatible dual-compartmental calcium imaging

After thorough comparison, CaYang1 and CaYin0.9 were considered as the best in their respective groups. In the previously chapter, I have showed that the four colors of FPs are spectrally compatible for simultaneous ratiometric FRET imaging. Using the same microscope setup, the spectral compatibility of the new $Ca^{2+}$ sensors was also examined.

CaYang1 fused with a calreticulin signal peptide and an ER retention sequence was expressed in HeLa cells and showed inclusive localization in the ER (**Figure 7.6**). CaYin0.9 has a molecular weight of ~100 kD. It is partially excluded from the nucleus when expressed in HeLa cells without any signal sequence. Probably its size is comparable to the limit for passive permeability of the nuclear envelope. CaYin0.9 was detected in both cell nucleus and cytoplasm, however, with lower concentration in the cell nucleus (**Figure 7.6**).

As a preliminary experiment, a cotransfected HeLa cell was imaged in HBSS buffer (**Figure 7.6**). This cell expressed CaYang1 in the ER and CaYin0.9 in cytoplasm. After imaging for about 2 minutes, the ionomycin was added to the cells. Ionomycin is a $Ca^{2+}$ ionophore that causes $Ca^{2+}$ release from the ER (initially at high $Ca^{2+}$ concentration) into the cell cytoplasm (initially at low $Ca^{2+}$ concentration). As expected, the FRET ratio (acceptor *vs* donor) of CaYang1 in the ER decreased, matched with the increase of CaYin0.9 FRET in the cytoplasm. After several more minutes, a high concentration of $Ca^{2+}$ was directly added into the buffer, the $Ca^{2+}$ concentrations in both cell compartments dramatically increased and caused a corresponding increase of FRET for both sensors.

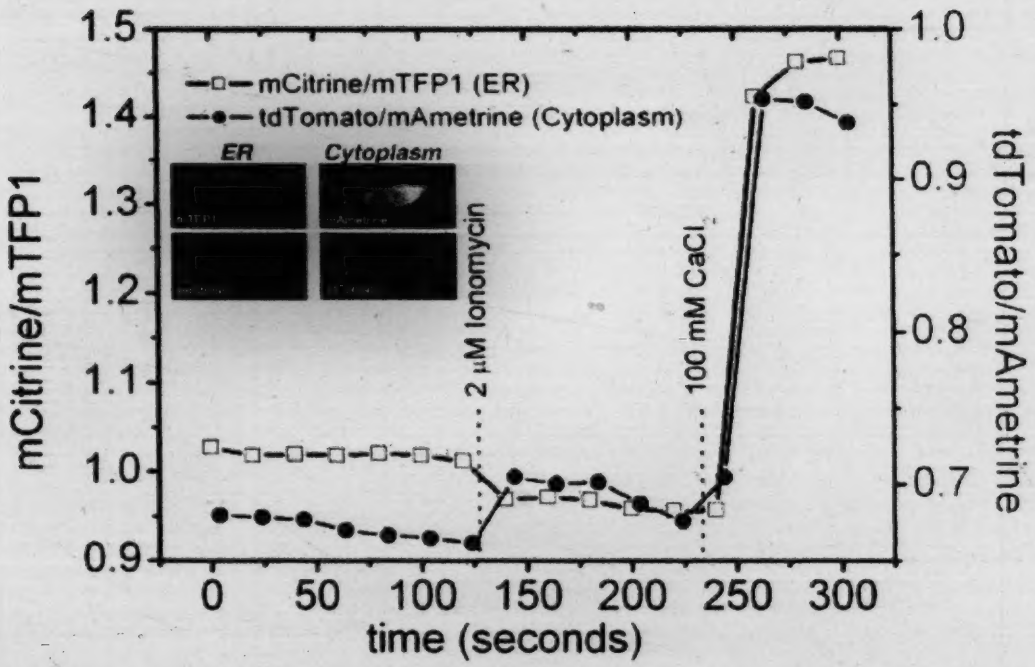


**Figure 7.6** The $Ca^{2+}$ response of a cotransfected HeLa cell expressing ER-targeted CaYang1 and non-targeted CaYin0.9. The insets are images showing the initial fluorescence of four individual channels.

## 7.4 CONCLUSIONS

The first described dual FRET pairs, mTFP and mCitrine together with mAmetrine and tdTomato, have been further expanded by the efforts described in this chapter. I demonstrated that cpVenus-173 could also be used as the FRET acceptor to mTFP1, and I also created cpmAmetrine-173, a new circularly permutated variant of mAmetrine, as an alternative FRET donor to tdTomato.

Creating $Ca^{2+}$ sensors is one of the most important applications of FPs. Here I also described the creation of compatible $Ca^{2+}$ sensors based on the compatible FRET pairs. After creating a dozen different constructs and comparing them for $Ca^{2+}$ response, CaYang1 and CaYin0.9 were identified as the sensors with the greatest dynamic range in their respective groups. The two sensors were optimized for ER and cytoplasm $Ca^{2+}$ imaging, respectively, and showed dramatic FRET increase when $Ca^{2+}$ concentration increased. In contrast, CaYin0.7 showed reversed $Ca^{2+}$ response with modest dynamic range. As a preliminary experiment, CaYang1 and CaYin0.9 were successfully used to

monitor $Ca^{2+}$ dynamics in mammalian cells simultaneously. Those results provided an initial point to further improve spectrally compatible dual $Ca^{2+}$ sensors.

# CHAPTER 8:

# CONCLUSIONS AND FUTURE WORK

Interest in FPs technologies has been growing at an remarkable rate ever since the cloning of the archetypal *Aequorea victoria* jellyfish green FP (avGFP) [113]. FPs with a variety of fluorescent colors, ranging from blue to the far-red, are now used in thousands of labs around the world as non-intrusive genetically encoded markers [68]. Although much work has already gone into the development of these various colors of FP, a few members in the 'toolbox' are still considerably less optimal than others. The attempt to overcome those problems and expand the application of FP technology is the main focus of this thesis.

Two of the earliest additions to the toolbox, BFP and CFP, occupy the high-energy end of the visible spectrum and were of concern to us because of their particularly poor properties [37]. In an effort to address the deficiencies of these protetins, I developed improved BFPs (e.g. EBFP2) by exploring the variety of blue chromophore structures. This work has provided new tools for researchers willing to use a blue FP, which had been considered of very little use because of the flaws of previous BFP variants. Furthermore, I monomerized tetrameric *Clavularia* FP484 to mTFP1, which has been proven to be a favourable alternative to existing CFP. mTFP1 is one of the brightest and most photostable FPs reported to date. The mechanism investigation of the spectral shift of mTFP1 led to another useful green FP, mWasabi [75].

In the process of engineering mTFP1, I discovered mTFP0.7, a reversibly photoswitchable version of mTFP1. This intriguing protein was subjected to extensive structural and photophysical characterization. The kinetics of the photochemistry and the energy barrier of the recovery have been measured. The x-ray crystal structure of fluorescent and dark states solved in collaboration with Prof. S.J. Remington [61] supported a chromophore cis-trans isomerization mechanism.

Due to the fact FPs have broad fluorescence excitation and emission profiles and the red or far-red FPs have low sensitised emission when used as FRET acceptors, only one FRET pair at a time is typically used for ratiometric FRET experiments [68]. My recent work created a new FP mAmetrine with long Stokes shift; and identified spectrally compatible FRET pairs, mAmetrine and tdTomato plus mTFP1 and mCitrine that can be imaged in the same cell. These new FRET pairs have been used to monitor caspase activation in apoptotic cells and identify the time difference of caspase-3 activation in cytoplasm and nucleus. To further extend the use of the dual FRET pairs, I also created compatible $Ca^{2+}$ sensors for

simultaneous $Ca^{2+}$ imaging in the ER and cytoplasm. This work provided an initial foundation for further improvement of spectrally compatible $Ca^{2+}$ sensors.

As for the future work, the photostability of mAmetrine remains as a big concern and this problem should be, and can be, tackled. Similar research could also be applied to mBlueberry2 and mKalama1, two bright blue FPs with insufficient photostability. Although EBFP2 is probably good enough for most applications, mBlueberry2 is extremely insensitive to pH change and could eventually become the preferred choice for imaging in low or variable pH environments. Building arrays of intense LEDs to photobleach the colonies would provide a selection pressure for photostability and has already been demonstrated to work well during the previous evolution process towards mTFP1.

The development of dual FRET pair is unquestionably an important step to expand the use of FPs into exciting new research areas. Further improvement of $Ca^{2+}$ sensors should be carried out and the sensors should be optimized for other cell compartments besides the ER and cytoplasm. Furthermore, the compatible FRET technique could be expanded to create many other biosensors, such as for kinase activity [162, 163], and histone methylation [72].

Continuing to fix the problems of FPs in the existing color palette is obviously another area that requires continued attention. YFP suffers from relative fast photobleaching in prolonged imaging experiments [68]. In addition, several recently report suggested that YFP was converted into a cyan fluorescent species after photobleaching under certain conditions [44, 45]. This problem may invalidate, or at least call into question, hundreds of previously published FRET experiments in which the efficiency was measured by acceptor photobleaching. Therefore a new yellow FP with improved properties is in high demand. Also the red and far-red fluorescent proteins still lack high brightness and maturation efficiency compared to other colors, because of the necessity of an extra oxidation step. Evolving brighter and more red-shifted FPs in this spectral range is a direction of high importance.

Since Shimomura's first observation of a greenish solution derived from jellyfish squeezate [36], the field of FP engineering and applications has made a great contribution to life science research. Researchers now have at their disposal a set of genetically encoded fluorophores that enable cells, tissues, and even whole animals to be investigated with a level of detail and subtlety that would otherwise be unimaginable. Some of the remaining challenges in this field include the development of photostable FPs, near-infrared FPs for deep

tissue imaging, multiple FRET pairs, and imaging modalities that break the diffraction barrier. The work described in this thesis is an example of the efforts trying to overcome some challenges. This work, together with parallel efforts in a handful of other labs around the world, will help to ensure that the future of FP-based imaging is a bright one.

# REFERENCES


1. Miyawaki A, Sawano A, Kogure T: **Lighting up cells: labelling proteins with fluorophores.** *Nat. Cell Biol.* 2003:S1-S7.
2. Giepmans BNG, Adams SR, Ellisman MH, Tsien RY: **The fluorescent toolbox for assessing protein location and function.** *Science* 2006, **312**:217-224.
3. Lutz S, Benkovic SJ: **Homology-independent protein engineering.** *Curr. Opin. Botechnol.* 2000, **11**:319-324.
4. Dahiyat BI, Sarisky CA, Mayo SL: ***De novo* protein design: towards fully automated sequence selection.** *J. Mol. Biol.* 1998, **279**:1023.
5. Wollacott AM, Zanghellini A, Murphy P, Baker D: **Prediction of structures of multidomain proteins from structures of the individual domains.** *Protein Sci.* 2007, **16**:165-175.
6. Jiang L, Althoff EA, Clemente FR, Doyle L, Rothlisberger D, Zanghellini A, Gallaher JL, Betker JL, Tanaka F, Barbas CF, III *et al*: ***De Novo* Computational Design of Retro-Aldol Enzymes.** *Science* 2008, **319**:1387-1391.
7. Darwin C: **On the Origin of Species by Means of Natural Selection, or the Preservation of Favoured Races in the Struggle for Life**: The Complete Work of Charles Darwin Online (revised in 2002); 1859.
8. Hutchison CA, Phillips S, Edgell MH, Gillam S, Jahnke P, Smith M: **Mutagenesis at a specific position in a DNA sequence.** *J. Biol. Chem.* 1978, **253**:6551-6560.
9. Wilkinson AJ, Fersht AR, Blow DM, Carter P, Winter G: **A large increase in enzyme-substrate affinity by protein engineering.** *Nature* 1984, **307**:187-188.
10. Jones PT, Dear PH, Foote J, Neuberger MS, Winter G: **Replacing the complementarity-determining regions in a human antibody with those from a mouse.** *Nature* 1986, **321**:522-525.
11. Wintrode PL, Miyazaki K, Arnold FH: **Cold-adaptation of a mesophilic subtilisin-like protease by laboratory evolution.** *J. Biol. Chem.* 2000, **275**:31635–31640.
12. Tobin MB, Gustafsson C, Huisman GW: **Directed evolution: the 'rational' basis for 'irrational' design.** *Curr. Opin. Struct. Biol.* 2000, **10**:421-427.
13. Brannigan JA, Wilkinson AJ: **Protein engineering 20 years on.** *Nat. Rev. Mol. Cell Biol.* 2002, **3**:964-970.

14. Umeno D, Tobias AV, Arnold FH: **Diversifying Carotenoid Biosynthetic Pathways by Directed Evolution**. *Microbiol Mol. Biol. Rev.* 2005, **69**:51-78.

15. Leung DW, Chen E, Goeddel DW: **A method for random mutagenesis of a defined DNA segment using a modified polymerase chain reaction**. *Techniques* 1989, **1**:11-15.

16. Giver L, Arnold FH: **Combinatorial protein design by *in vitro* recombination**. *Curr. Opin. Chem. Biol.* 1998, **2**:335-338.

17. Schmidt-Dannert C: **Directed evolution of single proteins, metabolic pathways, and viruses.** *Biochemistry* 2001, **40**:13125–13136.

18. Stemmer WPC: **Rapid evolution of a protein in vitro by DNA shuffling**. *Nature* 1994, **370**:389-391.

19. Rubin-Pitel S, Cho CM-H, Chen W, Zhao H: **Directed Evolution Tools in Bioproduct and Bioprocess Development**. In: *Bioprocessing for Value-Added Products from Renewable Resources: New Technologies and Applications.* Edited by Yang ST. New York: Elsevier Science; 2006: 49-72.

20. Wang L, Jackson WC, Steinbach PA, Tsien RY: **Evolution of new nonantibody proteins via iterative somatic hypermutation**. *Proc. Natl. Acad. Sci. USA* 2004, **101**:16745-16749.

21. Zhao H, Arnold FH: **Combinatorial protein design: strategies for screening protein libraries**. *Curr. Opin. Struct. Biol.* 1997, **7**:480-485.

22. Petrounia IP, Arnold FH: **Designed evolution of enzymatic properties**. *Curr. Opin. Botechnol.* 2000, **11**:325-330.

23. Campbell RE, Tour O, Palmer AE, Steinbach PA, Baird GS, Zacharias DA, Tsien RY: **A monomeric red fluorescent protein**. *Proc. Natl. Acad. Sci. USA* 2002, **99**:7877-7882.

24. Lakowicz JR: **Principles of Fluorescence Spectroscopy**, the 3rd edn. New York: Springer Science & Business Media, LLC; 2006.

25. Harvey EN: **A history of luminescence: from the earliest times until 1900**, vol. 44, 1957 edn. Philadelphia: The American Philosophical Society; 1957.

26. Herschel SJFW: **On a case of superfacial colour presented by a homogeneous liquid internally colorless** *Phil. Trans. Roy. Soc. (London)* 1845, **135**:143-145.

27. Stokes GG: **On the change of refrangibility of light**. *Phil. Trans. Roy. Soc. (London)* 1852, **142**:463-562.

28. Jablonski A: **Uber den mechanisms des photolumineszenz von farbstoffphosphoren**. *Z. Phys.* 1935, **94**:38-46.

29. Pawley JB: **Handbook of biological confocal microscopy,** the 3rd edn: Springer; 2006.

30. Förster T: **Intermolecular energy migration and fluorescence**. *Ann. Phys. (Leipzig)* 1948, **2**:55-75.

31. Hofmann M, Eggeling C, Jakobs S, Hell SW: **Breaking the diffraction barrier in fluorescence microscopy at low light intensities by using reversibly photoswitchable proteins**. *Proc. Natl. Acad. Sci. USA* 2005, **102**:17565-17569.

32. Betzig E, Patterson GH, Sougrat R, Lindwasser OW, Olenych S, Bonifacino JS, Davidson MW, Lippincott-Schwartz J, Hess HF: **Imaging Intracellular Fluorescent Proteins at Nanometer Resolution**. *Science* 2006, **313**:1642-1645.

33. Chen I, Ting AY: **Site-specific labeling of proteins with small molecules in live cells**. *Curr. Opin. Botechnol.* 2005, **16**:35-40.

34. Griffin BA, Adams SR, Tsien RY: **Specific covalent labeling of recombinant protein molecules inside live cells**. *Science* 1998, **281**:269-272.

35. Adams SR, Campbell RE, Gross LA, Martin BR, Walkup GK, Yao Y, Llopis J, Tsien RY: **New biarsenical ligands and tetracysteine motifs for protein labeling *in vitro* and *in vivo*: synthesis and biological applications**. *J. Am. Chem. Soc.* 2002, **124**:6063-6076.

36. Shimomura O, Johnson FH, Saiga Y: **Extraction, Purification and Properties of Aequorin, a Bioluminescent Protein from Luminous Hydromedusan, *Aequorea***. *J. Cell. Comp. Physiol.* 1962, **59**:223-239.

37. Tsien RY: **The green fluorescent protein**. *Annu. Rev. Biochem.* 1998, **67**:509-544.

38. Ormo M, Cubitt AB, Kallio K, Gross LA, Tsien RY, Remington SJ: **Crystal structure of the *Aequorea victoria* green fluorescent protein**. *Science* 1996, **273**:1392-1395.

39. Heim R, Prasher DC, Tsien RY: **Wavelength mutations and posttranslational autoxidation of green fluorescent protein**. *Proc. Natl. Acad. Sci. USA.* 1994, **91**:12501-12504.

40. Heim R, Cubitt AB, Tsien RY: **Improved green fluorescence**. *Nature* 1995, **373**:663-664.

41. Heim R, Tsien RY: **Engineering green fluorescent protein for improved brightness, longer wavelengths and fluorescence resonance energy transfer**. *Curr. Biol.* 1996, **6**:178-182.

42. Griesbeck O, Baird GS, Campbell RE, Zacharias DA, Tsien RY: **Reducing the environmental sensitivity of yellow fluorescent protein. Mechanism and applications**. *J. Biol. Chem.* 2001, **276**:29188-29194.

43. Nagai T, Ibata K, Park ES, Kubota M, Mikoshiba K, Miyawaki A: **A variant of yellow fluorescent protein with fast and efficient maturation for cell-biological applications**. *Nat. Botechnol.* 2002, **20**:87-90.

44. Valentin G: **Photoconversion of YFP into a CFP-like species during acceptor photobleaching FRET experiments**. *Nat. Meth.* 2005, **2**:801.

45. Kirber MT, Chen K, Keaney JF: **YFP photoconversion revisited: confirmation of the CFP-like species**. *Nat. Meth.* 2007, **4**:767-768.

46. Matz MV, Fradkov AF, Labas YA, Savitsky AP, Zaraisky AG, Markelov ML, Lukyanov SA: **Fluorescent proteins from nonbioluminescent Anthozoa species**. *Nat. Botechnol.* 1999, **17**:969-973.

47. Gurskaya NG, Savitsky AP, Yanushevich YG, Lukyanov SA, Lukyanov KA: **Color transitions in coral's fluorescent proteins by site-directed mutagenesis**. *BMC Biochem.* 2001, **2**:6.

48. Yanushevich YG, Staroverov DB, Savitsky AP, Fradkov AF, Gurskaya NG, Bulina ME, Lukyanov KA, Lukyanov SA: **A strategy for the generation of non-aggregating mutants of *Anthozoa* fluorescent proteins**. *FEBS Lett.* 2002, **511**:11-14.

49. Yarbrough D, Wachter RM, Kallio K, Matz MV, Remington SJ: **Refined crystal structure of DsRed, a red fluorescent protein from coral, at 2.0-A resolution**. *Proc. Natl. Acad. Sci. USA* 2001, **98**:462-467.

50. Shaner NC, Campbell RE, Steinbach PA, Giepmans BN, Palmer AE, Tsien RY: **Improved monomeric red, orange and yellow fluorescent proteins derived from *Discosoma sp.* red fluorescent protein.** *Nat. Botechnol.* 2004, **22**:1567-1572.

51. Wiedenmann J, Vallone B, Renzi F, Nienhaus K, Ivanchenko S, Rocker C, Nienhaus GU: **Red fluorescent protein eqFP611 and its genetically engineered dimeric variants.** *J. Biomed. Optics* 2005, **10**:014003-014007.

52. Shkrob MA, Yanushevich YG, Chudakov DM, Gurskaya NG, Labas YA, Poppnov SY, Mudrik NN, Lukyanov S, Lukyanov KA: **Far-red fluorescent proteins evolved from a blue chromoprotein from *Actinia equina*.** *Biochem. J.* 2005, **392**:649-654.

53. Merzlyak EM, Goedhart J, Shcherbo D, Bulina ME, Shcheglov AS, Fradkov AF, Gaintzeva A, Lukyanov KA, Lukyanov S, Gadella TWJ *et al*: **Bright monomeric red fluorescent protein with an extended fluorescence lifetime.** *Nat. Meth.* 2007, **4**:555-557.

54. Shcherbo D, Merzlyak EM, Chepurnykh TV, Fradkov AF, Ermakova GV, Solovieva EA, Lukyanov KA, Bogdanova EA, Zaraisky AG, Lukyanov S *et al*: **Bright far-red fluorescent protein for whole-body imaging.** *Nat. Meth.* 2007, **4**:741-746.

55. Lippincott-Schwartz J, Patterson GH: **Development and use of fluorescent protein markers in living cells.** *Science* 2003, **300**:87-91.

56. Lukyanov KA, Chudakov DM, Lukyanov S, Verkhusha VV: **Innovation: Photoactivatable fluorescent proteins.** *Nat. Rev. Mol. Cell Biol.* 2005, **6**:885-891.

57. Patterson GH, Lippincott-Schwartz J: **A photoactivatable GFP for selective photolabeling of proteins and cells.** *Science* 2002, **297**:1873-1877.

58. Cinelli RAG, Tozzini V, Pellegrini V, Beltram F, Cerullo G, Zavelani-Rossi M, De Silvestri S, Tyagi M, Giacca M: **Coherent Dynamics of Photoexcited Green Fluorescent Proteins.** *Phy. Rev. Lett.* 2001, **86**:3439.

59. McAnaney TB, Zeng W, Doe CFE, Bhanji N, Wakelin S, Pearson DS, Abbyad P, Shi X, Boxer SG, Bagshaw CR: **Protonation, Photobleaching, and Photoactivation of Yellow Fluorescent Protein (YFP 10C): A Unifying Mechanism.** *Biochemistry* 2005, **44**:5510-5524.

60. Ando R, Mizuno H, Miyawaki A: **Regulated fast nucleocytoplasmic shuttling observed by reversible protein highlighting.** *Science* 2004, **306**:1370-1373.

61. Henderson JN, Ai H-w, Campbell RE, Remington SJ: **Structural basis for reversible photobleaching of a green fluorescent protein homologue**. *Proc. Natl. Acad. Sci. USA* 2007, **104**:6672-6677.

62. Schwentker MA, Bock H, Hofmann M, Jakobs S, Bewersdorf J, Eggeling C, Hell SW: **Wide-field subdiffraction RESOLFT microscopy using fluorescent protein photoswitching**. *Microscopy Research and Technique* 2007, **70**:269-280.

63. Topell S, Hennecke J, Glockshuber R: **Circularly permuted variants of the green fluorescent protein**. *FEBS Lett.* 1999, **457**:283-289.

64. Baird GS, Zacharias DA, Tsien RY: **Circular permutation and receptor insertion within green fluorescent proteins**. *Proc. Natl. Acad. Sci. USA* 1999, **96**:11241-11246.

65. Nagai T, Sawano A, Park ES, Miyawaki A: **Circularly permuted green fluorescent proteins engineered to sense $Ca^{2+}$**. *Proc. Natl. Acad. Sci. USA* 2001, **98**:3197-3202.

66. Nakai J, Ohkura M, Imoto K: **A high signal-to-noise $Ca^{2+}$ probe composed of a single green fluorescent protein**. *Nat. Botechnol.* 2001, **19**:137-141.

67. Nagai T, Yamada S, Tominaga T, Ichikawa M, Miyawaki A: **Expanded dynamic range of fluorescent indicators for $Ca^{2+}$ by circularly permuted yellow fluorescent proteins**. *Proc. Natl. Acad. Sci. USA* 2004, **101**:10554-10559.

68. Shaner NC, Steinbach PA, Tsien RY: **A guide to choosing fluorescent proteins**. *Nat. Meth.* 2005, **2**:905-909.

69. Kogure T, Karasawa S, Araki T, Saito K, Kinjo M, Miyawaki A: **A fluorescent variant of a protein from the stony coral *Montipora* facilitates dual-color single-laser fluorescence cross-correlation spectroscopy**. *Nat. Botechnol.* 2006, **24**:577-581.

70. Miyawaki A, Llopis J, Heim R, McCaffery JM, Adams JA, Ikura M, Tsien RY: **Fluorescent indicators for $Ca^{2+}$ based on green fluorescent proteins and calmodulin**. *Nature* 1997, **388**:882-887.

71. Violin JD, Zhang J, Tsien RY, Newton AC: **A genetically encoded fluorescent reporter reveals oscillatory phosphorylation by protein kinase C**. *J. Cell. Biol.* 2003, **161**:899-909.

72. Lin CW, Jao CY, Ting AY: **Genetically encoded fluorescent reporters of histone methylation in living cells.** *J. Am. Chem. Soc.* 2004, **126**:5982-5983.

73. Ai H-w, Henderson JN, Remington SJ, Campbell RE: **Directed evolution of a monomeric, bright and photostable version of *Clavularia* cyan fluorescent protein: structural characterization and applications in fluorescence imaging.** *Biochem. J.* 2006, **400**:531-540.

74. Ai H-w, Campbell RE: **Teal fluorescent proteins: Characterization of a reversibly photoswitchable variant.** *Proc. SPIE* 2008, **6868**:68680D.

75. Ai H-w, Olenych SG, Wong P, Davidson MW, Campbell RE: **Hue-shifted monomeric variants of Clavularia cyan fluorescent protein: identification of the molecular determinants of color and applications in fluorescence imaging.** *BMC Biology* 2008, **6**:13.

76. Ai H-w, Shaner NC, Cheng Z, Tsien RY, Campbell RE: **Exploration of New Chromophore Structures Leads to the Identification of Improved Blue Fluorescent Proteins.** *Biochemistry* 2007, **46**:5904-5910.

77. Ai H-w, Hazelwood KL, Davidson MW, Campbell RE: **Fluorescent protein FRET pairs for ratiometric imaging of dual caspase sensors.** *Nat. Meth.* 2008, **5**:401-403.

78. Verkhusha VV, Lukyanov KA: **The molecular properties and applications of Anthozoa fluorescent proteins and chromoproteins.** *Nat. Botechnol.* 2004, **22**:289-296.

79. Zhang J, Campbell RE, Ting AY, Tsien RY: **Creating new fluorescent probes for cell biology.** *Nat. Rev. Mol. Cell Biol.* 2002, **3**:906-918.

80. Chudakov DM, Lukyanov S, Lukyanov KA: **Fluorescent proteins as a toolkit for *in vivo* imaging.** *Trends Botechnol.* 2005, **23**:605-613.

81. Yang F, Moss LG, Phillips GN, Jr.: **The molecular structure of green fluorescent protein.** *Nat. Biotechnol.* 1996, **14**:1246-1251.

82. Cody CW, Prasher DC, Westler WM, Prendergast FG, Ward WW: **Chemical structure of the hexapeptide chromophore of the *Aequorea* green-fluorescent protein.** *Biochemistry* 1993, **32**:1212-1218.

83. Chattoraj M, King BA, Bublitz GU, Boxer SG: **Ultra-fast excited state dynamics in green fluorescent protein: multiple states and proton transfer**. *Proc. Natl. Acad. Sci. USA* 1996, **93**:8362-8367.

84. Cormack BP, Valdivia RH, Falkow S: **FACS-optimized mutants of the green fluorescent protein (GFP)**. *Gene* 1996, **173**:33-38.

85. Rizzo MA, Springer GH, Granada B, Piston DW: **An improved cyan fluorescent protein variant useful for FRET**. *Nat. Biotechnol.* 2004, **22**:445-449.

86. Nguyen AW, Daugherty PS: **Evolutionary optimization of fluorescent proteins for intracellular FRET**. *Nat. Biotechnol.* 2005, **23**:355-360.

87. Rizzo MA, Piston DW: **High-contrast imaging of fluorescent protein FRET by fluorescence polarization microscopy**. *Biophys. J.* 2005, **88**:L14-16.

88. Carter RW, Schmale MC, Gibbs PD: **Cloning of anthozoan fluorescent protein genes**. *Comp. Biochem. Physiol. C* 2004, **138**:259-270.

89. Sun Y, Castner EW, Jr., Lawson CL, Falkowski PG: **Biophysical characterization of natural and mutant fluorescent proteins cloned from zooxanthellate corals**. *FEBS Lett.* 2004, **570**:175-183.

90. Kelmanson IV, Matz MV: **Molecular basis and evolutionary origins of color diversity in great star coral *Montastraea cavernosa* (Scleractinia: Faviida)**. *Mol. Biol. Evol.* 2003, **20**:1125-1133.

91. Shagin DA, Barsova EV, Yanushevich YG, Fradkov AF, Lukyanov KA, Labas YA, Semenova TN, Ugalde JA, Meyers A, Nunez JM *et al*: **GFP-like proteins as ubiquitous metazoan superfamily: evolution of functional features and structural complexity**. *Mol. Biol. Evol.* 2004, **21**:841-850.

92. Karasawa S, Araki T, Nagai T, Mizuno H, Miyawaki A: **Cyan-emitting and orange-emitting fluorescent proteins as a donor/acceptor pair for fluorescence resonance energy transfer**. *Biochem. J.* 2004, **381**:307-312.

93. Lauf U, Lopez P, Falk MM: **Expression of fluorescently tagged connexins: a novel approach to rescue function of oligomeric DsRed-tagged proteins**. *FEBS Lett.* 2001, **498**:11-15.

94. Gavin P, Devenish RJ, Prescott M: **An approach for reducing unwanted oligomerisation of DsRed fusion proteins.** *Biochem. Biophys. Res. Commun.* 2002, **298**:707-713.

95. Soling A, Simm A, Rainov N: **Intracellular localization of Herpes simplex virus type 1 thymidine kinase fused to different fluorescent proteins depends on choice of fluorescent tag.** *FEBS Lett.* 2002, **527**:153-158.

96. Karasawa S, Araki T, Yamamoto-Hino M, Miyawaki A: **A green-emitting fluorescent protein from Galaxeidae coral and its monomeric version for use in fluorescent labeling.** *J. Biol. Chem.* 2003, **278**:34167-34171.

97. Wiedenmann J, Ivanchenko S, Oswald F, Schmitt F, Rocker C, Salih A, Spindler KD, Nienhaus GU: **EosFP, a fluorescent marker protein with UV-inducible green-to-red fluorescence conversion.** *Proc. Natl. Acad. Sci. USA* 2004, **101**:15905-15910.

98. Gurskaya NG, Verkhusha VV, Shcheglov AS, Staroverov DB, Chepurnykh TV, Fradkov AF, Lukyanov S, Lukyanov KA: **Engineering of a monomeric green-to-red photoactivatable fluorescent protein induced by blue light.** *Nat. Biotechnol.* 2006, **24**:461-465.

99. Zacharias DA, Violin JD, Newton AC, Tsien RY: **Partitioning of lipid-modified monomeric GFPs into membrane microdomains of live cells.** *Science* 2002, **296**:913-916.

100. Fromant M, Blanquet S, Plateau P: **Direct random mutagenesis of gene-sized DNA fragments using polymerase chain reaction.** *Anal. Biochem.* 1995, **224**:347-353.

101. Cheng Z, Campbell RE: **Assessing the structural stability of designed beta-hairpin peptides in the cytoplasm of live cells.** *ChemBioChem* 2006, **7**:1147-1150.

102. Brannon JH, Magde D: **Absolute Quantum Yield Determination by Thermal Blooming - Fluorescein.** *J. Phys. Chem.* 1978, **82**:705-709.

103. Ward WW: **Biochemical and physical properties of GFP.** In: *Green Fluorescent Protein: Properties, Applications, and Protocols.* Edited by Chalfie MK, S. New York: Wiley; 1998: 45-75.

104. Bevis BJ, Glick BS: **Rapidly maturing variants of the *Discosoma* red fluorescent protein (DsRed).** *Nat. Biotechnol.* 2002, **20**:83-87.

105. Henderson JN, Remington SJ: **Crystal structures and mutational analysis of amFP486, a cyan fluorescent protein from *Anemonia majano***. *Proc. Natl. Acad. Sci. USA* 2005, **102**:12712-12717.

106. Holm L, Sander C: **Protein structure comparison by alignment of distance matrices**. *J. Mol. Biol.* 1993, **233**:123-138.

107. Holm L, Park J: **DaliLite workbench for protein structure comparison**. *Bioinformatics* 2000, **16**:566-567.

108. Nienhaus K, Nienhaus GU, Wiedenmann J, Nar H: **Structural basis for photo-induced protein cleavage and green-to-red conversion of fluorescent protein EosFP**. *Proc. Natl. Acad. Sci. USA* 2005, **102**:9156-9159.

109. Wall MA, Socolich M, Ranganathan R: **The structural basis for red fluorescence in the tetrameric GFP homolog DsRed**. *Nat. Struct. Biol.* 2000, **7**:1133-1138.

110. Henderson JN, Remington SJ: **The kindling fluorescent protein: a transient photoswitchable marker**. *Physiology (Bethesda)* 2006, **21**:162-170.

111. Miyawaki A, Tsien RY: **Monitoring protein conformations and interactions by fluorescence resonance energy transfer between mutants of green fluorescent protein**. *Methods Enzymol.* 2000, **327**:472-500.

112. Day RN, Booker CF, Periasamy A: **The characterization of an improved donor fluorescent protein for Forster resonance energy transfer microscopy**. *J. Biomed. Optics* 2008:in press.

113. Prasher DC, Eckenrode VK, Ward WW, Prendergast FG, Cormier MJ: **Primary structure of the *Aequorea victoria* green-fluorescent protein**. *Gene* 1992, **111**:229-233.

114. Chalfie M, Tu Y, Euskirchen G, Ward WW, Prasher DC: **Green fluorescent protein as a marker for gene expression**. *Science* 1994, **263**:802-805.

115. Inouye S, Tsuji FI: ***Aequorea* green fluorescent protein. Expression of the gene and fluorescence characteristics of the recombinant protein**. *FEBS Lett.* 1994, **341**:277-280.

116. Shaner NC, Patterson GH, Davidson MW: **Advances in fluorescent protein technology**. *J. Cell Sci.* 2007, **120**:4247-4260.

117. Dickson RM, Cubitt AB, Tsien RY, Moerner WE: **On/off blinking and switching behaviour of single molecules of green fluorescent protein.** *Nature* 1997, **388**:355-358.

118. Habuchi S, Ando R, Dedecker P, Verheijen W, Mizuno H, Miyawaki A, Hofkens J: **Reversible single-molecule photoswitching in the GFP-like fluorescent protein Dronpa.** *Proc. Natl. Acad. Sci. USA* 2005, **102**:9511-9516.

119. Quillin ML, Anstrom DM, Shu X, O'Leary S, Kallio K, Chudakov DM, Remington SJ: **Kindling fluorescent protein from *Anemonia sulcata*: dark-state structure at 1.38 A resolution.** *Biochemistry* 2005, **44**:5774-5787.

120. Ando R, Flors C, Mizuno H, Hofkens J, Miyawaki A: **Highlighted Generation of Fluorescence Signals Using Simultaneous Two-Color Irradiation on Dronpa Mutants.** *Biophys. J.* 2007, **92**:L97-99.

121. Wouters FS: **The physics and biology of fluorescence microscopy in the life sciences.** *Contemp. Phys.* 2006, **47**:239-255.

122. Ehrig T, O'Kane DJ, Prendergast FG: **Green-fluorescent protein mutants with altered fluorescence excitation spectra.** *FEBS Lett.* 1995, **367**:163-166.

123. Matz MV, Lukyanov KA, Lukyanov SA: **Family of the green fluorescent protein: journey to the end of the rainbow.** *Bioessays* 2002, **24**:953-959.

124. Marques MA, Lopez X, Varsano D, Castro A, Rubio A: **Time-dependent density-functional approach for biological chromophores: the case of the green fluorescent protein.** *Phys. Rev. Lett.* 2003, **90**:258101.

125. Budisa N, Pal PP, Alefelder S, Birle P, Krywcun T, Rubini M, Wenger W, Bae JH, Steiner T: **Probing the role of tryptophans in *Aequorea victoria* green fluorescent proteins with an expanded genetic code.** *Biol. Chem.* 2004, **385**:191-202.

126. Ward WW, Cormier MJ: **An energy transfer protein in coelenterate bioluminescence. Characterization of the *Renilla* green-fluorescent protein.** *J. Biol. Chem.* 1979, **254**:781-788.

127. Cubitt AB, Woollenweber LA, Heim R: **Understanding structure-function relationships in the *Aequorea victoria* green fluorescent protein.** *Methods Cell. Biol.* 1999, **58**:19-30.

128. Waldo GS, Standish BM, Berendzen J, Terwilliger TC: **Rapid protein-folding assay using green fluorescent protein**. *Nat. Biotechnol.* 1999, **17**:691-695.

129. Pedelacq JD, Cabantous S, Tran T, Terwilliger TC, Waldo GS: **Engineering and characterization of a superfolder green fluorescent protein**. *Nat. Biotechnol.* 2006, **24**:79-88.

130. Mitra RD, Silva CM, Youvan DC: **Fluorescence resonance energy transfer between blue-emitting and red-shifted excitation derivatives of the green fluorescent protein**. *Gene* 1996, **173**:13-17.

131. Piljic A, Schultz C: **Annexin A4 self-association modulates general membrane protein mobility in living cells**. *Mol. Biol. Cell* 2006, **17**:3318-3328.

132. Miyawaki A, Nagai T, Mizuno H: **Engineering fluorescent proteins**. *Adv. Biochem. Eng. Biotechnol.* 2005, **95**:1-15.

133. Shimomura O: **Structure of the Chromophore of *Aequorea* Green Fluorescent Protein**. *FEBS Lett.* 1979, **104**:220-222.

134. Gross LA, Baird GS, Hoffman RC, Baldridge KK, Tsien RY: **The structure of the chromophore within DsRed, a red fluorescent protein from coral**. *Proc. Natl. Acad. Sci. USA* 2000, **97**:11990-11995.

135. Wang S, Hazelrigg T: **Implications for bcd mRNA localization from spatial distribution of exu protein in Drosophila oogenesis**. *Nature* 1994, **369**:400-403.

136. Yang TT, Sinai P, Green G, Kitts PA, Chen YT, Lybarger L, Chervenak R, Patterson GH, Piston DW, Kain SR: **Improved fluorescence and dual color detection with enhanced blue and green variants of the green fluorescent protein**. *J. Biol. Chem.* 1998, **273**:8212-8216.

137. Mena MA, Treynor TP, Mayo SL, Daugherty PS: **Blue fluorescent proteins with enhanced brightness and photostability from a structurally targeted library**. *Nat. Biotechnol.* 2006, **24**:1569-1571.

138. Treynor TP, Vizcarra CL, Nedelcu D, Mayo SL: **Computationally designed libraries of fluorescent proteins evaluated by preservation and diversity of function**. *Proc. Natl. Acad. Sci. USA* 2007, **104**:48-53.

139. Adams MJ, Highfield JG, Kirkbright GF: **Determination of Absolute Fluorescence Quantum Efficiency of Quinine Bisulfate in Aqueous-Medium by Optoacoustic Spectrometry**. *Anal. Chem.* 1977, **49**:1850-1852.

140. Zapata-Hommer O, Griesbeck O: **Efficiently folding and circularly permuted variants of the Sapphire mutant of GFP**. *BMC Biotechnol.* 2003, **3**:5.

141. Chudakov DM, Verkhusha VV, Staroverov DB, Souslova EA, Lukyanov S, Lukyanov KA: **Photoswitchable cyan fluorescent protein for protein tracking**. *Nat. Biotechnol.* 2004, **22**:1435-1439.

142. Wachter RM, King BA, Heim R, Kallio K, Tsien RY, Boxer SG, Remington SJ: **Crystal structure and photodynamic behavior of the blue emission variant Y66H/Y145F of green fluorescent protein**. *Biochemistry* 1997, **36**:9759-9765.

143. Wu X, Simone J, Hewgill D, Siegel R, Lipsky PE, He L: **Measurement of two caspase activities simultaneously in living cells by a novel dual FRET fluorescent indicator probe**. *Cytometry A* 2006, **69**:477-486.

144. Anna Peyker ORPIHB: **Imaging Activation of Two Ras Isoforms Simultaneously in a Single Cell**. *ChemBioChem* 2005, **6**:78-85.

145. Kawai H, Suzuki T, Kobayashi T, Sakurai H, Ohata H, Honda K, Momose K, Namekata I, Tanaka H, Shigenobu K *et al*: **Simultaneous real-time detection of initiator- and effector-caspase activation by double fluorescence resonance energy transfer analysis.** *J. Pharmacol. Sci.* 2005, **97**:361-368.

146. Evdokimov AG, Pokross ME, Egorov NS, Zaraisky AG, Yampolsky IV, Merzlyak EM, Shkoporov AN, Sander I, Lukyanov KA, Chudakov DM: **Structural basis for the fast maturation of *Arthropoda* green fluorescent protein** *EMBO reports* 2006, **7**:1006-1012.

147. Abramoff MD, Magelhaes PJ, Ram SJ: **Image Processing with ImageJ**. *Biophotonics International* 2004, **11**:36 – 42.

148. Xu X, Gerard AL, Huang BC, Anderson DC, Payan DG, Luo Y: **Detection of programmed cell death using fluorescence energy transfer**. *Nucleic Acids Res.* 1998, **26**:2034-2035.

149. Ferrando-May E: **Nucleocytoplasmic transport in apoptosis**. *Cell Death Differ.* 2005, **12**:1263-1276.

150. Rudolf R, Mongillo M, Rizzuto R, Pozzan T: **Looking forward to seeing calcium.** *Nat. Rev. Mol. Cell Biol.* 2003, **4**:579-586.

151. Soderling TR: **The $Ca^{2+}$-calmodulin-dependent protein kinase cascade.** *Trends Biochem. Sci.* 1999, **24**:232-236.

152. Roderick H, Bootman M: **Redoxing calcium from the ER.** *Cell* 2005, **120**(1):4-5.

153. Tsien RY: **New calcium indicators and buffers with high selectivity against magnesium and protons: design, sythesis, and properties of prototype structures.** *Biochemistry* 1980, **19**:2396-2404.

154. Shimomura O: **A short history of aequorin.** *Biol. Bull.* 1995, **189**:1-5.

155. Cork RJ, Strautman AF, Robinson KR: **Measuring Cytoplasmic Calcium: A Review of Three Methods With Emphasis on the Practical Aspects of Their Use.** *Biol. Bull.* 1989, **176**:25-30.

156. Romoser VA, Hinkle PM, Persechini A: **Detection in living cells of $Ca^{2+}$-dependent changes in the fluorescence emission of an indicator composed of two green fluorescent protein variants linked by a calmodulin-binding sequence.** *J. Biol. Chem.* 1997, **272**:13270-13274.

157. Truong K, Sawano A, Mizuno H, Hama H, Tong KI, Mal TK, Miyawaki A, Ikura M: **FRET-based in vivo $Ca^{2+}$ imaging by a new calmodulin-GFP fusion molecule.** *Nat. Struct. Biol.* 2001, **8**:1069-1073.

158. Palmer AE, Tsien RY: **Measuring calcium signaling using genetically targetable fluorescent indicators.** *Nat. Protocols* 2006, **1**:1057-1065.

159. Palmer AE, Jin C, Reed JC, Tsien RY: **Bcl-2-mediated alterations in endoplasmic reticulum $Ca^{2+}$ analyzed with an improved genetically encoded fluorescent sensor.** *Proc. Natl. Acad. Sci. USA* 2004, **101**:17404-17409.

160. Palmer AE, Giacomello M, Kortemme T, Hires SA, Lev-Ram V, Baker D, Tsien RY: **$Ca^{2+}$ Indicators Based on Computationally Redesigned Calmodulin-Peptide Pairs.** *Chem. Biol.* 2006, **13**:521-530.

161. Wikipedia: **Yin and yang.** In: *Wikipedia, The Free Encyclopedia.* 2008.

162. Zhang J, Ma Y, Taylor SS, Tsien RY: **Genetically encoded reporters of protein kinase A activity reveal impact of substrate tethering.** *Proc. Natl. Acad. Sci. USA* 2001, **98**:14997-15002.

163. Ting AY, Kain KH, Klemke RL, Tsien RY: **Genetically encoded fluorescent reporters of protein tyrosine kinase activities in living cells**. *Proc. Natl. Acad. Sci. USA* 2001, **98**:15003-15008.